Report No. K-TRAN: KSU-14-2 ▪ FINAL REPORT ▪ December 2016

Best Practices for Concrete Pumping

Kyle A. Riding, Ph.D., P.E.
Jan Vosahlik

Kansas State University Transportation Center

Dimitri Feys, Ph.D.

Missouri University of Science and Technology

Travis Malone, P.E.
Will Lindquist, Ph.D., P.E.

Kansas Department of Transportation

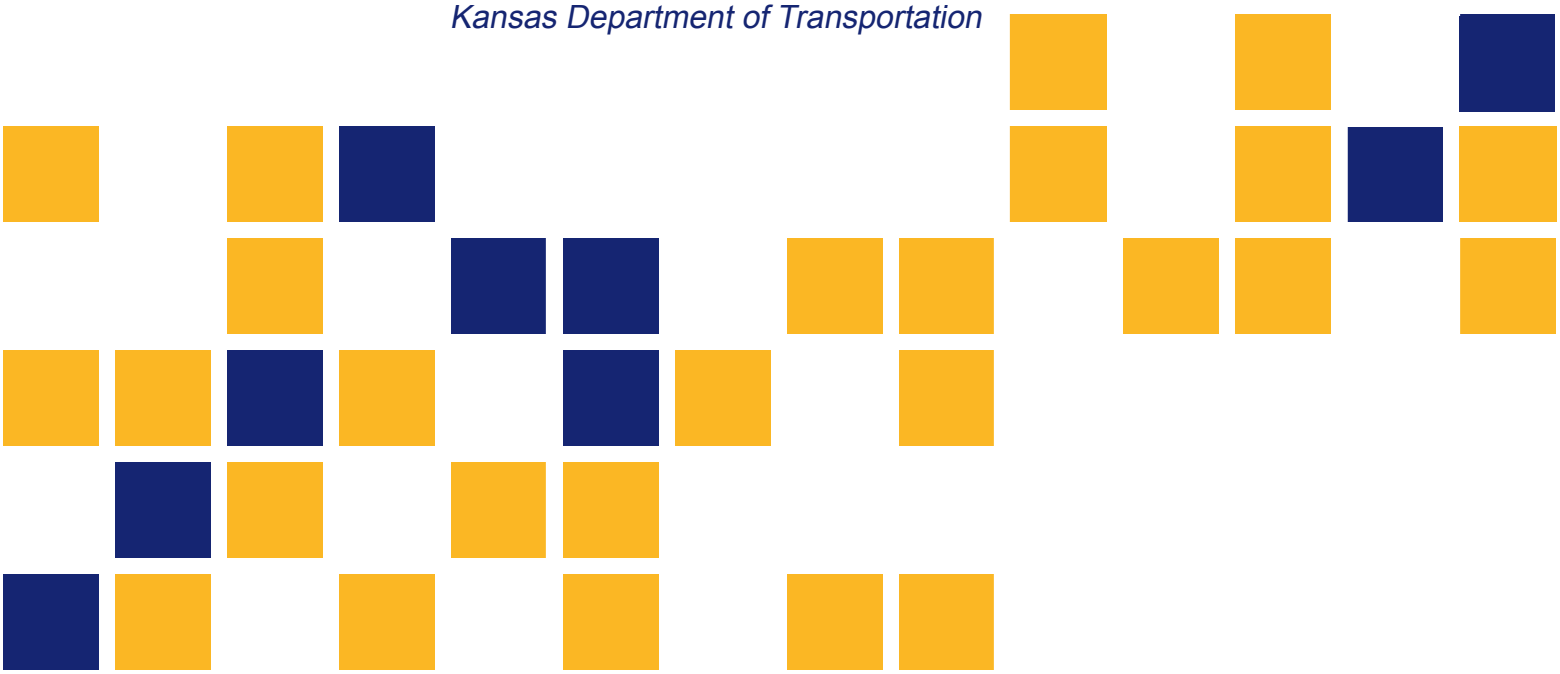

1 Report No. K-TRAN: KSU-14-2	**2 Government Accession No.**	**3 Recipient Catalog No.**
4 Title and Subtitle Best Practices for Concrete Pumping		**5 Report Date** December 2016 **6 Performing Organization Code**
7 Author(s) Kyle A. Riding, Ph.D., P.E., Jan Vosahlik, Dimitri Feys, Ph.D., Travis Malone, P.E., Will Lindquist, Ph.D., P.E.		**7 Performing Organization Report No.**
9 Performing Organization Name and Address Kansas State University Transportation Center Department of Civil Engineering 2118 Fiedler Hall Manhattan, KS 66506-5000		**10 Work Unit No. (TRAIS)** **11 Contract or Grant No.** C1995
12 Sponsoring Agency Name and Address Kansas Department of Transportation Bureau of Research 2300 SW Van Buren Topeka, Kansas 66611-1195		**13 Type of Report and Period Covered** Final Report January 2014–May 2016 **14 Sponsoring Agency Code** RE-0623-01
15 Supplementary Notes For more information write to address in block 9.		

Pumping is one of the major placement techniques used in the concrete industry to deliver concrete from the mixing truck to the formwork. Although concrete pumping has been used to place concrete since the 1960s, there is still a lack of exact knowledge supported by research evidence as to what affects concrete pumpability and how pumping changes concrete properties. A three-phase research study was carried out to (1) investigate performance of pumped concrete in field conditions, (2) identify concrete properties affecting pumpability, and (3) assess the effects of pumping on the concrete air void system. In the first phase of the research program, six Kansas Department of Transportation (KDOT) project sites were visited during the summer of 2015, and concrete was sampled before and after pumping. In addition to measuring fresh concrete properties as well as performing hardened air void analysis of all sampled mixtures, rheological and tribological tests were performed on sampled concrete. The second phase of the study consisted of a full-scale controlled pumping experiment. During the experiment, three different concrete mixtures were pumped, and both fresh and hardened properties of the concrete were determined. Additionally, the pumping system was equipped with strain gauges to measure pumping pressures. Finally, the third phase of the study consisted of measuring the rheological and tribological properties of 35 concrete mixtures in order to determine the effect of various concrete components on pumpability.

17 Key Words Concrete Pumping, Pumpability, Concrete Properties, Air Void System		**18 Distribution Statement** No restrictions. This document is available to the public through the National Technical Information Service www.ntis.gov.	
19 Security Classification (of this report) Unclassified	**20 Security Classification (of this page)** Unclassified	**21 No. of pages** 122	**22 Price**

Form DOT F 1700.7 (8-72)

This page intentionally left blank.

Best Practices for Concrete Pumping

Final Report

Prepared by

Kyle A. Riding, Ph.D., P.E.
Jan Vosahlik

Kansas State University Transportation Center

Dimitri Feys, Ph.D.

Missouri University of Science and Technology

Travis Malone, P.E.
Will Lindquist, Ph.D., P.E.

Kansas Department of Transportation

A Report on Research Sponsored by

THE KANSAS DEPARTMENT OF TRANSPORTATION
TOPEKA, KANSAS

and

KANSAS STATE UNIVERSITY TRANSPORTATION CENTER
MANHATTAN, KANSAS

December 2016

PREFACE

The Kansas Department of Transportation's (KDOT) Kansas Transportation Research and New-Developments (K-TRAN) Research Program funded this research project. It is an ongoing, cooperative and comprehensive research program addressing transportation needs of the state of Kansas utilizing academic and research resources from KDOT, Kansas State University and the University of Kansas. Transportation professionals in KDOT and the universities jointly develop the projects included in the research program.

NOTICE

The authors and the state of Kansas do not endorse products or manufacturers. Trade and manufacturers names appear herein solely because they are considered essential to the object of this report.

This information is available in alternative accessible formats. To obtain an alternative format, contact the Office of Public Affairs, Kansas Department of Transportation, 700 SW Harrison, 2nd Floor – West Wing, Topeka, Kansas 66603-3745 or phone (785) 296-3585 (Voice) (TDD).

DISCLAIMER

The contents of this report reflect the views of the authors who are responsible for the facts and accuracy of the data presented herein. The contents do not necessarily reflect the views or the policies of the state of Kansas. This report does not constitute a standard, specification or regulation.

Abstract

Pumping is one of the major placement techniques used in the concrete industry to deliver concrete from the mixing truck to the formwork. Although concrete pumping has been used to place concrete since the 1960s, there is still a lack of exact knowledge supported by research evidence as to what affects concrete pumpability and how pumping changes concrete properties. A three-phase research study was carried out to (1) investigate performance of pumped concrete in field conditions, (2) identify concrete properties affecting pumpability, and (3) assess the effects of pumping on the concrete air void system. In the first phase of the research program, six Kansas Department of Transportation (KDOT) project sites were visited during the summer of 2015, and concrete was sampled before and after pumping. In addition to measuring fresh concrete properties as well as performing hardened air void analysis of all sampled mixtures, rheological and tribological tests were performed on sampled concrete. The second phase of the study consisted of a full-scale controlled pumping experiment. During the experiment, three different concrete mixtures were pumped, and both fresh and hardened properties of the concrete were determined. Additionally, the pumping system was equipped with strain gauges to measure pumping pressures. Finally, the third phase of the study consisted of measuring the rheological and tribological properties of 35 concrete mixtures in order to determine the effect of various concrete components on pumpability.

Acknowledgments

The authors wish to acknowledge the financial support of the Kansas Department of Transportation (KDOT) for this project. The cooperation and help of KDOT project monitors Dr. Will Lindquist and Travis Malone is greatly appreciated.

The field testing part of this project would not be possible without the help of Mr. Jason Thompson, Mr. Nathan Jeffries, and the construction crew from TranSystems. Their help with arranging site visits and help with samples collection is gratefully acknowledged. Additionally, the authors would like to express thanks to Ms. Amy Pope, KDOT Field Engineering Administrator, for her help with the field work on the I-70 over Kaw Drive project.

The full-scale controlled experiment was only possible with the tremendous help of ACI Concrete Placement and Fordyce Concrete Company. The authors would like to thank Mr. Matt Kaminski and Mr. Nate Rutledge from ACI Concrete Placement for their help, advice, and particularly for providing their pump, equipment, and personnel for the experiment. The authors also wish to express their thanks to Frank Schilling and Ronnie Tucker from Fordyce Concrete Company. Their gracious donation of concrete as well as providing space for the experiment is gratefully acknowledged.

The authors also wish to express their gratitude to Mr. Andy Kultgen from Con Forms for his advice, help, and donation of pumping equipment for this study.

The authors would also like to thank SIKA Corporation US, Active Minerals International, and Ash Grove Cement Company for donations of materials for the laboratory part of this study.

Lastly, the authors would like to thank the following Kansas State University students and staff for their tremendous help with this project: Mr. Cale Armstrong, Mr. Ryan Benteman, Mr. Jason Cane, Mr. Koby Daily, Mr. Aref Dastgerdi, Mr. Cody Delaney, Mr. Abraham Fangman, Dr. Ahmad Ghadban, Mr. Casey Keller, and Mrs. Yadira Porras.

Table of Contents

List of Tables

List of Figures

This page intentionally left blank.

Chapter 1: Introduction

1.1 Research Background

Concrete pumping is one of the most common techniques for the transport and placement of fresh concrete on the job site. Developed in the early 1960s, the concrete pumping technology has significantly evolved since its early days. Concrete pumps are used to deliver concrete of various properties to great distances both horizontally and vertically, including at the most prestigious and challenging projects around the world.

Pumped concrete goes through different states and stages throughout the pumping process. First, concrete is dropped from the mixing truck into the pump hopper, agitated, and eventually pushed into one of the pump's pistons. Shortly after that, concrete is exposed to a large pressure shock in order to be pushed by the piston and through the pipeline. During the pumping process, concrete is sheared, pushed as a plug, or both. Finally, fresh concrete arrives at the location of placement, where it is depressurized and dropped into the formwork. After such a diverse experience, concrete that is placed can have very different properties from the material that was initially delivered in the mixing truck.

1.2 Scope of the Research

A three-phase study was conducted at Kansas State University (KSU) to investigate the effect of concrete pumping on concrete properties. The first phase of the research program, the field testing campaign, was conducted in the summer of 2015. Six Kansas Department of Transportation (KDOT) construction sites were visited. Concrete before and after pumping was investigated. The second part of the study took place in November 2015 when a full-scale, controlled pumping experiment was conducted. In this experiment, the controlled research environment allowed for more precise measurements and assessment of concrete properties after pumping, including pumping pressure monitoring. Finally, the third component of the project consisted of a laboratory study investigating rheological and tribological properties of concrete mixtures to assess the effects of mix proportioning on these properties.

Chapter 2: Literature Review

2.1 Concrete Pumps

The most common type of concrete pump in use is a high-capacity dual-piston pump (ACI 304.2R-96, 1996; Jacobsen, Mork, Lee, & Haugan, 2008; Khatib, 2013). Many different piston concrete pumps are available for purchase, but they are the same conceptually. The three major parts of a piston pump are: (1) a concrete receiving hopper, (2) a valve system, and (3) a power transmission system (Cooke, 1990). The hopper is commonly equipped with an agitator that prevents aggregate segregation and allows fresh concrete to flow smoothly into the pistons (ACI 304.2R-96, 1996; Fisher, 1994). The pump performs in two cycles: during the first cycle, concrete is drawn into one of the cylinders, utilizing suction created by the retreating piston, while the second piston moves in the opposite direction and discharges concrete into the pipeline. In the second cycle, pistons reverse their roles from the first cycle. Most pumps are driven by hydraulic cylinders powered by hydraulic pumps; however, some older models of piston pumps are still driven by a mechanical system (ACI 304.2R-96, 1996). Other, less common, types of concrete pumps include worm and peristatic pumps (Cooke, 1990).

An essential element of each piston pump is a valve system that can be used to distinguish one type of pump from another. The valve ensures that concrete coming from two cylinders can be pushed through one line while providing a constant flow rate of concrete for the entire pumping circuit (ACI 304.2R-96, 1996). However, concrete pressure has been proven to fluctuate as piston position in the cylinders changes (Jacobsen et al., 2008). Negative pressure in the system was also observed when the piston retreated immediately before the controlling valve opened for the discharging piston. As each of the major concrete pump manufacturers has developed their own valves, many types of valves or valve systems are available on the market. Some of the most utilized valve types include gate valve, flapper valve, hollow-tube valve, rock valve, S-valve, C-valve, or ball valves.

Concrete pumps can be classified on the basis of their drive (mechanical/hydraulic), type of valve (hollow-core tube, ball, gate), or mobility. The three most common types of concrete pumps based on mobility are boom pumps, truck-mounted line pumps, and trailer pumps.

Boom pumps are commonly deployed for large projects in which big volumes of concrete must be pumped typically for long distances, such as a bridge deck or residential building construction. Modern boom pumps are state-of-the-art machines that require well-trained operators to oversee the pumping process. The major advantages of boom pumps include their ability to pump large volumes of concrete over a short period of time, and not needing an external pumping line for concrete because the pump is equipped with a boom.

Truck-mounted line pumps are essentially boom pumps without a long boom and corresponding pumping line. These pumps offer high power, and thus can be utilized at a large-scale construction site while providing higher mobility than traditional boom pumps. The disadvantage of a truck-mounted pump is that these machines require installation of conventional pipelines to distribute the concrete on site, hence the use of a truck-mounted pump is more labor intensive than utilization of a boom pump. However, truck-mounted pumps are very often used in space-limited working conditions. Trailer pumps are used to deliver concrete on small job sites, such as urban housing developments, or less traditional concrete applications, such as the shotcrete industry.

In addition to the concrete pump, other parts of the pumping circuit greatly influence the quality and safety of concrete pumping. Once concrete leaves the pump, it is transported through a pumpline to its final destination, usually flowing through a system of bends, reducers, and fittings. The entire assemblage interacts with pumped concrete and significantly influences pumping quality (flow rate, pumping pressure) as well as fresh concrete properties after discharge. The pumping line is composed of tightly connected pipe segments to provide a system for transportation of the pressurized concrete. Standard material for a concrete pipe is steel, and it must be rated to sustain a pressure of 85 bars (1,232 psi) according to current Concrete Pump Manufacturers Association (CPMA) standard.

2.2 Concrete Rheology

2.2.1 Introduction

Rheology is the science dealing with the deformation and flow of matter. Understanding the rheology of concrete is a key to characterization of fresh concrete parameters when it is

transported and placed in the formwork. For many decades, only the slump was used to assess whether or not concrete can be pumped. However, many recent studies revealed that rheological properties of concrete in a liquid-like state control its behavior during the pumping process (Feys, Khayat, Perez-Schell, & Khatib, 2015; Kaplan, 2001; Khatib, 2013).

Concrete is a combination of several constituents in various states. Cement, supplementary cementitious materials (SCM), and coarse and fine aggregates are solid materials, whereas water and chemical admixtures are fluids. Therefore, fresh concrete can be considered a suspension of solid particles dispersed in a liquid medium. Solid materials have specific characteristics that make them clearly distinguishable from liquids because they retain a fixed volume and shape, they are not compressible, and they do not flow. These macro-properties are a reflection of the internal arrangement of particles that form solids (atoms, molecules, ions); these particles are tightly packed, often in a regular pattern (Roussel, 2012). When a small load is applied, most solid materials experience a deformation that is linearly proportional to the magnitude of stress and, upon removal of the load, the material reverts to its original shape. This deformation regime, referred to as elastic, is defined by Hooke's law, described in its general form by Equations 2.1 and 2.2.

$$\sigma = E\varepsilon \qquad \textbf{Equation 2.1}$$

$$\tau = G\gamma \qquad \textbf{Equation 2.2}$$

Where:

σ and τ are normal and shear stress, respectively,

ε and γ are corresponding deformations, and

E and G are material constants that define the rate of deformation (modulus of elasticity or Young's modulus, and shear modulus).

2.2.2 Steady-Shear Rheology Fundamentals

Unlike solids, fluids do not retain a fixed shape. Their deformation characteristics define them very well: they have zero shear modulus. In other words, they continually flow under an

applied shear stress. The elasticity theory defines stress as a force divided by the area over which the stress is applied, and the strain is relative deformation caused by the stress. For shear deformation, previous definitions can be mathematically expressed as:

$$\tau = \frac{P}{A} \qquad \textbf{Equation 2.3}$$

Where:

τ is shear stress,

P is applied force, and

A is the area over which the force is applied, and

$$\gamma = \frac{x}{d} \qquad \textbf{Equation 2.4}$$

Where:

x is element deformation of the element, and

d is element height, as illustrated in Figure 2.1a.

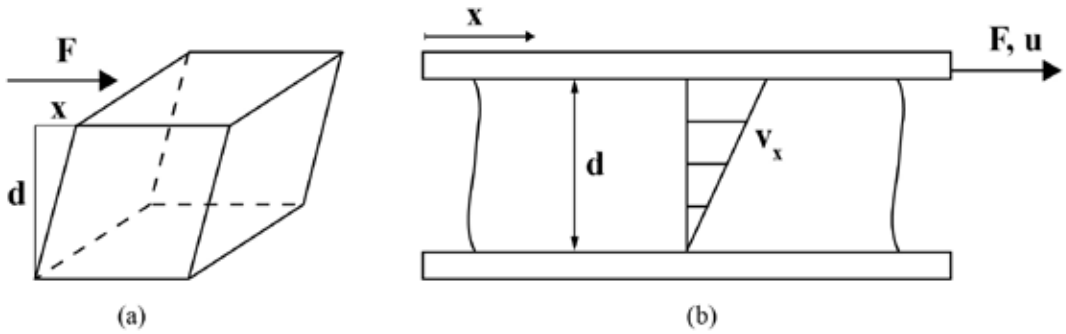

Figure 2.1: Steady-Shear Deformation
Adapted from Barnes, Hutton, and Walters (1989)

Consider two solid parallel plates with fluid filling the space between plates, as shown in Figure 2.1b. Assuming no slip between surfaces and force F action on the upper plate, the rate of shear strain with respect to time can be expressed as shown in Equation 2.5.

$$\dot{\gamma} = \frac{d\gamma}{dt} = \frac{dx}{hdt} = \frac{u}{h} \qquad \textbf{Equation 2.5}$$

The term $\dot{\gamma}$ is a basic deformation parameter of a fluid matter, referred to as rate of strain, velocity gradient, or shear rate.

2.2.3 Newtonian Fluids

Newtonian fluids and non-Newtonian fluids are two common classifications of fluids (Barnes, Hutton, & Walters, 1989; Bird, Armstrong, & Hassager, 1987). The relationship between shear stress τ and shear rate $\dot{\gamma}$ is linear for a Newtonian fluid. The slope in the equation that describes this relationship is viscosity, also designated as apparent or shear viscosity, and typically denoted κ. Because it represents resistance of a fluid to flow, viscosity can be visualized as internal friction between fluid layers. Shear behavior of a Newtonian fluid can be formulated by Equation 2.6.

$$\tau = \kappa\dot{\gamma} \qquad \textbf{Equation 2.6}$$

Constant shear rate is not the only requirement for a fluid to be characterized as Newtonian. Additional characteristics of Newtonian behavior are (Barnes et al., 1989):

1. Shear viscosity is constant and does not vary with shear rate.
2. The only stress generated in simple shear flow is shear stress τ. The two normal stresses are zero.
3. Viscosity is constant with respect to time of shearing, and stress in the liquid falls to zero immediately when shearing stops.
4. Viscosities measured in various types of deformation are always in proportion to one another. For example, the viscosity measured in a uniaxial extensional flow is always three times the value measured in simple shear flow.

2.2.4 Non-Newtonian Fluids

Fluids that do not meet one of the requirements for Newtonian fluids are considered to be non-Newtonian liquids. These types of fluids often fail to meet the first requirement of

Newtonian fluids that viscosity is independent of shear rate. Shear stress for non-Newtonian fluid is expressed by Equation 2.7 (J. E. Wallevik, 2006).

$$\tau = \kappa(\dot{\gamma})\dot{\gamma} \qquad \textbf{Equation 2.7}$$

Viscosity can increase with shear rate, causing liquids to demonstrate behavior consistent with shear-thickening materials, such as Silly Putty, a silicone polymer-based toy. However, when viscosity decreases with an increase in shear rate, the fluid experiences shear-thinning. Modern paints or ketchup are both shear-thinning fluids.

Many fluids, including fresh concrete, must overcome an initial value of stress in order to flow. For example, Bingham fluid does not flow until the yield stress is exceeded. Once the yield stress τ_0 is achieved, Bingham fluid behaves as a Newtonian fluid, with a constant value of plastic viscosity μ_p as expressed in Equation 2.8.

$$\tau = \tau_0 + \mu_p\dot{\gamma} \qquad \textbf{Equation 2.8}$$

2.2.5 Flow Characterization of Cement-Based Materials

The Bingham fluid model is the most commonly used rheological model for concrete. However, the Bingham model is not a universal equation and it might be quite problematic to implement in order to characterize the behavior of all existing types of concrete. For example, non-linear behavior was reported for fresh, self-compacting concrete (Heirman, Vandewalle, Van Gemert, & Wallevik, 2008). The Herschel-Bulkley model was successfully applied to describe the non-linear concrete flow regime (Barnes et al., 1989). This model is based on the general power-law model as shown in Equation 2.9:

$$\kappa = K\dot{\kappa}^{n-1} \qquad \textbf{Equation 2.9}$$

Where:

K is consistency (or flow coefficient), and

n is power law index.

As described by Equation 2.10, the Herschel-Bulkley equation is developed from the power-law model by adding the yield stress component:

$$\tau = \tau_0 + K\dot{\kappa}^n, \tau \geq \tau_0 \qquad \textbf{Equation 2.10}$$

When $n > 1$, the fluid experiences shear-thickening; when $n < 1$, shear-thinning behavior is observed; and when $n = 1$, the fluid behaves according to the Bingham model. Flow curves for these models are shown in Figure 2.2.

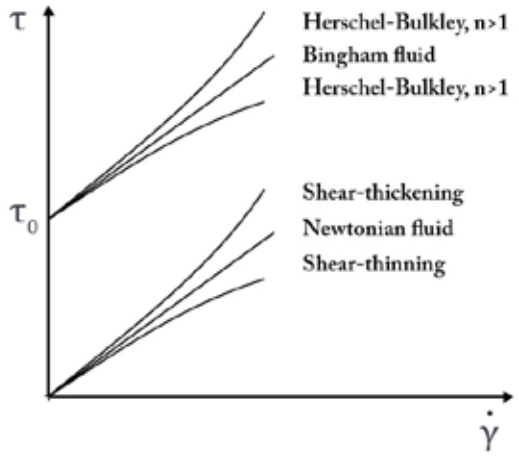

Figure 2.2: Fluid Rheological Models
Adapted from J. E. Wallevik (2006) and Khatib (2013)

Mathematical models characterizing rheological properties of fresh concrete are valid only if steady state flow is reached. These models assume that concrete properties do not change with time. However, a transient state always exists between two successive steady states (Roussel & Gram, 2014). For example, the initial seconds of concrete testing in a rheometer are a transient state between two boundary states: concrete at rest and concrete subjected to constant rotational velocity. There are three phenomena that are typical of the transient flow of fresh concrete: thixotropy, structural breakdown, and loss of workability (Khatib, 2013).

2.2.5.1 Thixotropy

Thixotropy is a decrease of apparent viscosity under shear stress, followed by gradual recovery when stress is removed. This is a reversible process (Harris, 1977). The thixotropy effect in fresh concrete is associated with the colloidal nature of the suspension. When concrete is left undisturbed, attracting forces acting on the particles result in a formation of connections between these particles. A coagulation effect can be observed, leading to increase in viscosity. If energy is supplied to the system, connections are broken, the suspension de-flocculates, and viscosity decreases. This time-dependent phenomena must be taken into account for rheological testing of fresh concrete because incorrect results could be obtained in absence of time-dependent consideration (O. H. Wallevik, Feys, Wallevik, & Khayat, 2015). Concrete must be “pre-sheared” before rheological or tribological tests to eliminate the thixotropy effect and achieve equilibrium.

2.2.5.2 Structural Breakdown

The term structural breakdown refers to a phenomenon in which connections formed by the hydration process of cement are broken. Within a few seconds of initial contact between cement and water, cement particles with charged surfaces can floculate and hydration products can begin to form, forming a bridging membrane. However, as soon as the cement paste is agitated, this bridging membrane breaks. This process is considered irreversible (J. E. Wallevik, 2009).

2.2.5.3 Loss of Workability

Loss of workability is a phenomenon characterized by reduction of fresh concrete workability over time due to formation of permanent connections in the concrete matrix. These connections are either chemical bonds created by hydration of cement grains, or they are connections formed by coagulation processes.

2.3 Rheometry and Concrete Rheometers

Rheometry is a discipline that focuses on experimental determination of mechanical properties of substances classified as fluids (Harris, 1977). For concrete, the primary objective of rheometry is to measure rheological parameters of fresh concrete, especially viscosity and yield stress. The relationship between general stress tensor σ_{ij} and strain rate tensor d_{ij} must be known in order to successfully characterize the general flow of fluid matter. However, obtaining this relationship is a complex problem. A primary objective of rheometry is to simplify this relationship. The simplification is achieved by subjecting the fluid to a simple shear which leaves only one component of the strain rate tensor non-zero. In addition, if the shear rate $\dot{\gamma}$ is constant, simple shear is homogeneous. Theoretically, ideal homogeneous simple shear can be achieved by inserting fluid matter between two plates of an infinite surface area and imposing different velocity on each plate. Various geometries have been used to simulate homogeneous shear on finite geometries (Roussel, 2012). The three main geometries are (1) parallel plates, (2) cone and plate, (3) and Couette (or coaxial) cylinder, as shown in Figure 2.3. All of these geometries have been used with concrete (Heirman et al., 2008; Ferraris & Martys, 2003). Unfortunately, the ideal geometrical configuration for concrete rheometer is unknown as several studies have revealed significant discrepancies among current devices (Ferraris & Martys, 2003; Khatib, 2013).

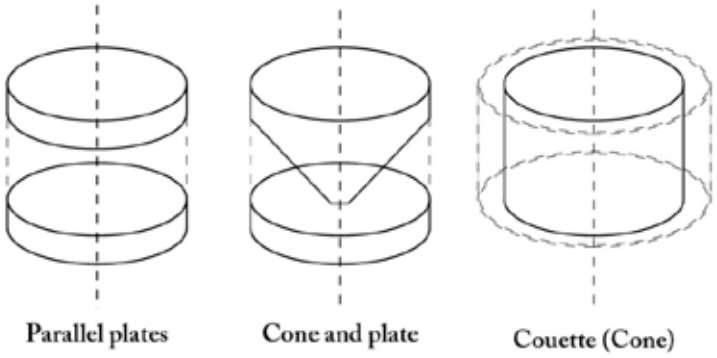

Figure 2.3: Rheological Geometries
Adapted from Roussel (2012)

Several models of concrete rheometers have been developed and are used to characterize rheological properties of fresh concrete. Unfortunately, the rheological parameters calculated

from the measured values from these rheometers produce different results when testing the same concrete mixture; however, rheometers can be correlated to each other (Ferraris & Martys, 2003). Nevertheless, the real rheological properties of concrete are still, to some extent, unknown. However, values of Bingham parameters obtained from these rheometers are still valuable and can be used as relative parameters when attempting to understand behavior of various types of concrete.

2.4 Concrete Flow in Pipes

Fresh concrete can be characterized as a suspension of rock and sand particles in cement paste, or as a suspension of rock particles in grout. Particle size, shape, and ratio of solid particles to overall volume of the suspension are critical parameters that determine fresh concrete behavior. Fresh concrete can be distinguished in two states: unsaturated concrete and saturated concrete (Roussel, 2012).

When concrete is unsaturated, the concentration of solid particles relative to the content of the liquid phase is such that the particles form a network through direct contact. The stress transfer is frictional. In this stress regime, stress transfer is dominated by inter-particle forces and their contact. Coulomb's Law of Friction (friction force is proportional to the friction coefficient and normal force acting on the surface) must be applied for unsaturated concrete, resulting in a nonlinear pressure loss in pipelines during pumping. Saturated concrete, however, contains enough paste to lubricate all solid particles so that the particles are not in direct contact. If solid particles do come into direct contact, the stress transfer mode is considered to be hydrodynamic. In the hydrodynamic stress regime, concrete flow is dependent on the shear rate in the interstitial liquid (mortar or grout) that fills the space between particles. Rheological properties of liquids in this mode (without normal force present during flow) are independent of applied pressure, thereby allowing application of rheology. For saturated concrete, pressure loss in the pipeline is linear (assuming no variations in pipe geometry, shape, or material). The comparison of pressure evolution over the pipe length for both saturated and unsaturated concrete is shown in Figure 2.4.

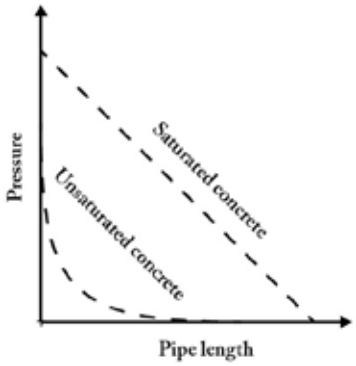

Figure 2.4: Pressure Development for Saturated and Unsaturated Concrete
Adapted from Browne and Bamforth (1977)

The saturation state of concrete is the fundamental parameter that determines whether or not concrete can be pumped. Browne and Bamforth (1977) carried out a pioneering study on pumpability and developed analytical formulas for saturated and unsaturated concrete in order to calculate the distance concrete can be pumped, taking into account various parameters such as mix properties, pipeline length, and pump pressure. The maximum pumpable distance X_{max} for saturated and unsaturated flow can be obtained from Equation 2.11 and 2.12, respectively.

$$X_{max} = \frac{DP_0}{4R} \qquad \textbf{Equation 2.11}$$

$$X_{max} = -\frac{DP_0}{4\mu k}\log\frac{A}{P_0\mu k + A} \qquad \textbf{Equation 2.12}$$

Where:
D is diameter of the pipe,
R flow resistance coefficient,
P_0 is pump pressure,
μ is concrete viscosity, and
A is adhesive stress.

An example calculation in their paper showed that concrete mix in saturated state can be pumped approximately 250 meters, while the same mix in unsaturated flow mode can be pumped only 1 meter. Unsaturated flow must be avoided in order for concrete to be pumpable.

2.4.1 Flow Zones

If saturated concrete is pumped through a pipeline, two or three zones of different properties and behavior can be observed, depending on the concrete type (Feys, De Schutter, & Verhoeven, 2013; Kaplan, de Larrard, & Sedran, 2005; Newman & Choo, 2003). A general model with three flow zones is presented in Figure 2.5. The inner zone, called the plug, is comprised of concrete that is not sheared during pumping because the shear stress did not exceed the value of yield stress. In the second zone, the value of shear stress is equal to or higher than the yield stress; therefore, concrete is sheared as it moves in this zone. Pumped material in the third zone is also sheared, but rheological properties of this zone, the lubrication layer, differ from sheared concrete in the second zone. A plug flow regime with two distinguished zones (lubrication layer and plug) is typical for conventional vibrated concrete (CVC) because CVC has a higher yield stress than self-consolidating concrete (SCC). Therefore, shear stress in the pipeline is not sufficient to overcome concrete yield stress and cause shearing of a portion of the concrete profile. In this flow regime, only the lubrication layer is sheared.

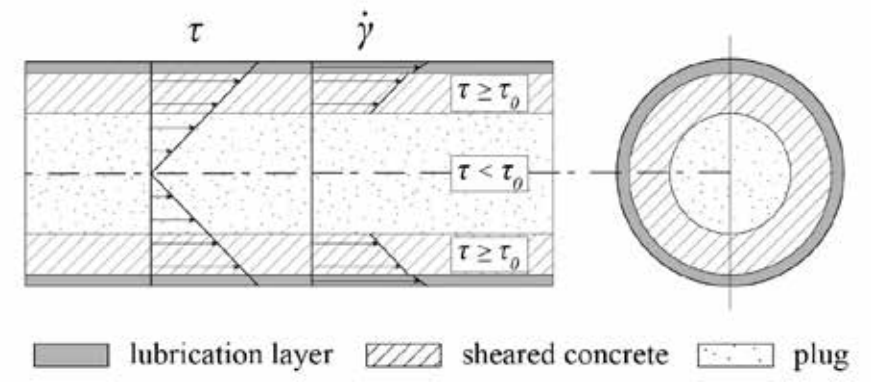

Figure 2.5: Flow Zones in a Pipe
Adapted from Khatib (2013)

2.4.2 Lubrication Layer

The zone adjacent to the pipe surface is called the lubrication layer, also referred to as slippage, slip, or boundary layer. Existence of the lubrication layer was first predicted in the 1960s (Choi, Roussel, Kim, & Kim, 2013). This zone reduces friction between the wall of the pipe and concrete and allows the concrete mass, or the plug, to be moved through the pipeline.

To date, the slip layer composition is not exactly known. It is assumed that it is comprised of cement paste, and possibly of fine aggregate particles, with thickness estimated to be between 1 and 5 mm (Browne & Bamforth, 1977; Choi et al., 2013; Jacobsen, Haugan, Hammer, & Kalogiannidis, 2009). Choi et al. (2013) reported that layer thickness is independent of flow rate, but that it is related to the mix design of pumped concrete and the pipe diameter.

Two mutually nonexclusive phenomena have been linked to the process of boundary layer formation. First, the suggestion has been made that large particles migrate towards the center of the pipeline due to a shear gradient in the pipeline (Jacobsen et al., 2009). In addition, due to shear stress distribution over the pipe cross section, water droplets and fine materials migrate in the opposite direction, i.e., towards the pipe wall (Khatib, 2013). Second, paste content around the pipe wall increases within a zone of thickness of *d/2*, where *d* is maximum aggregate size, as a result of a loose packing of coarse aggregate in close proximity to the pipe wall.

2.5 Flow Models

2.5.1 Energy Equilibrium

Concrete pumping must obey the law of energy conservation. For any fluid that flows in a pipe, this law is traditionally described by Bernoulli's equation, as expressed in Equation 2.13:

$$h_1 + \frac{v_1^2}{2g} + \frac{p_1}{\rho_1 g} = h_2 + \frac{v_2^2}{2g} + \frac{p_2}{\rho_2 g} \qquad \textbf{Equation 2.13}$$

Where:

$h_{1,2}$ is elevation above reference level,

$v_{1,2}$ is fluid velocity,

g is gravitational constant,

$p_{1,2}$ is pressure, and

$\rho_{1,2}$ is fluid density.

Bernoulli's equation can be extended to account for energy exchange in the pipe, yielding the steady-flow energy equation (Equation 2.14):

$$\left(h_1 + \frac{v_1^2}{2g} + \frac{p_1}{\rho_1 g}\right) = \left(h_2 + \frac{v_2^2}{2g} + \frac{p_2}{\rho_2 g}\right) + \Delta F - h_{pump} \qquad \textbf{Equation 2.14}$$

Where:

ΔF is the sum of minor and friction pressure losses, and

h_{pump} is the pump head.

Equation 2.14 states that pumping pressure must balance for pressure change, elevation change, kinetic energy (velocity), and pressure losses. Pressure losses can be categorized as (1) minor losses and (2) friction losses. Minor losses in pumping circuits, frequently associated with bends and elbows, are typically converted to pressure losses in an equivalent straight section. However, these approximations are non-consistent for various pumping applications; therefore, their applicability is questionable (Khatib, 2013).

2.5.2 Momentum Conservation

Other significant equations that describe concrete flow in pipes include the Hagen-Poiseuille and Buckingham-Reiner equations. However, the following requirements are necessary in order to apply these equations (Roussel, 2012): (1) fully developed, isothermal, and steady flow in the pipe; (2) one-dimensional flow (no radial or tangential flow component); (3) incompressible and homogeneous liquid; (4) no slippage at the wall; and (5) laminar flow condition. If these conditions are met, a conservation of momentum law must be valid between two points in a pipe section of a uniform radius *R* and length *L* (Khatib, 2013). The pressure loss over a pipeline segment is balanced by friction force acting on the pipe wall (Figure 2.6). Shear stress distribution over the pipe can be considered linear, with maximum value at the walls and zero value in the middle of the center of the pipe section.

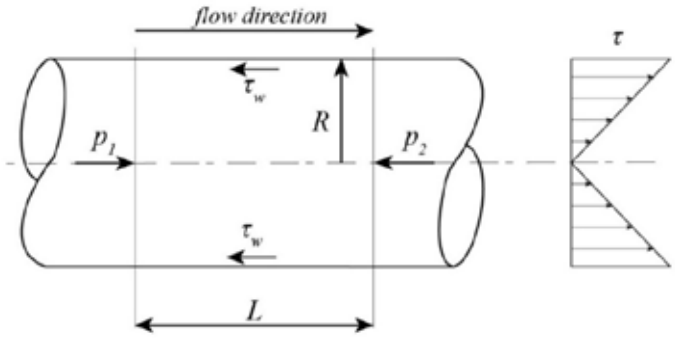

Figure 2.6: Force Analysis in Pipe Flow
Adapted from Khatib (2013)

These relationships are defined by Equation 2.15, or in an alternate form by Equation 2.16.

$$p_1\pi R^2 - p_2\pi R^2 - 2\pi R\tau_w L = 0 \qquad \textbf{Equation 2.15}$$

$$\tau_w = \frac{\Delta p}{L}\frac{R}{2} \qquad \textbf{Equation 2.16}$$

2.5.3 Kaplan's Model

Kaplan et al. (2005) utilized his experimental pumping circuit that was 486 feet (148 m) long to investigate conventional concrete behavior during pumping. His model was based on the observation that two diverse flows are present in a pipe when concrete is sheared after the yield stress τ_0 of concrete is reached: a slip flow Q_g and a shear flow Q_c. The model assumed that these flows are related to the total flow in the pump Q_{total} as follows:

$$Q_{total} = \begin{cases} Q_g, & \tau_i \leq \tau_0 \\ Q_g + Q_{c,} & \tau_i > \tau_0 \end{cases} \qquad \textbf{Equation 2.17}$$

Where:

τ_i is shear stress applied to concrete as a result of pumping.

Based on these assumptions, a model that relates flow rate and pressure was developed and split into two parts: before shear flow occurs and after shear flow occurs, as shown in Equation 2.18 and Equation 2.19, respectively.

$$P = \frac{2L}{R}\left(\frac{Q}{3600\pi R^2 k_r}\eta + \tau_0\right) \quad \textbf{Equation 2.18}$$

$$P = \frac{2L}{R}\left(v_g\eta + \tau_0\right) \quad \textbf{Equation 2.19}$$

Where:

P is pressure,

L is length of the pipe,

R is pipe radius,

Q is flow rate,

k_r is filling coefficient,

η is viscous constant (obtained from a tribometer),

τ_0 is concrete yield stress, and

v_g is slip rate, calculated according to Equation 2.20.

$$v_g = \frac{v_p R_p^2 - \frac{R^3}{4\mu}\tau_{0i} + \frac{R^3}{3\mu}\tau_0}{R^2 + \frac{R^3}{4\mu}\eta} \quad \textbf{Equation 2.20}$$

Where:

v_p is velocity of the pump piston,

R_p is piston radius,

τ_{0i} is interface yield stress (obtained from a tribometer), and

μ is concrete plastic viscosity.

The pressure-flow relationship based on Kaplan's model is shown in Figure 2.7.

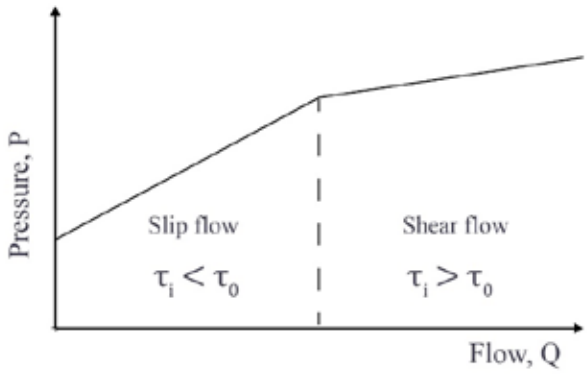

Figure 2.7: Kaplan's Model
Adapted from Kaplan et al. (2005)

Kaplan successfully validated his model by comparing pressure data obtained from a pumping experiment to job site measurements. Kaplan's research is groundbreaking because he demonstrated and proved, analytically and experimentally, that CVC is often not sheared during pumping but is slipped in the pipe because of the lubrication layer. His model and subsequent experimental data also showed that friction loss is not dependent on pumping pressure; all his rate/pressure curves showed a linear character, proving that pumping pressure is a function of slip rate. Additionally, Kaplan (2001) and Chapdelaine (2007) suggested that bends in the pumping circuit do not significantly increase pressure loss during pumping of CVC, which is contrary to practical pumping guidelines.

2.5.4 Khatib's Model

Kaplan's model was further expanded by Khatib (2013). As discussed in Section 2.4.1, a maximum of three zones of concrete can be distinguished in pumped concrete in the pipeline. Based on rheological properties of individual layers and the linear shear stress distribution, the shear rate can be derived for each zone. By integrating shear rate with respect to the radius, a velocity profile can be obtained. Subsequently, flow rate *Q* can be derived for each layer by integrating the velocity profile over the cross-sectional area of the pipe. Finally, the flow rate as a function of concrete and lubrication layer rheological properties and the pressure loss per unit length can be expressed as shown in Equation 2.21.

$$Q = \frac{\pi}{24R^4\Delta p^3\mu_c\mu_{ll}}(-12\mu_{ll}\Delta p^4R^7t_{ll} + 18\mu_{ll}\Delta p^4R^6t_{ll}^2 - 12\mu_{ll}\Delta p^4R^5t_{ll}^3 - 8\tau_{0c}R^7\mu_{ll}\Delta p^3 + 12\mu_cR^7\Delta p^4t_{ll} - 18\mu_cR^6\Delta p^4t_{ll}^2 + 12\mu_cR^5\Delta p^4t_{ll}^3 + 24\tau_{0c}R^6\mu_{ll}\Delta p^3t_{ll} - 24\tau_{0c}R^5\mu_{ll}\Delta p^3t_{ll}^2 + 8\tau_{0c}R^4\mu_{ll}\Delta p^3t_{ll}^3 - 24\mu_c\tau_{0l}R^6\Delta p^3t_{ll} + 24\mu_c\tau_{0l}R^5\Delta p^3t_{ll}^2 - 8\mu_c\tau_{0l}R^4\Delta p^3t_{ll}^3 + 16\tau_{0c}^4R^4\mu_{ll} + 3\mu_{ll}\Delta p^4R^8 + 3\mu_{ll}R^4\Delta p^4t_{ll}^4 - 3\mu_cR^4\Delta p^4t_{ll}^4)$$

Equation 2.21

Where:

Q is total flow rate across the pipe section,

R is radius of the pipe,

Δp is pressure loss per unit length of the pipe,

μ_c is plastic viscosity of concrete,

μ_{ll} is plastic viscosity of the lubrication layer,

τ_{0c} is yield stress of concrete,

τ_{ll} is yield stress of lubrication layer, and

t_{ll} is the thickness of the lubrication.

As the thickness of the lubrication layer is not known, this model can be used to perform useful numerical simulations based on various assumptions; however, it cannot be directly applied to estimate pumping pressure for job site applications.

Chapter 3: Methodology

3.1 Introduction

Three experimental studies were carried out as part of this project: a field testing campaign in the summer of 2015 as described in Chapter 4, a full-scale pumping experiment as described in Chapter 5, and a laboratory study as described in Chapter 6. Experimental methods and techniques utilized in all three studies were similar, therefore a full description of these methods is provided in this chapter.

3.2 Fresh Concrete Properties

Standard tests to evaluate properties of fresh concrete were adopted in all three experimental programs. The following fresh concrete properties were measured in accordance with respective ASTM standards:

- Slump (ASTM C143, 2012)
- Air void content (ASTM C231, 2010)
- Unit weight (ASTM C138, 2013)
- Temperature (ASTM C1064, 2004)

Additionally, two non-standard devices used to assess performance of fresh concrete were deployed for the purposes of this project: (1) the Super Air Meter (SAM), and (2) the ICAR (International Center for Aggregate Research) rheometer. The ICAR rheometer was modified so that both rheological and tribological measurement could be performed using a single device in both field and laboratory conditions. The newly developed tribometer was calibrated and a correction method for the bottom effect of the rotary cylinder was developed.

3.2.1 Super Air Meter

The Super Air Meter (SAM) is a newly developed device to characterize properties of the air void system of fresh concrete (Ley & Tabb, 2014). The device operates on a similar principle as the regular pressure air meter; however, the test itself consists of two sequences during which the concrete sample is pressurized in three consecutive steps up to a pressure of 45 psi. A resultant value that is reported by the device, the SAM number, is believed to be an indicator of

the air void distribution and bubble sizes in fresh concrete. The device manufacturer claims that a frost-durable concrete should have a SAM number smaller than 0.20. This device also reports the total air content of fresh concrete samples. This value is measured during the first test sequence using identical procedure to one described in ASTM C231.

The following procedure was used for testing concrete with the Super Air Meter:

1. Fill the bottom chamber of the device with fresh concrete following ASTM C231.
2. Pressure the upper chamber to 14.5 psi with petcocks on the lid open.
3. Close both petcocks, allow the pressure value to stabilize.
4. Press a lever on the lid to open the valve, hit the bottom chamber with a mallet several times, and take readings. In this step, the value of total air content is obtained.
5. Pressure the upper chamber to 30 psi, allow pressure to stabilize, press the lever on the lid to open the valve, hit the bottom chamber with a mallet several times and take readings.
6. Pressure the upper chamber to 45 psi, allow pressure to stabilize, press the lever on the lid to open the valve, hit the bottom chamber with a mallet several times, and take readings.
7. Release the pressure from the top chamber, and repeat Steps 2–7.

3.2.2 Rheological Measurements – ICAR Rheometer

The ICAR rheometer is a coaxial, portable field rheometer developed at the University of Texas at Austin (Koehler, Fowler, Ferraris, & Amziane, 2006). The device consists of five major components: (1) a container with vertical ribs to prevent concrete slippage; (2) a driver head equipped with an electric motor and torque meter; (3) a four-blade vane; (4) a frame to attach the driver head to the container; and (5) a laptop to control the test. All rheometer components are shown in Figure 3.1.

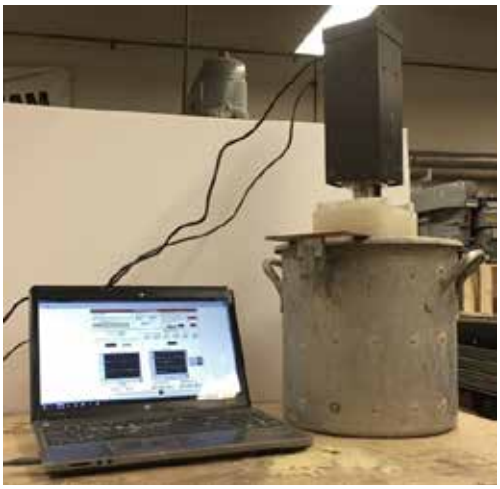

Figure 3.1: ICAR Rheometer

The ICAR rheometer uses a coaxial geometry: shear flow is induced by the vane revolving around its longitudinal axis while the container remains in still position during the test. Multiple container sizes are available for various maximum aggregate sizes. Static and dynamic tests can be performed using the ICAR rheometer. A static test is performed under a constant vane speed (0.025 rev/sec), and the increase in torque is recorded to calculate static yield stress. A dynamic test must be employed in order to measure Bingham parameters of fresh concrete (dynamic yield stress τ_0 and plastic viscosity μ_p). At the beginning of the dynamic test, the vane is rotated at a high speed (0.5 rev/sec) in order to pre-shear the concrete, reach the equilibrium state, and avoid thixotropic distortion of the measurement. After the initial "breakdown" stage, a set of decreasing vane velocities (the manufacturer recommends at least six steps) is imposed on the concrete sample, and corresponding values of torque for each step are recorded. The test procedure used in this study is outlined in Figure 3.2.

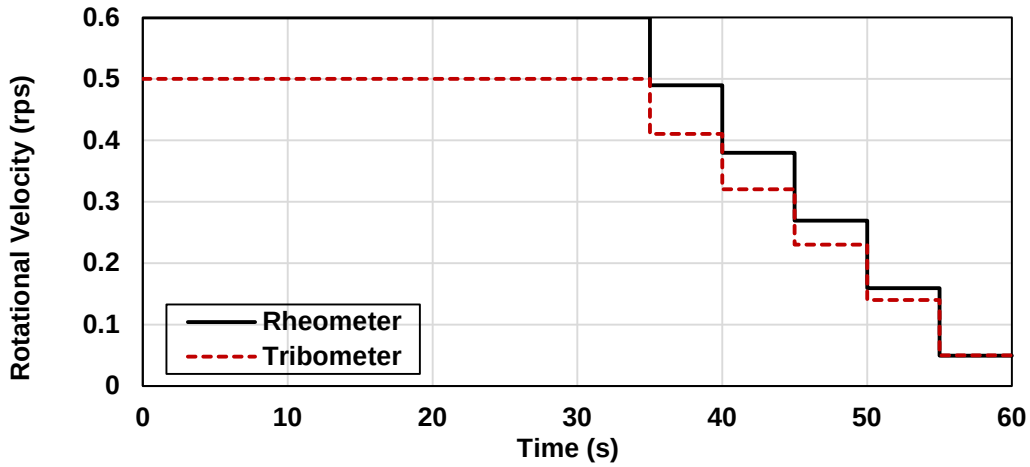

Figure 3.2: ICAR Rheometer and Tribometer Testing Procedures

The device is equipped with software that allows for an automated analysis of measured data. However, for purposes of this study, raw data recorded by the device (measured torque and corresponding rotational velocity) were further analyzed to account for the effect of plug flow. Plug flow in a rheometer can occur when sheared stress applied on a tested concrete sample is lower than the concrete yield stress, creating a condition when only a portion of the concrete is sheared (O. H. Wallevik et al., 2015).

The Reiner-Rivlin equation can be used to obtain yield stress τ_0 and plastic viscosity μ_p from recorded torque and rotational velocities (Feys, Wallevik, Yahia, Khayat, & Wallevik, 2013). Reiner-Rivlin equations for yield stress and plastic viscosity are shown in Equations 3.1 and 3.2, respectively.

$$\tau_0 = \frac{\frac{1}{R_i^2} - \frac{1}{R_o^2}}{4\pi h \, ln\left(\frac{R_i}{R_o}\right)} G \qquad \textbf{Equation 3.1}$$

$$\mu_p = \frac{\frac{1}{R_i^2} - \frac{1}{R_o^2}}{8\pi^2 h} H$$ **Equation 3.2**

Where:

R_i is radius of the cylinder (four-blade vane in case of the ICAR rheometer),

R_o is radius of the container,

h is height of the cylinder (vane), and

G and H are intercept and slope of the torque-rotational velocity curve, respectively.

In order to account for the plug flow condition, an iterative procedure must be carried out (O. H. Wallevik et al., 2015). First, one must determine the radius of the plug for each rotational velocity using Equation 3.3.

$$R_p = \sqrt{\frac{T}{2\pi\tau_0 h}}$$ **Equation 3.3**

Where:

R_p is plug radius.

Second, the shear rate at the inner cylinder can be computed using Equation 3.4.

$$\dot{\gamma}(R_i) = \frac{2}{R_i^2}\left(\frac{1}{R_i^2} - \frac{1}{R_s^2}\right)^{-1}\left[\omega + \frac{\tau_0}{\mu}\ln\left(\frac{R_s}{R_i}\right)\right] - \frac{\tau_0}{\mu}$$ **Equation 3.4**

Where:

$\dot{\gamma}$ is shear rate,

ω is angular velocity of the rheometer, and

$R_s = \min(R_o, R_p)$.

The plug radius as well as the shear rate depends on yield stress and plastic viscosity, which are unknown. Therefore, the iterative procedure with assumed initial values is necessary to obtain the real rheological parameters.

It is important to note that concrete rheological measurements are challenging due to the non-homogenous nature of fresh concrete. Several studies in the past revealed several inconsistencies in measurement of absolute values among various concrete rheometers; however, a correlation between rheometers was found (Ferraris & Martys, 2003; Khatib, 2013; O. H. Wallevik et al., 2015). Therefore, to some extent, the true rheological properties of concrete are still unknown; however, rheometers can be used as a relative comparative tool to assess behavior of different concretes.

3.2.3 Lubrication Layer Properties – ICAR-Based Tribometer

A concrete tribometer is a device based on a similar principle as a regular concentric cylinder rheometer. While concrete rheometers usually have roughened or ribbed surfaces, a tribometer typically consists of a concentric smooth-wall cylinder (inner cylinder) that is immersed in a cylindrical container (outer cylinder) filled with concrete during the test. The outer cylinder remains stationary as the inner cylinder rotates around its axis. The lubrication layer is formed on the wall of the inner cylinder, simulating the shear effect that is present in a pipeline during pumping. Similar to rheological measurements, torque and corresponding rotational velocities are recorded.

A concrete tribometer utilizing the ICAR rheometer was made for the purposes of this study. The design of the tribometer head was based on a tribometer developed at the Université de Sherbrooke (Feys, Khayat, Perez-Schell, & Khatib, 2014). The standard four-blade vane for rheological measurements was replaced by a stainless steel cylinder to perform tribological measurements. The cylinder had a conical-shaped bottom with diameter of 5 inches and height of 8 inches, with the conical part height of 2 inches. A comparison of the rheometer vane and the tribometer head is shown in Figure 3.3.

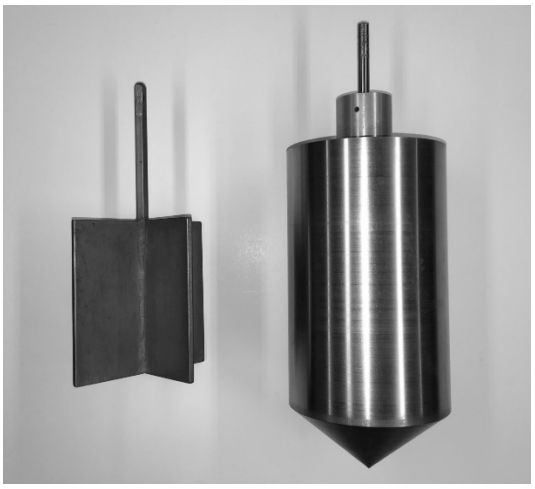

Figure 3.3: Rheometer Vane and Tribometer Head

The adopted experimental method follows a similar procedure to that used for rheological measurements. Concrete is pre-sheared for a prolonged amount of time to create the lubrication layer and to avoid any thixotropic behavior. Subsequently, various rotational velocities (with decreasing speeds) are imposed on the cylinder, holding each velocity level constant for a certain period of time while the resulting torque for each velocity is registered by the device. There are two different aspects of the test procedure that are different from the original rheometer practice: (1) concrete is pre-sheared for 30 seconds as opposed to 20 seconds in the case of rheological measurements in order to provide sufficient time to create the lubrication layer, and (2) the maximum rotational velocity allowed by the device (0.6 rps) is used (as opposed to velocity of 0.5 rps implemented for rheology). The rotational speed used in the procedure is outlined in Figure 3.2.

In order to determine properties of the lubrication layer, data were treated according to the procedure described in Feys et al. (2015). Three different flow conditions can be observed during the test based on the rheological properties of tested concrete: (1) only the lubrication layer is sheared, (2) both the lubrication layer and concrete are sheared, or (3) the lubrication layer is sheared and concrete is partially sheared. The shear stress τ and the strain rate $\dot{\gamma}$ evolution between the inner and outer cylinder as a function of distance between the inner and outer cylinder r were calculated according to Equation 3.5 and Equation 3.6, respectively.

$$\tau(r) = \frac{T}{2\pi h}\frac{1}{r^2}$$ **Equation 3.5**

$$\dot{\gamma}(r) = \frac{\frac{T}{2\pi h}\frac{1}{r^2} - \tau_0}{\mu_p}$$ **Equation 3.6**

Where:

T is registered torque,

h is height of the cylinder,

τ_0 is yield stress of concrete, and

μ_p is concrete plastic viscosity.

By integrating the strain rate over the radius, one can obtain the velocity gradient between the inner and outer cylinder. As the outer cylinder is stationary, the velocity at the outer cylinder is zero; hence, the velocity at the boundary between concrete and the lubrication layer can be obtained. Since the actual thickness of the lubrication layer is unknown, the rotational velocity of concrete N_i is calculated at the inner cylinder (and not at the lubrication layer-concrete boundary) according to Equation 3.7.

$$N_i = \frac{T}{8\pi^2 h\mu_p}\left(\frac{1}{R_i^2} - \frac{1}{R_o^2}\right) - \frac{\tau_0}{2\pi\mu_p}\ln\left(\frac{R_o}{R_i}\right)$$ **Equation 3.7**

Where:

T is measured torque,

h is height of the cylinder,

μ_p is plastic viscosity of concrete,

τ_0 is yield stress of concrete,

R_i is the inner cylinder radius, and

R_o is the outer cylinder (container) radius.

The rotational velocity N_i is a rotational velocity that corresponds to a rotational velocity that would produce the same amount of torque in a concentric cylinder rheometer, without formation of the lubrication layer (i.e., without a slip).

To determine the flow regime for a particular rotational speed, one must calculate the plug R_p using Equation 3.3. When only the lubrication layer is sheared ($R_p < R_i$), N_{ii} will be zero as concrete does not flow at all. In case of a partially-sheared concrete sample ($R_i < R_p < R_o$), the radius of the outer cylinder (container) R_o must be replaced by the plug radius R_p in Equation 3.7. Finally, when both the lubrication layer and concrete are sheared ($R_p > R_o$), Equation 3.7 shall be used with no modification.

To obtain lubrication layer properties, a value of the velocity difference that is facilitated by the lubrication layer, N_{LL}, should be calculated according to Equation 3.8.

$$N_{LL} = N - N_i \qquad \textbf{Equation 3.8}$$

Where:

N is imposed rotational velocity by the device, and

N_i is calculated according to Equation 3.7.

Finally, the linear velocity-shear stress relationship ($\tau - V$ curve) can be obtained for the lubrication layer. From this relationship, the viscous constant η_{LL} and yield stress of the lubrication layer $\tau_{0,LL}$ can be determined according to Equation 3.9.

$$\tau_{LL} = \tau_{0,LL} + \eta_{LL} V \qquad \textbf{Equation 3.9}$$

Where:

τ_{LL} is shear stress calculated using Equation 3.10, and

V is the linear velocity calculated according to Equation 3.11.

$$\tau_{LL} = \frac{T}{2\pi R_i^2 h} \qquad \textbf{Equation 3.10}$$

$$V = 2\pi R_i N_{LL}$$ **Equation 3.11**

Where:

T is the recorded value of torque for a particular imposed rotational velocity,

R_i^2 is radius of the inner cylinder,

h is the height of the inner cylinder,

R_i is radius of the inner cylinder, and

N_{LL} is calculated according to Equation 3.8.

3.3 Air Void System Characterization

An automated method of hardened air void analysis developed at Kansas State University was utilized to characterize the properties of concrete air void system. This method is based on an image analysis approach originally developed by Peterson (2008) and is described in detail in Riding, Esmaeily, and Vosahlik (2015).

Chapter 4: Field Testing Campaign

4.1 Introduction

A field testing campaign was carried out in the summer of 2015 to evaluate the effect of pumping on placed concrete. Six bridge-deck projects located in Eastern Kansas were selected in cooperation with KDOT to be part of this investigation. Each of the selected job sites was visited by a KSU research team at the day of the deck placement, and fresh concrete properties were measured before and after pumping in order to quantify the effect of pumping on concrete in field conditions. Additionally, samples for hardened air void analysis were made so that the influence of pumping on quality of the air void system could be evaluated.

4.2 Experimental Methods

4.2.1 Project Sites

All visited job sites were selected after consultation with KDOT. Five sites selected to be part of this study were located in Lawrence, KS, and were part of the K-10 South Lawrence Trafficway (SLT) project. One additional site located on I-70 near Kansas City, KS, was also part of the field investigation. An overview of the investigated project sites is shown in Table 4.1.

Table 4.1: Field Testing Campaign Sites

KSU Site ID	Project	KDOT Project #	Bridge	Mix Design
K-10 Haskell	SLT	10-23 K-8392-04	Bridge 10-23-10.71 (169) (mainline WB K-10 over Haskell Ave)	1PL1501A
I-70 Kaw	I-70	7070-105 KA-3865-01	Bridge No. 70-105-14.37 (096) WB	1PMC082B
K-10 Naismith #1	SLT	10-23 K-8392-04	Bridge 10-23-9.56 (164) (mainline K-10 over Naismith Creek WB)	1PL1501A
K-10 East	SLT	10-23 K-8392-04	Bridge 10-23-13.66 (184) (Ramp EB23-EB10 over K10)	1PL1501A
K-10 Louisiana	SLT	10-23 K-8392-04	Bridge 10-23-8.97 (163) (Louisiana St over K-10)	1PL1505A
K-10 Naismith #2	SLT	10-23 K-8392-04	Bridge 10-23-9.57 (165) (mainline K-10 over Naismith Creek EB)	1PL1505A

4.2.2 Concrete Sampling, Testing, and Mixture Designs

At each visited site, concrete was sampled before and after pumping. Concrete before pumping was sampled directly as discharged from the truck whereas concrete after pumping was sampled from the bridge deck. After the concrete was sampled from the truck, the team waited until the concrete ready-mix truck was halfway through discharging the concrete load to the pump truck until the concrete was sampled. The concrete was sampled from the bridge deck and not from the end of the hose to ensure that the concrete was representative of in-place concrete.

Obtained samples of concrete, both before and after pumping, were used to quantify concrete fresh properties (slump, air content, unit weight, temperature, and rheological and tribological properties), as described in Section 3.2. Mix designs of tested concretes are shown in Table 4.2 and Table 4.3. As admixture dosages varied on the SLT project, they are shown separately in Table 4.3. Samples were also made for hardened air void testing.

Table 4.2: SLT Mix Proportions, Bridges 169, 164, and 184 – KDOT CMS#1PL1501A

Component	Product/Type	Producer	Weight (lbs/cy)
Cement	Type I/II	Buzzi Unicem	423
Slag	N/A	Holcim	141
Coarse Aggregate	SCA-3 Limestone	APAC KS	1816
Fine Aggregate	FA-A Natural Sand	Penny's Concrete	1211
Water	City Water – Lawrence		231
Chemical Admixtures			**Dosage (oz/cy)**
Air-Entraining Agent			4.0
High Range Water Reducer			39.0
Water Reducer and Set Retarder			14.1
w/cm			0.41

Table 4.3: SLT Admixture Dosage, Bridges 169, 164, and 184 – KDOT CMS#1PL1501A

Bridge		169	164	184	163	163	165
Date		6/1/2015	7/14/2015	7/28/2015	8/12/2015	8/12/2015	8/13/2015
Time		N/A	N/A	N/A	5:30–7:30 AM	After 7:30 AM	N/A
Admixture	**Product**	**Dosage (oz/cy)**					
AEA	WR Grace Daravair 1400	8.5	14	12.5	10	9.7	10.3
WR	WR Grace ADVA 140	50	39	39	39	43	39
Retarder	WR Grace Recover	14.1	0	14.1	14.1	14.1	0

Table 4.4: I-70 over Kaw Drive – KDOT CMS Design #1PMC082

Component	**Product/Type Specification**	**Source**	**Producer**	**Weight (lbs/cy)**
Cement	Type I/II		Ash Grove	405
Fly Ash	Class F – Durapoz F		Ash Grove	105
Coarse Aggregate	SCA-4 Limestone	Stamper Quarry	Hunt Martin	1718
Fine Aggregate (lbs)	FA-A Sand	Plant #11	Holiday Sand	1389
Water (lbs)	City Water – Kansas City, KS			231
Chemical Admixtures				**Dosage (oz/cy)**
Air-Entraining Agent		Euclid AEA 92		3.8
High Range Water Reducer		Euclid WR-91		38.0
Water Reducer and Set Retarder		Eucon Retarder 100/Euclid Plastol		0
w/cm				0.43

4.3 Results and Discussion

Complete results of the field testing campaign are presented in Appendix A.

Changes in slump due are pumping is shown in Figure 4.1. No particular trend over all sites visited was observed between the slump value before and after pumping. Out of the total of 13 investigated concretes before and after pumping, five mixes experienced an increase in the slump after pumping, whereas the slump decreased in eight cases after pumping. The greatest

recorded decrease in the slump value was 2.75 inches, and the maximum slump increase after pumping was 1.5 inches.

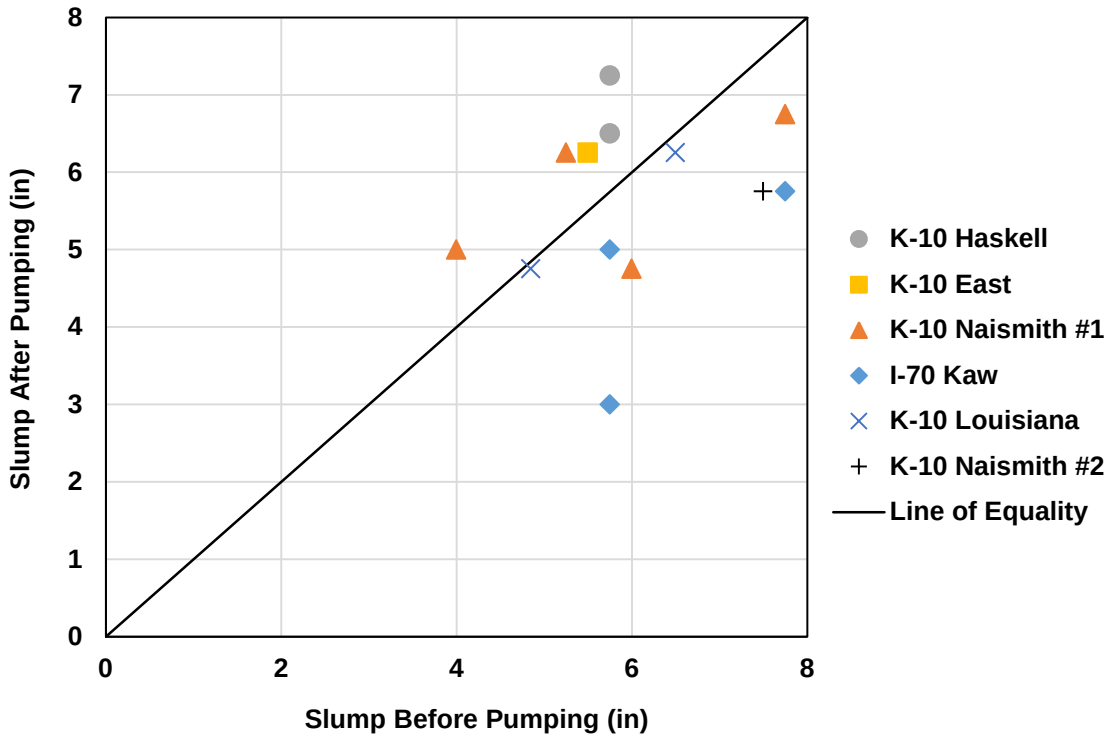

Figure 4.1: Slump Before and After Pumping – Field Testing

Evolution of the fresh concrete air content is shown in Figure 4.2. In all but two cases (11 out 13), an increase in the total air void content was observed after pumping. Maximum recorded rise was 3.6% and the smallest recorded increase was 0.8%. The only concrete to show a decrease in air content was that measured at the I-70 over Kaw Drive bridge project. The mix design utilized on this project used a different air-entraining agent (Euclid AEA 92S) than the AEA that was used in other concretes (WR Grace Daravair 1400) investigated during this field testing campaign. Additionally, bridge decks on the SLT project generally had a larger thickness than the I-70 deck, which was 8.5 inches thick. Considering the hypothesis that a re-mixing phenomenon occurs after concrete is discharged from the pump, allowing more air to be entrapped and entrained in the mix, one would expect a more significant increase of air content when concrete is pumped into a deeper formwork (SLT project) and a smaller increase or even

decrease in the air volume when concrete is pumped into a shallow formwork (I-70 project). Findings of this test campaign correspond with this hypothesis.

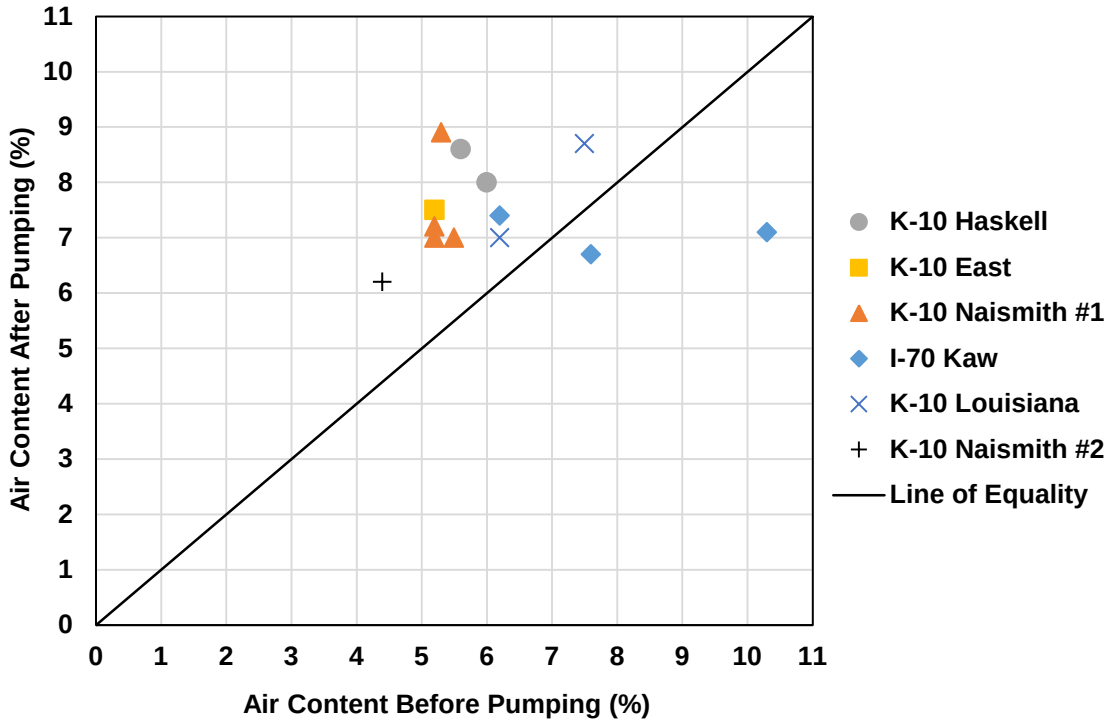

Figure 4.2: Fresh Concrete Air Content Before and After Pumping – Field Testing

Changes in the SAM number before and after pumping are presented in Figure 4.3. None of the tested concretes had a SAM number value smaller than 0.20 both before and after pumping, which is the manufacturer's recommended value in order to achieve freeze-thaw durability. Four mixes tested before pumping and two mixes tested after pumping had a SAM number less than 0.20. Results of the SAM testing suggest that the air void system size and distribution can significantly change due to pumping. Approximately half of the tested concrete mixtures after pumping exhibited increase in the SAM number. This suggests that the air void system of concrete that was pumped will be composed of larger air bubbles than the air void system of concrete before pumping. However, it is unknown whether the Super Air Meter test is applicable to pumped concrete, as this test utilizes over-pressurization to calculate the SAM number. The exact principle and mechanism of the SAM test is not known at the time; however,

the developer of the test claims that an increased pressure applied to fresh concrete causes small air bubbles to disappear from the mix (Ley, 2015). If this hypothesis is correct, a similar behavior would have to be observed during pumping when concrete is exposed to significantly higher pressures than 45 psi, which is the maximum pressure utilized in the SAM. Hence, the applicability of the SAM test on pumped concrete needs to be validated as concrete tested in the SAM already went through at least one cycle of over-pressurization.

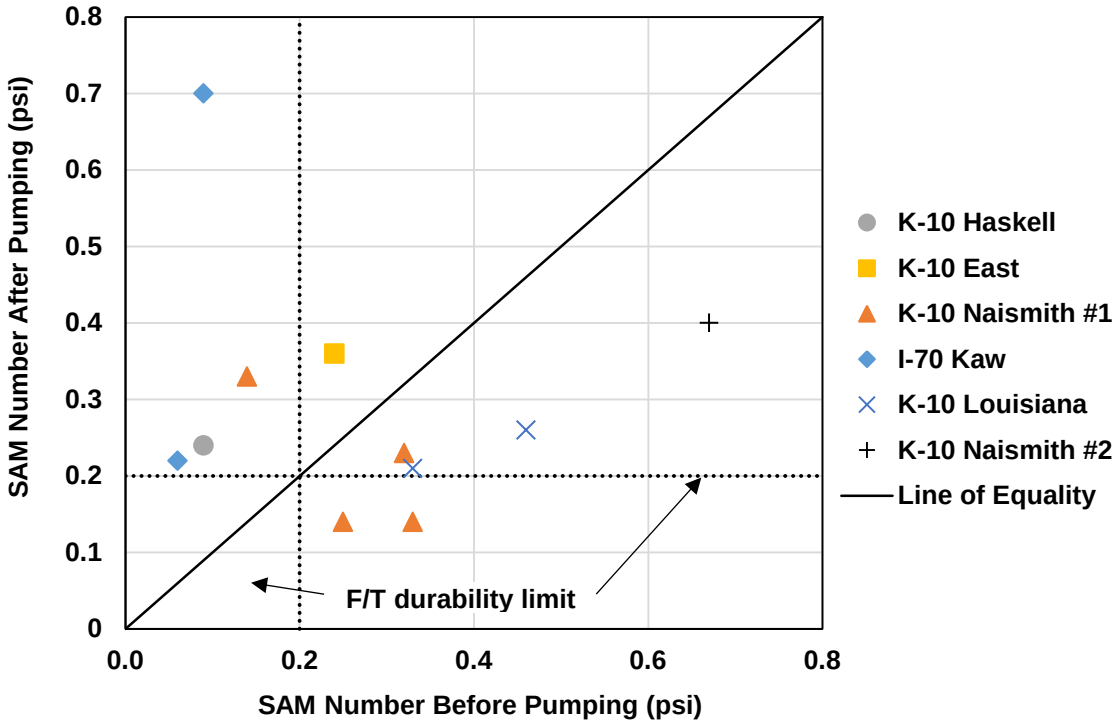

Figure 4.3: SAM Number Before and After Pumping – Field Testing

Hardened air void content and spacing factor before and after pumping are shown in Figure 4.4 and Figure 4.5, respectively. The total air void content increased in all cases but one after pumping and the results of hardened air void analysis were in a good agreement with fresh air content. Spacing factor increased after pumping in four out of 10 instances. It is notable that five mixtures had initial spacing factor greater than 0.008 inches, which is the recommended maximum value. However, after pumping, spacing factor decreased below the limit value. Similarly to the increase in the total air void content, this can be attributed to the effect of mixing

action when concrete is discharged from the pipeline. Additionally, all tested samples after pumping had values lower than 0.008 inches, therefore meeting requirements for freeze-thaw durability. This observation supports the proposed hypothesis that the Super Air Meter test is not applicable to pumped concrete.

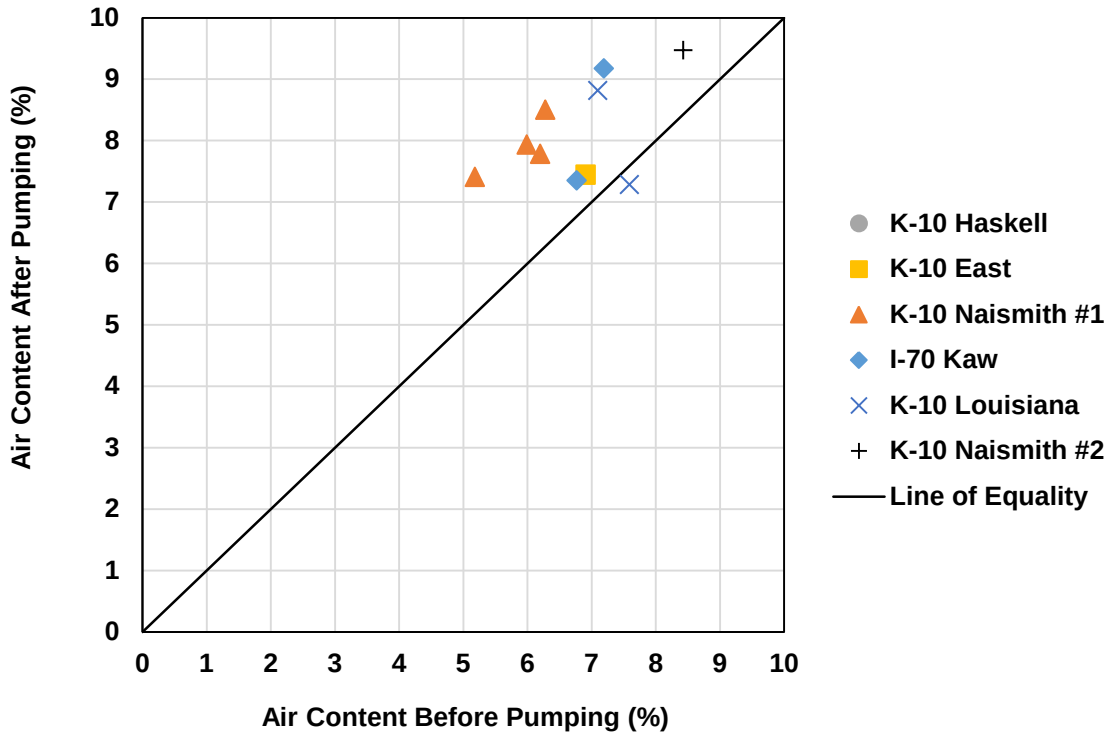

Figure 4.4: Hardened Air Void Content Before and After Pumping – Field Testing

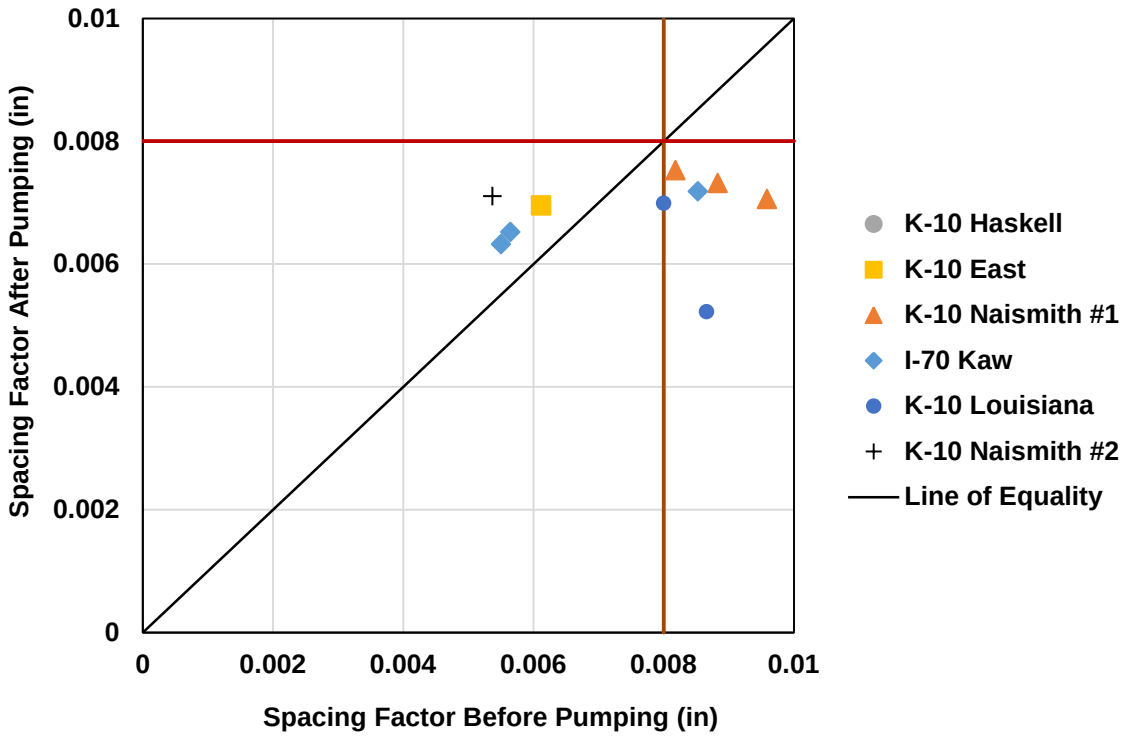

Figure 4.5: Spacing Factor Before and After Pumping – Field Testing

Figure 4.6, Figure 4.7, and Figure 4.8 show yield stress, plastic viscosity, and viscous constant, respectively, before and after pumping. No particular trend was observed in terms of a property change, be it yield stress, plastic viscosity, or viscous constant, due to pumping. The value of yield stress remained the same or decreased for all but two mixes, whereas the plastic viscosity and viscous constant decreased in approximately half of the cases. The precision and accuracy of conducted rheological and tribological testing was somewhat limited in the field conditions. As two sets of concretes (before and after pumping) had to be tested at the same time, concrete after pumping was generally tested 10 to 15 minutes after the test on concrete before pumping was conducted. This could have possibly resulted in slightly changed rheological and tribological properties of pumped concrete due to the stiffening effect.

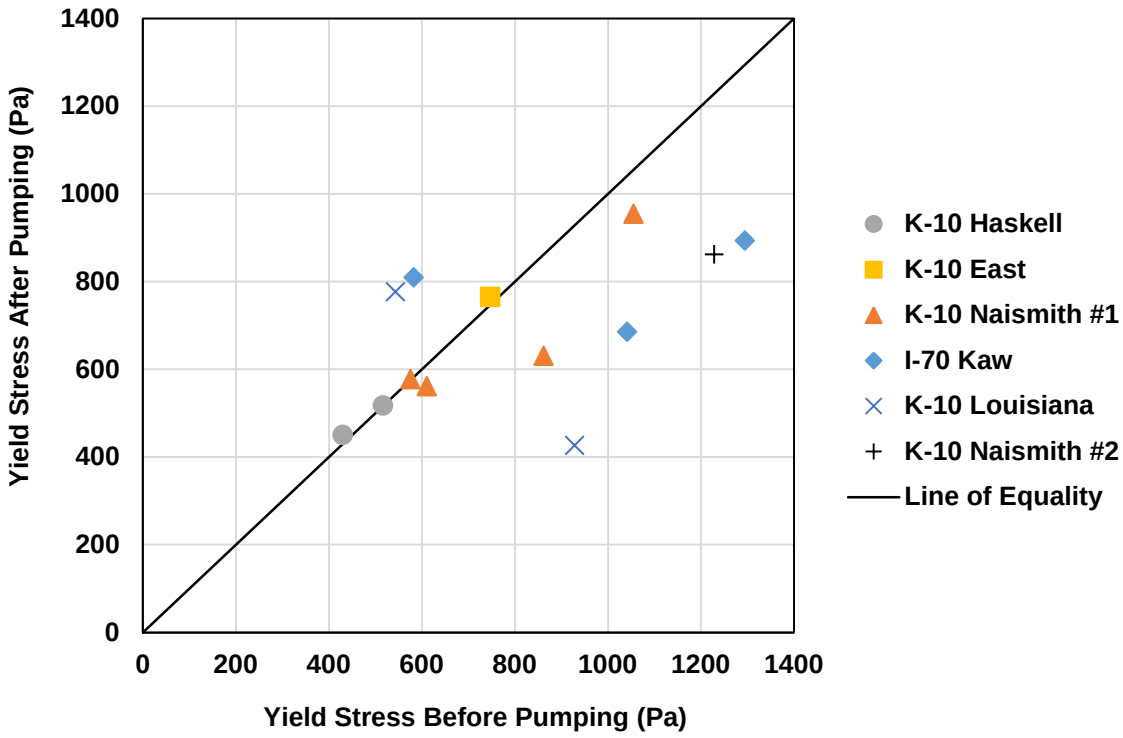

Figure 4.6: Yield Stress Before and After Pumping – Field Testing

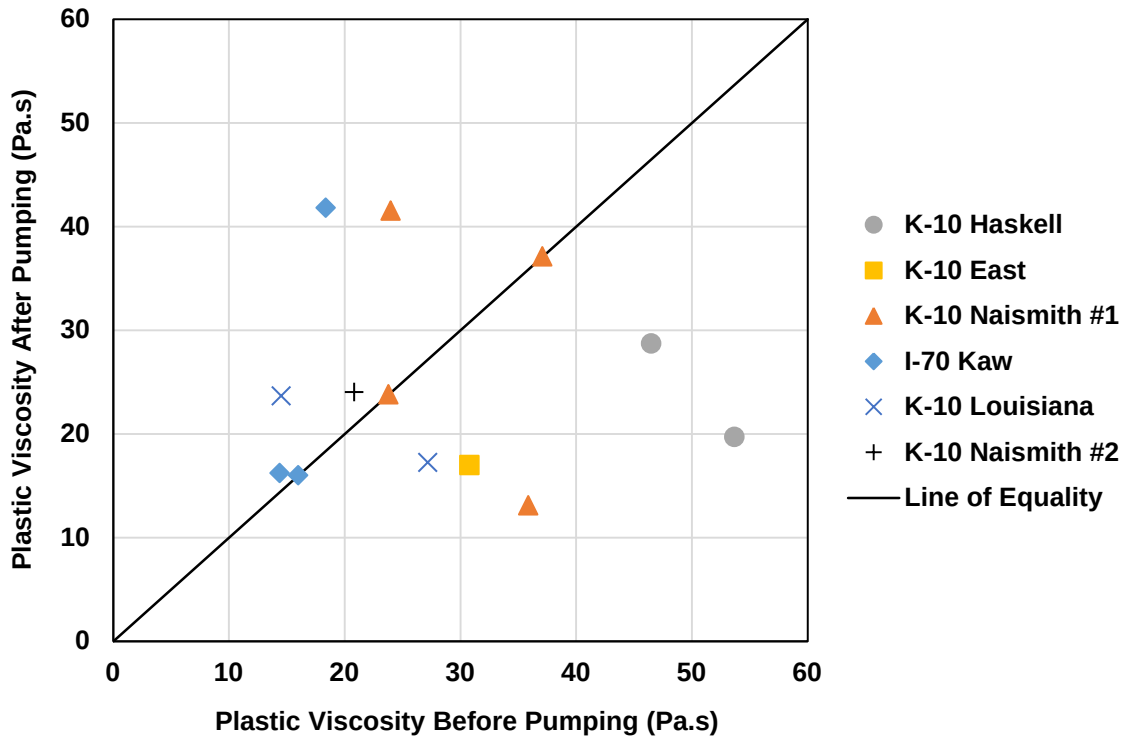

Figure 4.7: Plastic Viscosity Before and After Pumping – Field Testing

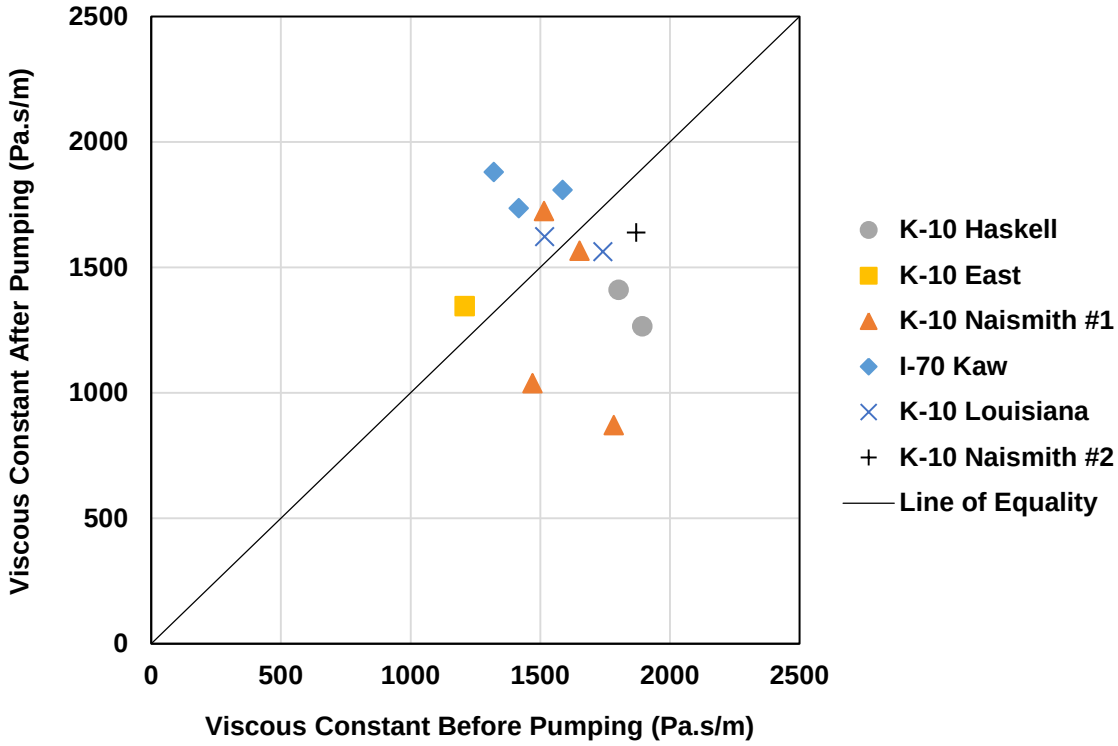

Figure 4.8: Viscous Constant Before and After Pumping – Field Testing

4.4 Summary and Recommendations

Six KDOT field sites were visited in the summer of 2015 to investigate the effect of pumping on concrete properties. At each site, concrete was sampled directly from the ready-mix truck and simultaneously after leaving the pumping line.

No direct relationship between pumping and workability (i.e., slump, plastic viscosity, and yield stress) was observed. In eight out of 13 cases, slump decreased after pumping, which is in agreement with results obtained by other researchers (Ghafoori, Diawara, Nyknahad, Barfield, & Islam, 2012; Yazdani, Bergin, & Majtaba, 2000). Therefore, it is recommended to continue with the practice of sampling and testing concrete slump at the final point of placement in order to ensure adequate workability of concrete for trouble-free placement (KDOT, 2015). It is also advised to design specific mixtures that are supposed to be pumped close the upper limit of slump as it is reasonable to expect slump loss after pumping. Additionally, it is recommended to require a reasonable aggregate moisture control plan, as it has been found that mixtures batched

with dry coarse aggregate having high absorption capacity (or with lightweight aggregate) can experience significant slump decrease after pumping due to excessive water intake under elevated pumping pressure (Yonezawa et al., 1988).

The field study has shown that the air void system can be significantly affected by pumping. In the vast majority of cases, total air void content increased after pumping. Therefore, it is encouraged to continue the practice of sampling concrete at the point of placement. When sampling concrete after pumping, it is advised to avoid the common practice of collecting the fresh concrete directly into a sampling container (i.e., bucket or wheelbarrow). The mechanism of air void change after pumping is directly related to the impact and mixing action of discharged concrete; therefore, a non-representative sample could be obtained by directly filling the sampling container. The spacing factor after pumping tended to decrease, supporting the assumption that the additional mixing action of discharged concrete can help stabilize additional air voids in the placed concrete. This research showed that not only the total air void system, but also air void size distribution can be altered by pumping; therefore, it is advised to require hardened air void analysis for projects where a high-quality air void system is central to the long-term durability of the structure.

Results obtained using the Super Air Meter were not consistent with hardened air void analysis data. The authors of this study raised concern about applicability of the SAM device on pumped concrete. Therefore, we suggest that a further investigation is carried out to examine whether the Super Air Meter can be reliably used for pumped concrete.

Chapter 5: Full-Scale Controlled Pumping Experiment

5.1 Introduction

A full-scale, controlled pumping experiment was conducted in November 2015 at the Fordyce Concrete Co. plant in Kansas City, KS, in cooperation with ACI Concrete Placement. The goal of this testing was to collect more detailed data on concrete pumping performance in a controlled environment. Three mix designs, two concrete pump boom arrangements, and various concrete flow rates were investigated in this experiment. In addition to testing concrete before and after pumping, the flow rate was measured and the pumping circuit was instrumented with strain gauges calibrated to pressure in order to quantify actual pumping pressures.

5.2 Experimental Program

5.2.1 Test Setup

The general overview of the test setup is shown in Figure 5.1. The experiment was conducted at the property of Fordyce Concrete Co. at Central Ave in Kansas City, KS. A Schwing concrete boom pump (Schwing 2023-5 S 46 SX) operated by ACI Concrete Placement was used throughout the experiment. The length of the pump boom was 151 feet (46 meters) and the volume of pump piston was 0.11 cubic yards.

Figure 5.1: Full-Scale Pumping Experiment Setup

The boom orientation was switched between the "A" configuration and the "flat" configuration during the test, as shown in Figure 5.2. These two configurations represent the most common situations that occur in the field. The A configuration can be typically seen on projects where concrete needs to be pumped horizontally, such as a bridge deck placement with the concrete pump located underneath the bridge. The flat configuration is typical when the pump is stationed at the same level as the structure.

(a) (b)

Figure 5.2: Boom Configuration: (a) A Configuration, (b) Flat Configuration

5.2.2 Concrete Sampling, Testing, and Mix Designs

A total of 11 pumping rounds were conducted during the experiment, varying the pump speed and boom configuration. Three different concrete mixtures were donated by the Fordyce Concrete Co. for this project. All three mixes had w/cm of 0.43 and were based on existing mix designs routinely used on KDOT projects. Mix proportions are shown in Table 5.1.

Table 5.1: Mix Proportions – Pumping Experiment

Component	Specification	Producer	Mix A	Mix B	Mix C
Cement (lbs)	Type I/II	Ash Grove	510	510	408
Fly Ash (lbs)	Durapoz (Class F)	Ash Grove	0	0	102
Coarse Aggregate (lbs)	SCA-4 Limestone	Hunt Martin Stamper	1570	1886	1875
Fine Aggregate (lbs)	FAA (MA-3)	Holliday Sand Plant #3	1570	1257	1250
Water (lbs)	City Water		219*	219	219
w/cm			0.43*	0.43	0.43

*1.25 gallons per cubic yard of water added in the truck (w/cm increased to 0.45)

Mix A was not initially pumpable; therefore, it was decided to add an additional 1.25 gallons of water per cubic yard of concrete to the mix. After the water addition, the mix was successfully pumped.

Concrete was delivered from the adjacent ready-mix plant in three trucks. The total volume of concrete made for Mixtures A, B and C was 8, 4, and 8 cubic yards, respectively. Concrete marked as “before pumping” was sampled directly from the mixing truck. For Mix A, sampling was done before the first pumping cycle, after three pumping cycles, and after the last pumping cycle. For Mixes B and C, concrete was sampled before the first pumping cycle and after the last cycle.

During each pumping cycle, approximately 1.1 cubic yards of concrete (equivalent to 10 strokes of the pump) were pumped in order to replace previously pumped concrete with new material and to ensure that newly pumped concrete was sampled. Concrete flow rate was determined by measuring the time required for five strokes of the pump. Using the volume of each piston, the actual flow rate was computed according to Equation 5.1.

$$Q = \frac{0.25\pi D_p^2 L_p}{5t}$$ **Equation 5.1**

Where:

Q is flow rate,

D_p is piston diameter,

L_p is length of the piston, and

t is time required for five stokes of the pump.

The pump was fully folded and cleaned with water after each truck was emptied in order to prevent concretes with different properties from mixing in the pump system. Each concrete sample (both before and after pumping) underwent a series of tests to determine its fresh properties, as discussed in Section 3.2. Additionally, hardened air void specimens were made and later analyzed using the methods described in Section 3.3.

5.2.3 Pressure Monitoring

In order to monitor hydraulic pressures in the pipeline during the pumping operation, the pumping circuit was instrumented with strain gauges. Three locations along the pipeline were selected: (1) at the end of the deck pipe (Gauge A); (2) second pipe segment of the boom section 2 (Gauge B); and (3) first pipe segment of the boom section 3 (Gauge C). Gauges A, B, and C were located 15, 41.25, and 80.5 feet from the pump hopper, respectively. Gauge positioning is shown in Figure 5.3.

Figure 5.3: Pipe Strain Gauge Locations

Vishay Micro-Measurements CEA-06-125UW-350 electric resistance strain gauges (gauge resistance 350 ohms) were mounted on the pipe surface perpendicular to the pipe longitudinal axis to measure hoop stresses generated by pressure inside the pipe. The M-Bond AE-10 system was used to mount gages on pipes. Gauges were mounted on chemically cleaned surfaces and cured for 12 hours at a curing temperature of 125 °F. Finally, gauges were covered with Micro-Measurements M-Coat W-1 protective coating. An example of a fully mounted and wired strain gauge is shown in Figure 5.4.

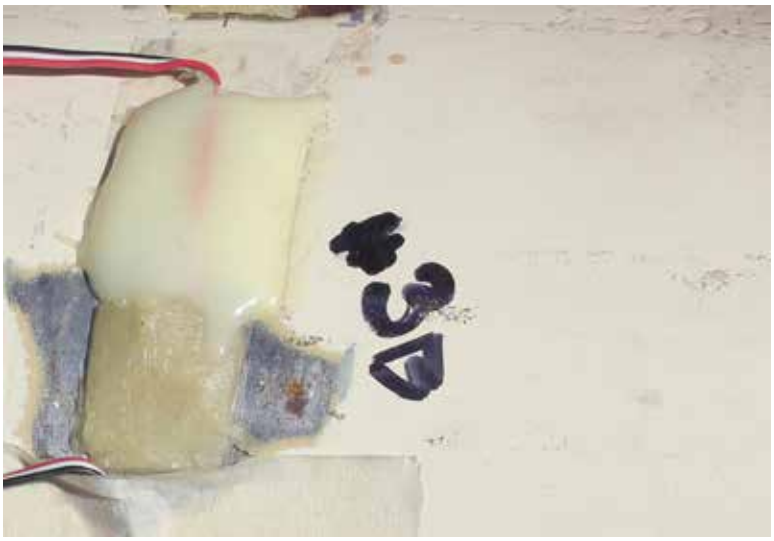

Figure 5.4: Mounted Strain Gauge

Campbell Scientific CR800 and Accsense VersaLog Model BR data loggers were used to record data provided by strain gauges. A CR800 logger was collecting readings from Gauge A and VersaLog data loggers were used to collect data from Gauges B and C. Both devices operated at a sampling rate of 30 Hz (30 readings per second). In order to complete the Wheatstone bridge required to detect resistance changes in strain gauges, Omega BCM-1 bridge completion modules were used. Figure 5.5 shows the data collection systems used. Two Anker Astro E7 batteries were used for each VersaLog data logger to provide an external power source required to achieve the sampling rate of 30 Hz.

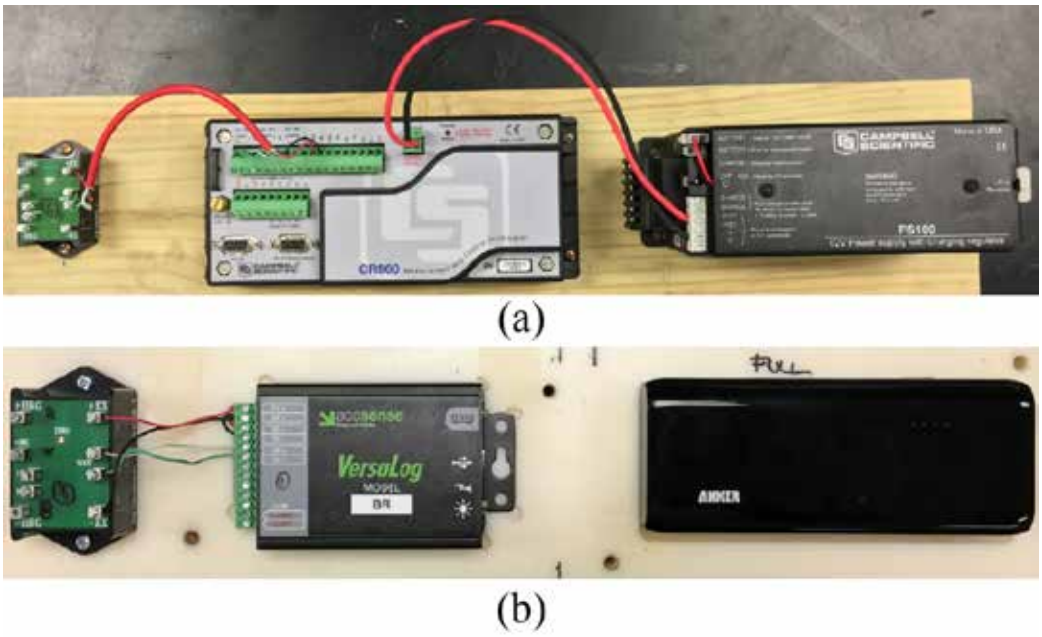

Figure 5.5: (a) Campbell Scientific CR800 System, (b) VersaLog System with Anker Battery

In addition to strain gauges, two pipes were instrumented with Type T thermocouple wires embedded in a highly thermally conductive epoxy (Omega 101) to account for temperature-induced strains. Temperature was sampled once per minute using an Omega OM-CP-IFC200 data logger. The complete data acquisition system used for Gages B and C mounted on a pump pipe is shown in Figure 5.6.

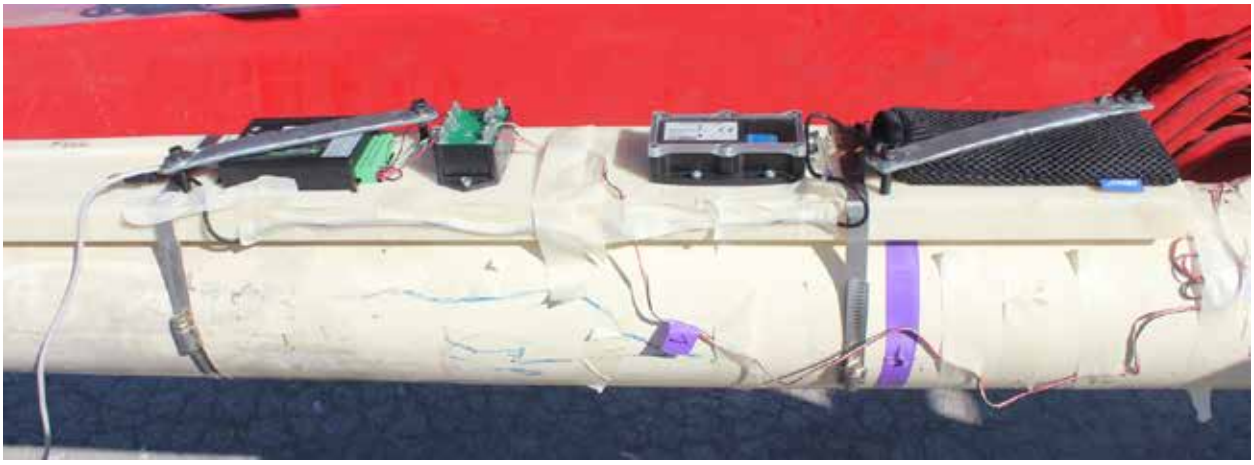

Figure 5.6: Data Acquisition System

Since it is very difficult to perfectly align the strain gauges on the circular surface of the pipe, all strain gauges were individually calibrated in a laboratory using known hydraulic pressure. The calibration also eliminated the need for testing of exact pipe material mechanical properties. The calibration procedure consisted of the following steps: (1) record strain at atmospheric pressure; (2) fill the system with water (pipe is aligned in a horizontal direction); (3) apply 800–1,000 psi pressure using a hand pump and record strains; and (4) release pressure in 100 psi decrements and record the corresponding strain for each step. Using the measured data, calibration (pressure-strain) curves were obtained for each strain gauge, as shown in Figure 5.7.

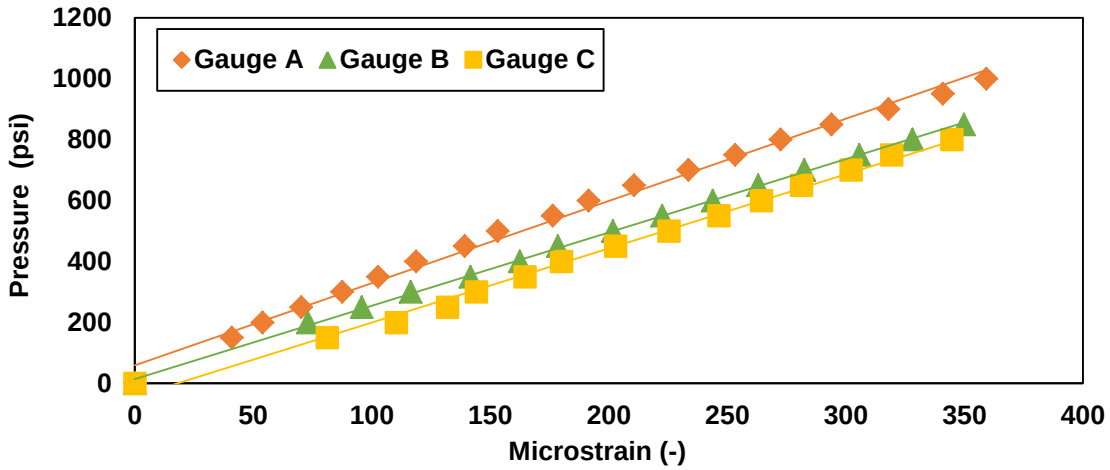

Figure 5.7: Strain Gauge Calibration Curves

Additionally, pipes were placed in an outdoor environment in order to determine the effect of temperature on measured strains. Pipes were left outdoors in direct sunlight for a 12-hour temperature cycle, resulting in temperature difference of approximately 30 °F.

5.3 Results and Discussion

Complete results of the full-scale experiment are presented in Appendix B.

5.3.1 Pumping Pressure

Pumping pressure as a function of the gauge distance from the pump hopper is shown in Figure 5.8. Pumping pressure decreased linearly as the distance from the hopper increased, as expected.

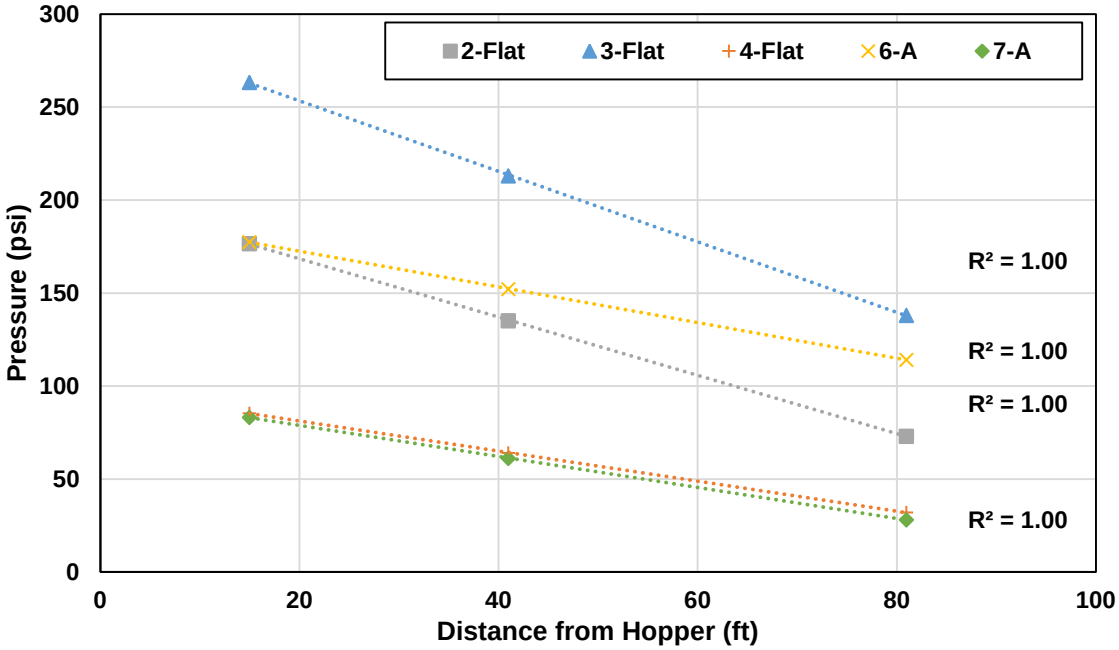

Figure 5.8: Pumping Pressure vs. Distance from the Hopper – Mix B and C

Due to a data logger malfunction, data for the Gauge A for Mix 1 were lost. However, the linear relationship between the gauge location and the distance from the hopper allowed for extrapolation of missing data, as shown in Figure 5.9.

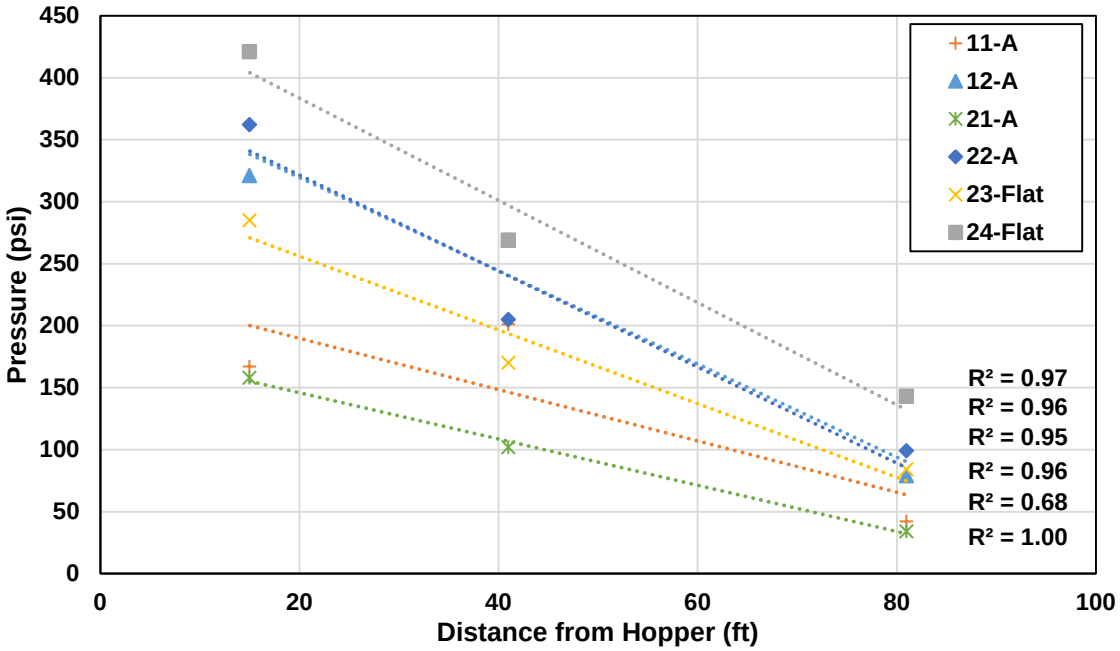

Figure 5.9: Pumping Pressure vs. Distance from the Hopper – Mix A

The maximum pumping pressure recorded was 421 psi at Gauge A when Mix 3 was pumped at a flow rate of 1.18 cubic feet per second, with the pump boom in a flat configuration. The recorded pressure profile revealed that the pump pressure during pumping was not constant but changed with every stroke of the piston. The concrete experienced large pressure shocks over a relatively short period of time, as shown in Figure 5.10. In this particular case, the pressure spiked from 0 psi to approximately 400 psi in 1.5 seconds. Similar trends were observed for all tested mixes.

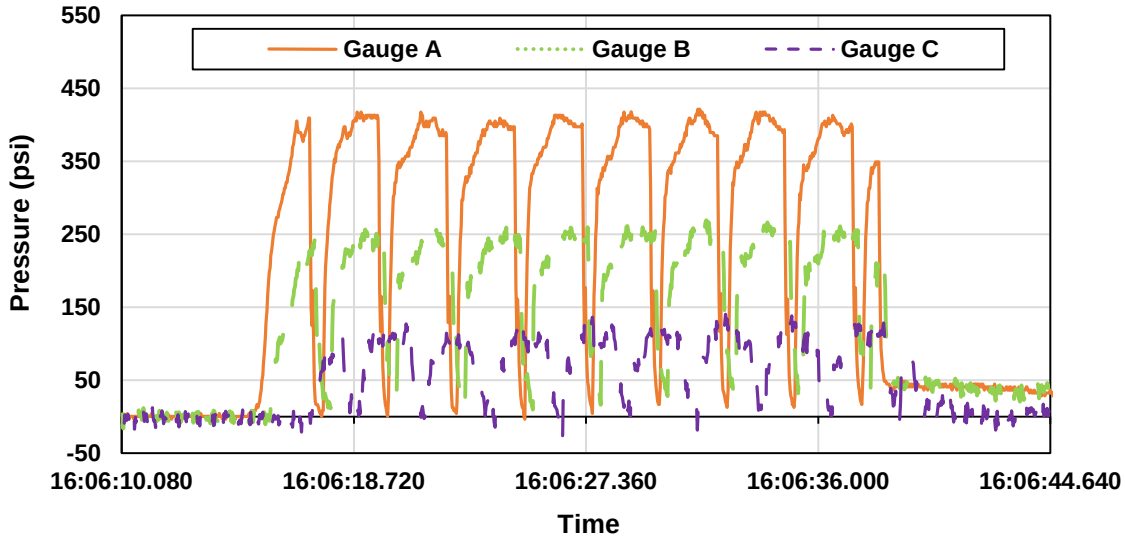

Figure 5.10: Recorded Pressure Profile during Pumping

Additionally, negative pressures exerted on concrete were observed in several instances, such as the case shown in Figure 5.11. The existence of a negative pressure during the pumping cycle suggests that suction, or vacuum, is created for a small period of time when the pump piston is retracting. The suction effect of the pump piston has been proposed as one of the possible factors contributing to the changes of the air void system due to pumping. Interestingly, significant negative pressures value (i.e., greater than 10 psi) were only observed when the boom was in the “A” configuration.

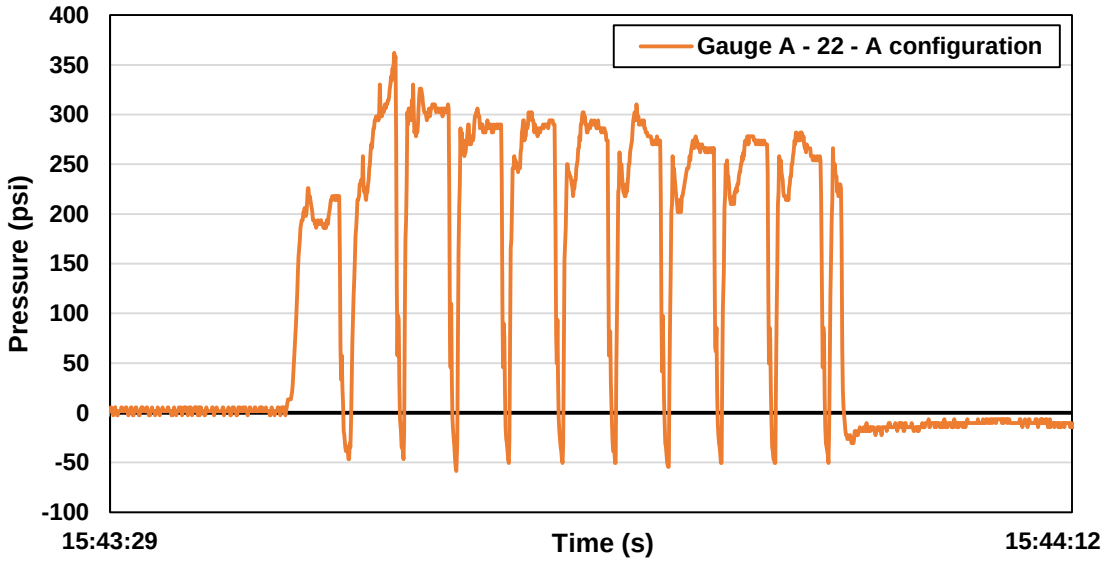

Figure 5.11: Negative Pressures – Pumping Experiment

Figure 5.12 and Figure 5.13 show the relationship between pumping pressure and flow rate for a pump boom in the "flat" and "A" configurations, respectively. Pumping pressure linearly increased with the flow rate growth, independent of the boom configuration.

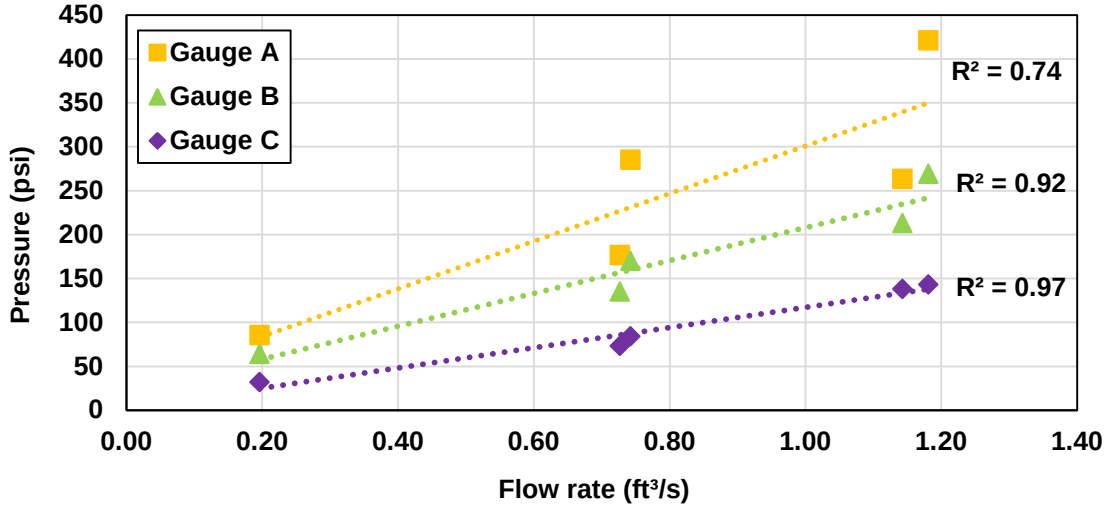

Figure 5.12: Pressure vs. Flow Rate (Flat Configuration)

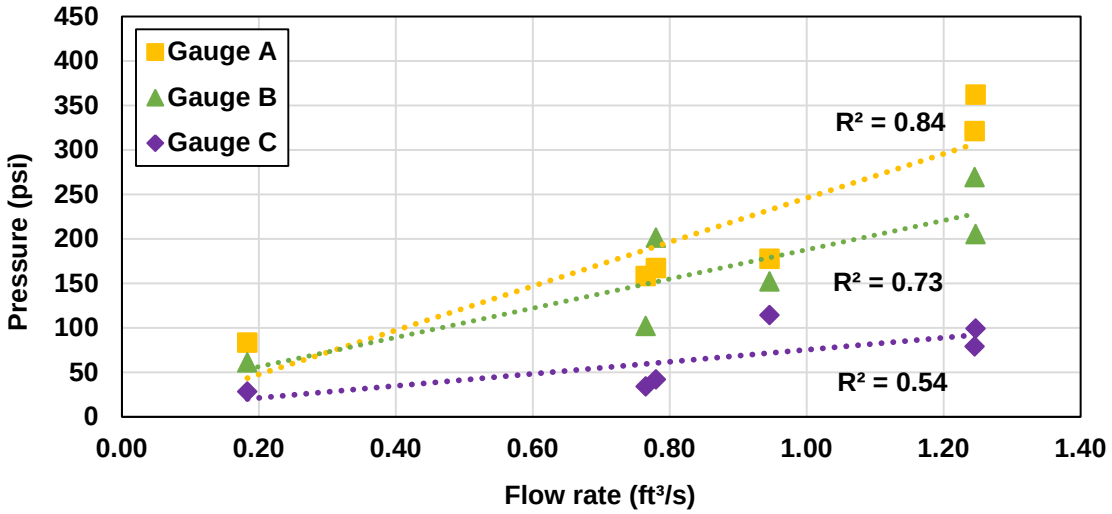

Figure 5.13: Pressure vs. Flow Rate (A Configuration)

The comparison of pumping pressures between the "flat" and "A" boom configurations is shown in Figure 5.14, Figure 5.15, and Figure 5.16 for Gauges A, B, and C, respectively. It is clear that the pumping pressure required for concrete to be pumped at a certain flow rate is higher when the boom was setup in the "flat" configuration than when it was arranged in the "A" configuration. To explain the difference between the two configurations, one must factor the gravity into the pressure analysis. In the "A" configuration, concrete that reached the peak of the boom is boosted by the gravity effect in the downward part of the pipeline. Therefore, essentially half of the pumped concrete mass is significantly affected by the free gravitational flow, whereas in the case of the "flat" configuration, almost all of the concrete mass must be moved by the pump, hence the higher overall pressure.

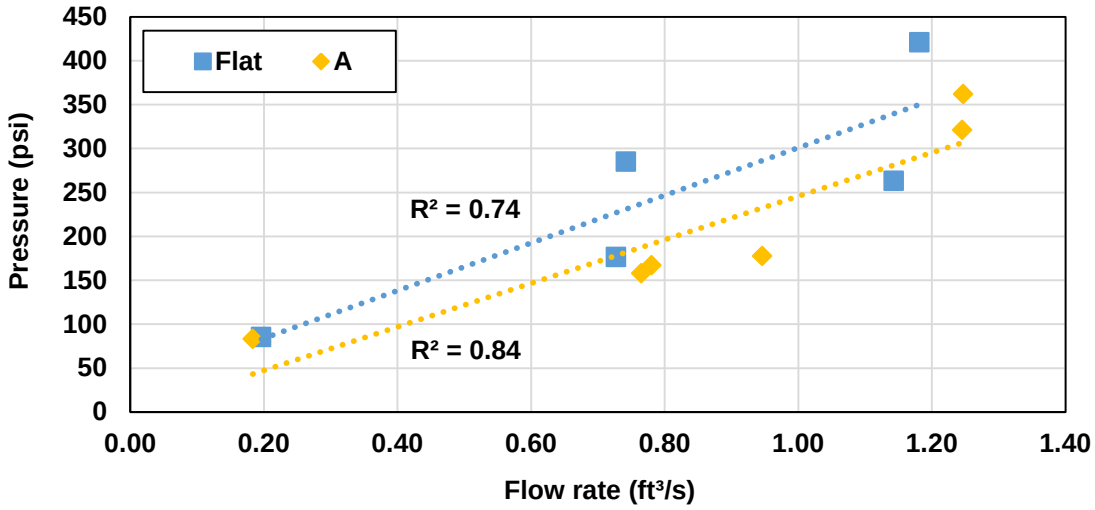

Figure 5.14: Pressure vs. Flow Rate (Gauge A)

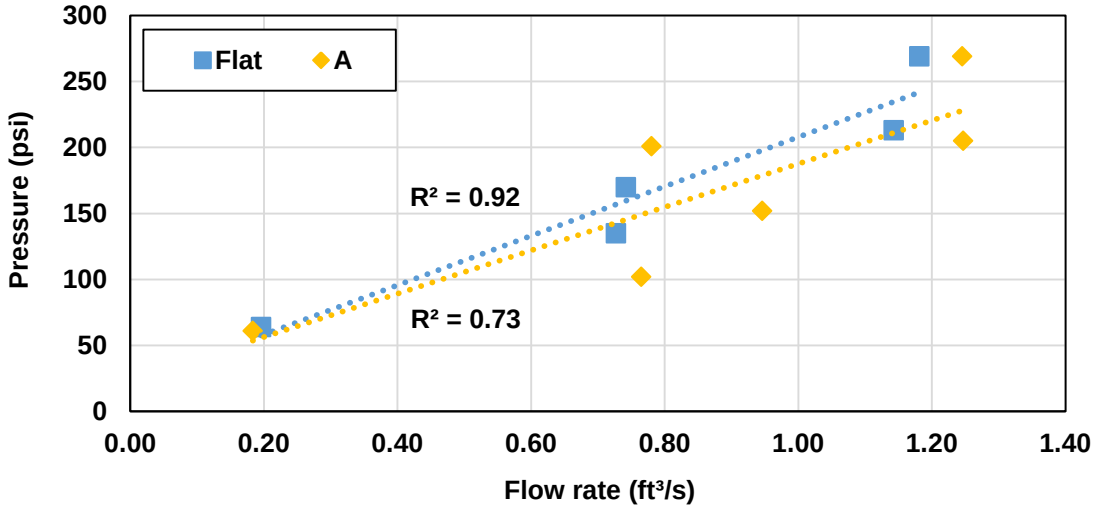

Figure 5.15: Pressure vs. Flow Rate (Gauge B)

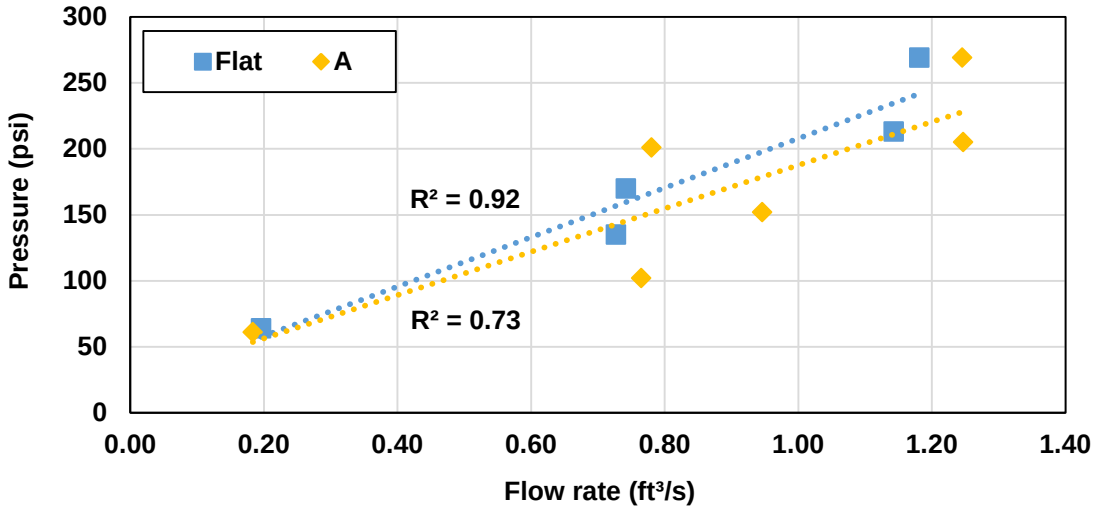

Figure 5.16: Pressure vs. Flow Rate (Gauge C)

5.3.2 Concrete Properties

Slump and fresh concrete air void content before and after pumping are shown in Figure 5.17 and Figure 5.18, respectively. Both of these concrete properties decreased after pumping for all boom configurations. The decrease in slump can be attributed to decrease of free water in the mix that contributes to overall workability. Mixing water is forced into aggregate pores under the pumping pressure and it is not immediately released once the pressure is removed. The decrease in the total air content is in sharp contrast with observations made during the field testing campaign, as mostly an increase in the air content was measured in the field. However, a decrease in the air content was observed in one instance of the field testing (I-70 over Kaw Drive), a project with a relatively shallow formwork. The nature of the pumping experiment was rather similar to this project as concrete was pumped on the ground, without any significant mixing action present after its discharge from the pump line. This supports the hypothesis that the re-mixing phenomenon is responsible for stabilizing additional bubbles upon release of concrete to the formwork. A shallow formwork would also provide more impact upon discharge than concrete discharged onto a thicker layer concrete. The same type of air-entraining agent (Euclid AEA 92S) was used in mixtures on both the I-70 project and during the pumping experiment. There is not enough evidence to support a claim that this particular admixture would

perform differently than others when utilized on projects when concrete is pumped; however, it is suggested that the type of AEA and its effect on changes in the air void system after pumping need to be investigated in the future.

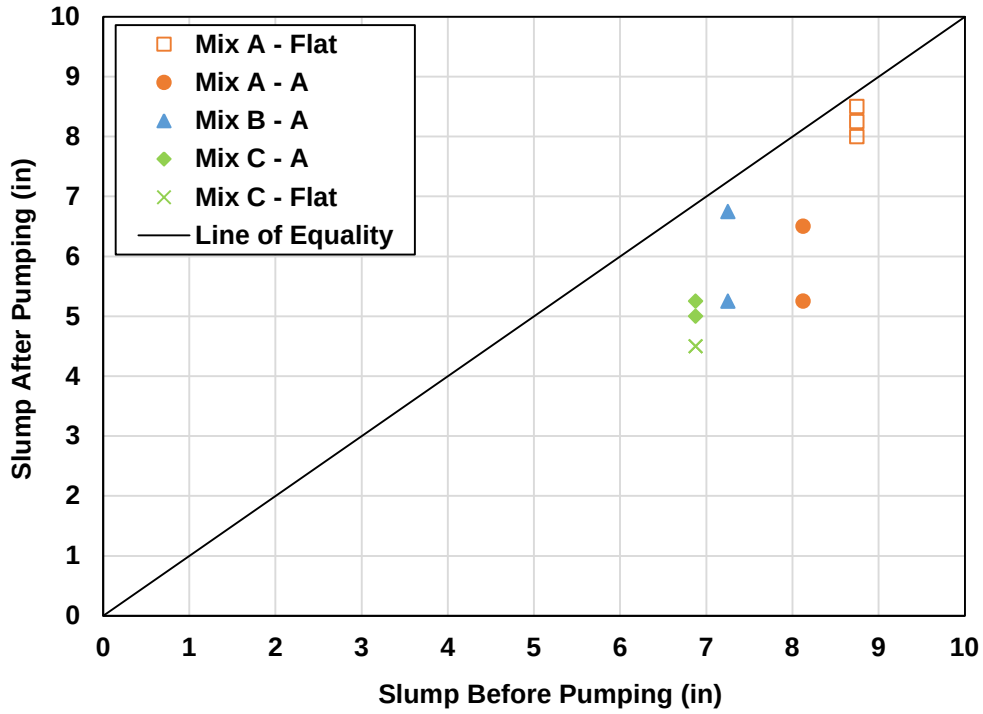

Figure 5.17: Slump Before and After Pumping – Pumping Experiment

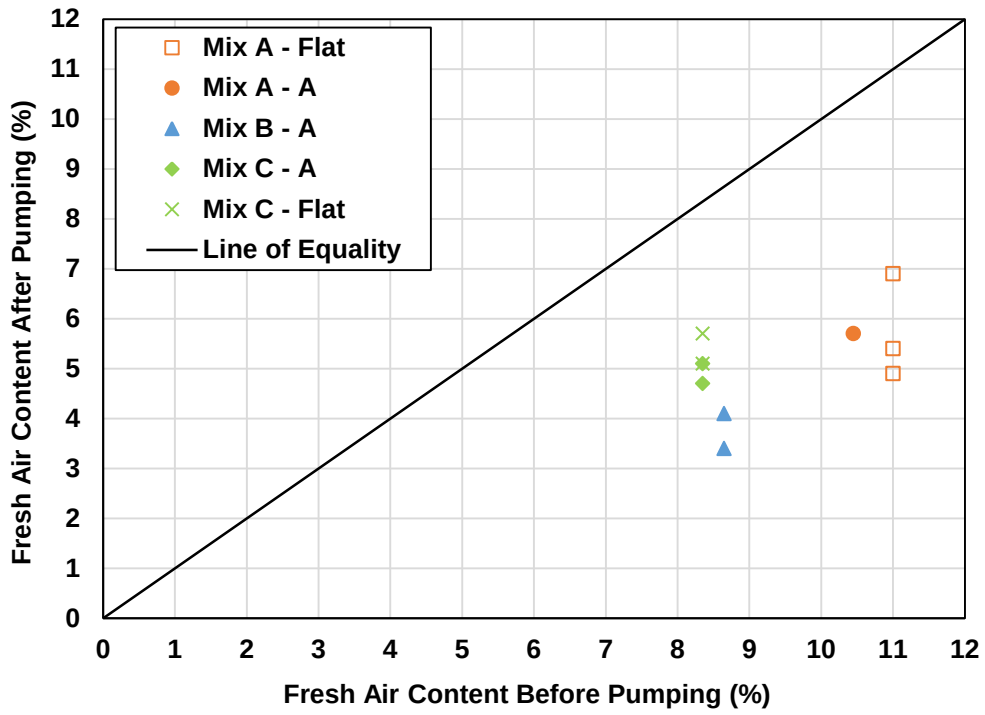

Figure 5.18: Fresh Air Content Before and After Pumping – Pumping Experiment

The SAM number before and pumping is presented in Figure 5.19. Similar to the observations made during the field testing campaign, some of the mixes exhibited greater SAM number values than what was recommended by the SAM manufacturer for a frost-durable concrete (0.20 psi). Additionally, the SAM number increased in all instances but one after pumping. This suggests that pumping can significantly affect the air void system and could possibly negatively alter the freeze-thaw performance of pumped concrete due to the reduction of fine air voids in the mixture after pumping. However, no particular relationship between the change of the SAM number and boom configuration was observed during the pumping experiment.

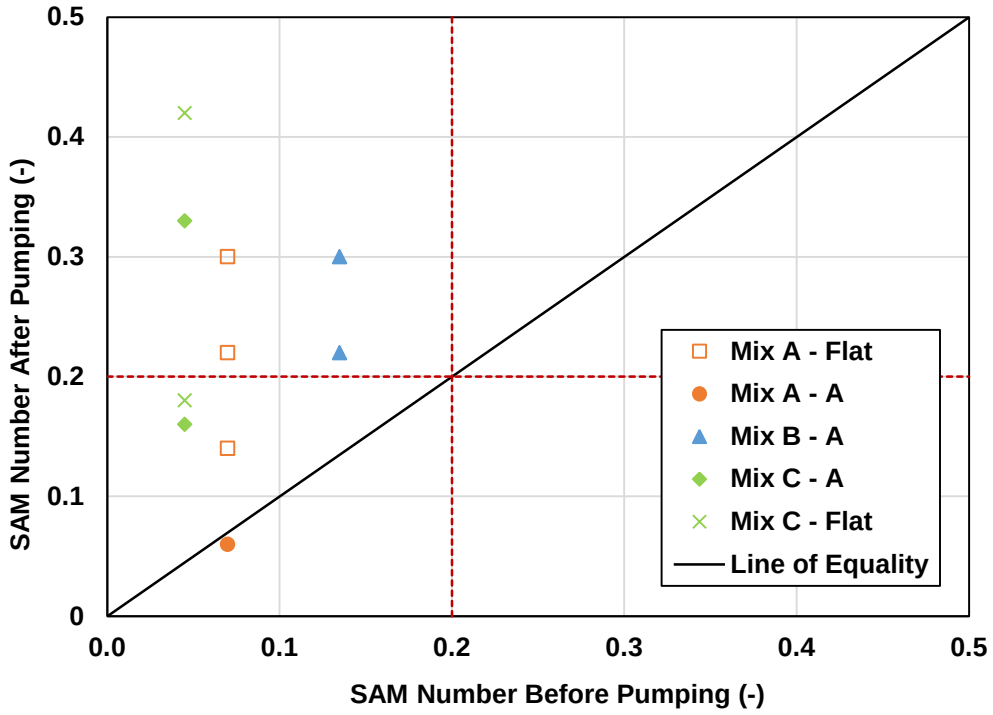

Figure 5.19: SAM Number Before and After Pumping – Pumping Experiment

Figure 5.20, Figure 5.21, and Figure 5.22 show values, both before and after pumping, of yield stress, plastic viscosity, and viscous constant, respectively. Both yield stress and plastic viscosity tended to increase after pumping. As for the yield stress, eight mixes out of 11 measured concretes had a higher yield stress value after pumping than before pumping, and all tested mixes showed an increase in plastic viscosity after pumping. The opposite trend was observed for the viscous constant. All investigated concrete mixes had a lower value of viscous constant after pumping. It is notable that although three different mix designs were incorporated into this study, the viscous constant had a small variation within the sample set, both before and after pumping.

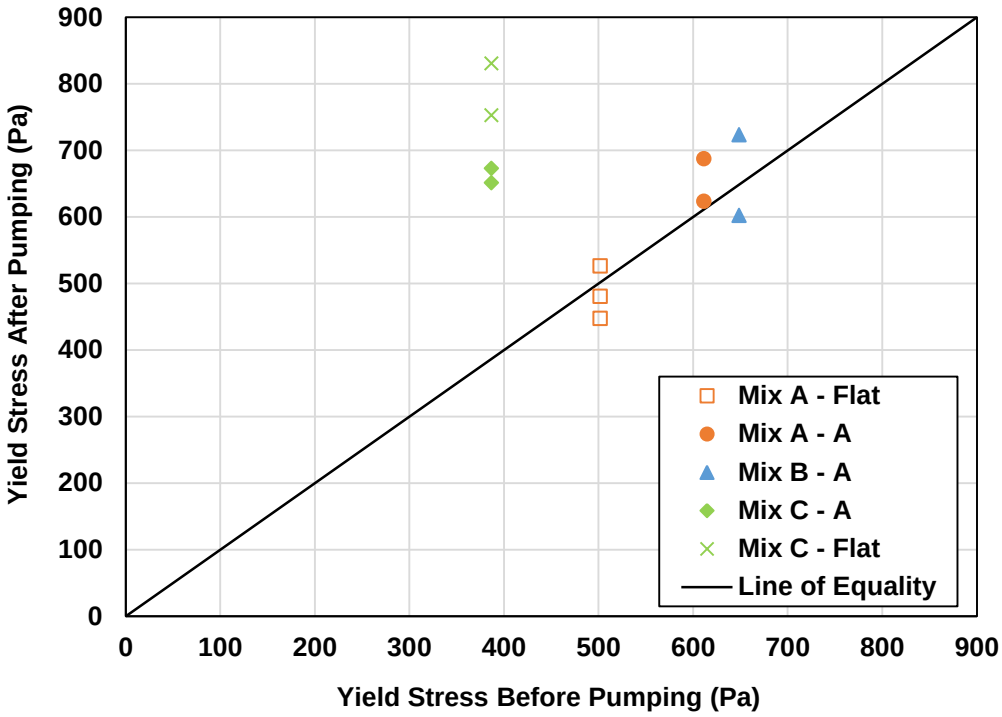

Figure 5.20: Yield Stress Before and After Pumping – Pumping Experiment

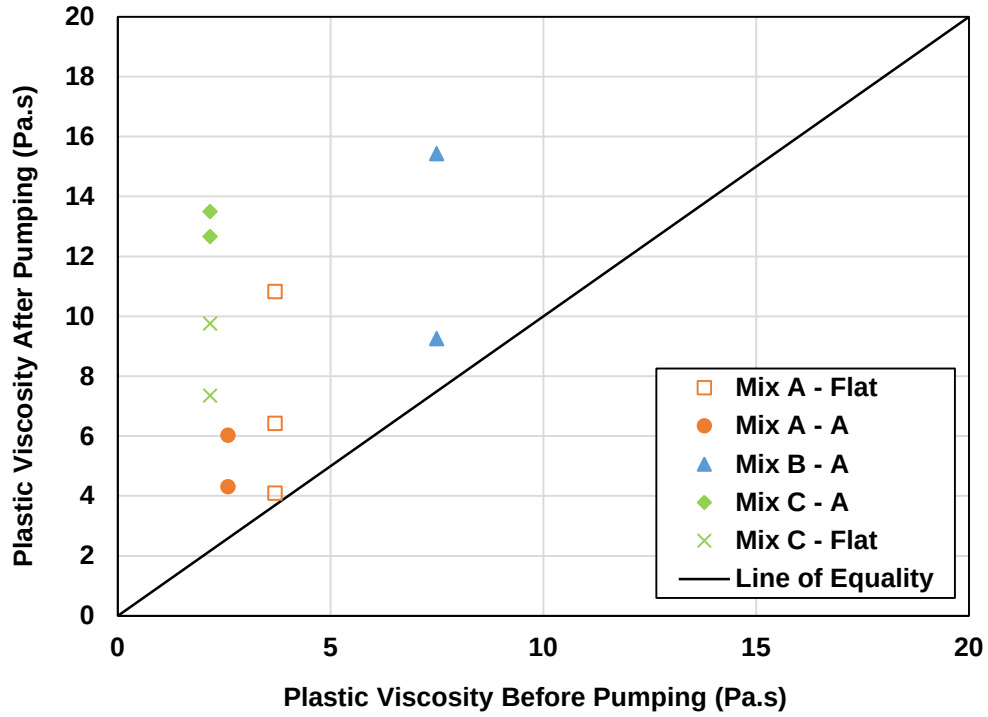

Figure 5.21: Plastic Viscosity Before and After Pumping – Pumping Experiment

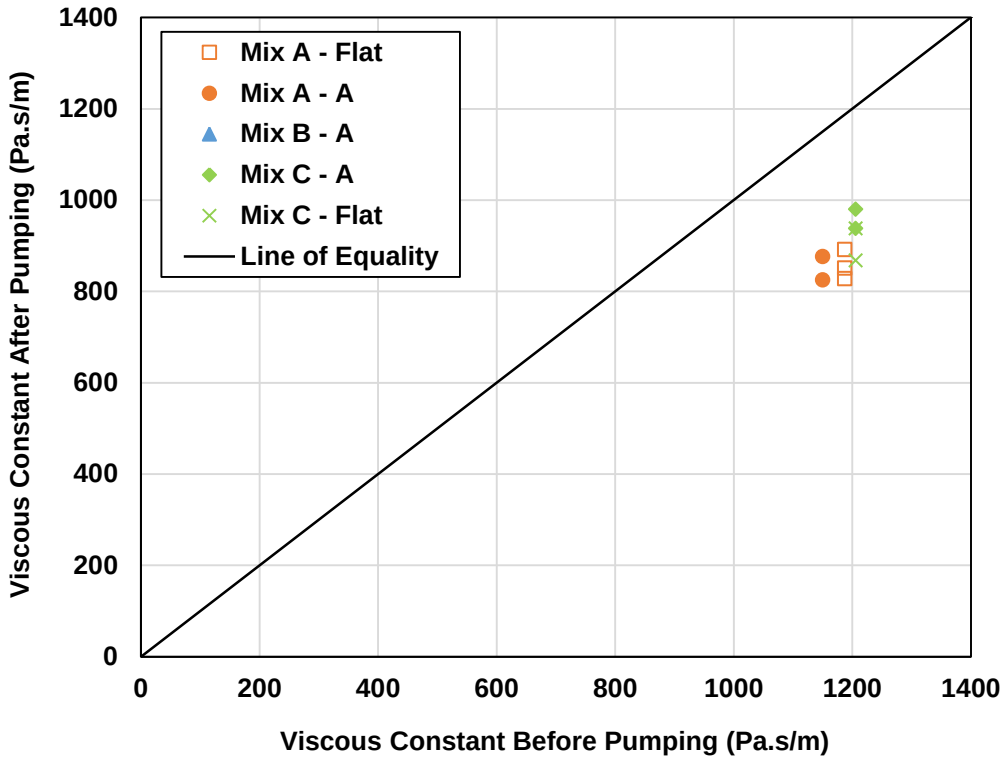

Figure 5.22: Viscous Constant Before and After Pumping – Pumping Experiment

The hardened air void content and spacing factor before and after pumping are shown in Figure 5.23 and Figure 5.24, respectively. The total air void content decreased after pumping, and the spacing factor increased after the concrete was pumped. Pumping increased the spacing factor, potentially making it more susceptible to freeze-thaw; however, freeze-thaw testing is needed to confirm this. Four of the tested mixes had a spacing factor greater than 0.008 inches, which is the recommended limit of spacing factor for frost-durable concrete. Three mechanisms explaining the nature of the air void system change due to pumping have been proposed: (1) the suction effect causing expansion and swelling of air bubbles in zones of negative pressure in the pipeline (Chapdelaine, 2007); (2) impact of concrete when discharged or when it reaches an elbow in the pipeline (Yingling, Mullings, & Gaynor, 1992); and (3) the pressure-dissolution mechanism causing air bubbles to dissolve in water due to increased pressure and subsequent nucleation of dissolved air on the surface of large, existing bubbles (Dyer, 1991). Additionally, the authors believe that the mixing action that might occur after concrete is discharged from the

line can help entrain additional air voids. The nature of these mechanisms is such that they all can occur simultaneously. In fact, during this testing campaign, negative pressure was recorded in several instances (the suction effect mechanism), was subjected to different levels of pressure (pressure-dissolution mechanism), and finally was discharged directly on the ground (the impact mechanism). Comparing results of the pumping experiment and the field testing program, it is apparent that very different trends of change of the air void system were observed as air content tended to increase after pumping during the field testing, whereas a decrease was recorded during the pumping experiment. This can be attributed to the mixing action effect, as no or very little mixing action was generated during the full-scale experiment (no "new" air stabilized in the mix), whereas a significant mixing action occurred on almost all visited job sites (additional air voids stabilized in the mix).

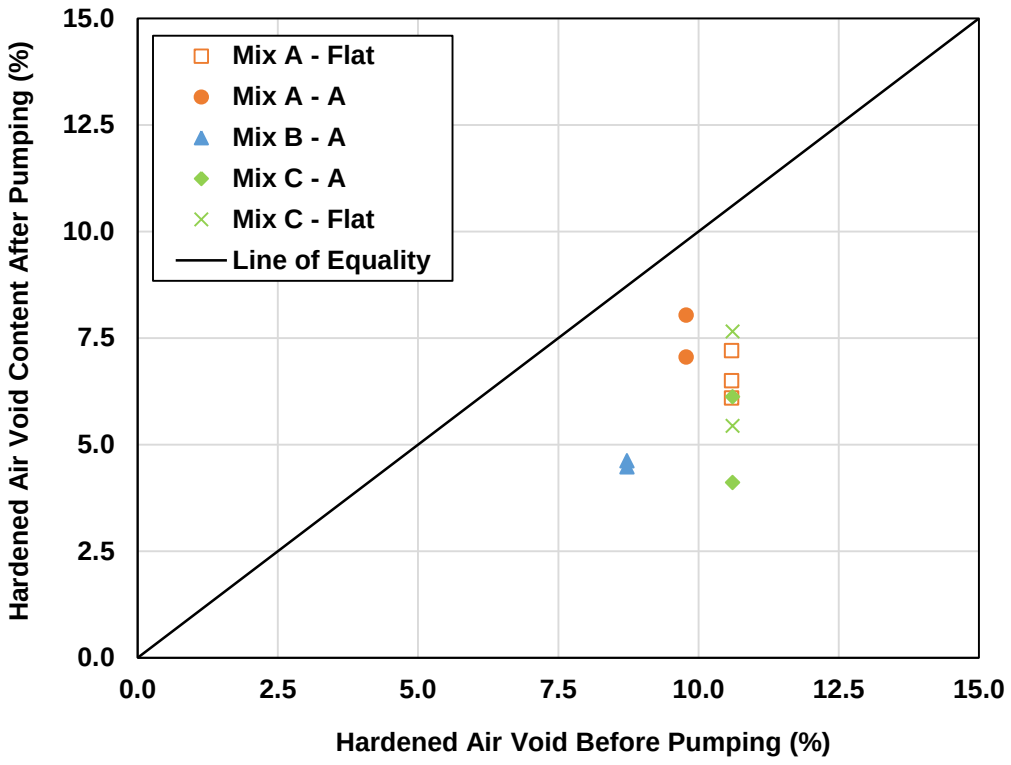

Figure 5.23: Hardened Air Void Before and After Pumping – Pumping Experiment

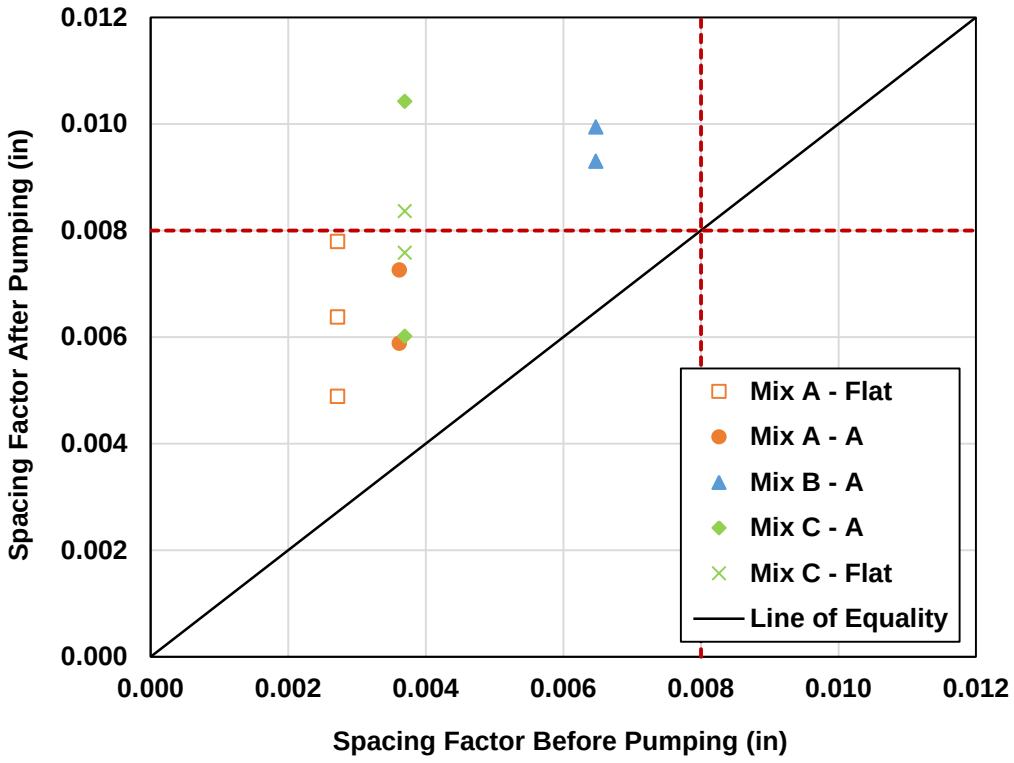

Figure 5.24: Spacing Factor Before and After Pumping – Pumping Experiment

5.3.3 Concrete Properties and Pumping Pressure

Figures 5.25 through 5.31 show maximum pumping pressure versus change in slump, fresh air void content, SAM number, yield stress, plastic viscosity, viscous constant, hardened air void content, and spacing factor, respectively. There was no relationship found between a property change and applied pressure for all cases but air void content and spacing factor. The change in slump is more likely associated with aggregate moisture level than pressure. Additionally, the reduction in the total air content after pumping could have possibly contributed to the loss of slump. Absolute change in spacing factor correlated well with the pumping pressure and was independent of the boom configuration or mix design. This observation suggests that the pressure-dissolution mechanism is a major factor affecting changes in the air void system, since concrete that experienced higher pressure also saw a higher change in the spacing factor value. However, additional research is needed to provide better understanding of the mechanisms governing changes in the air void system due to pumping.

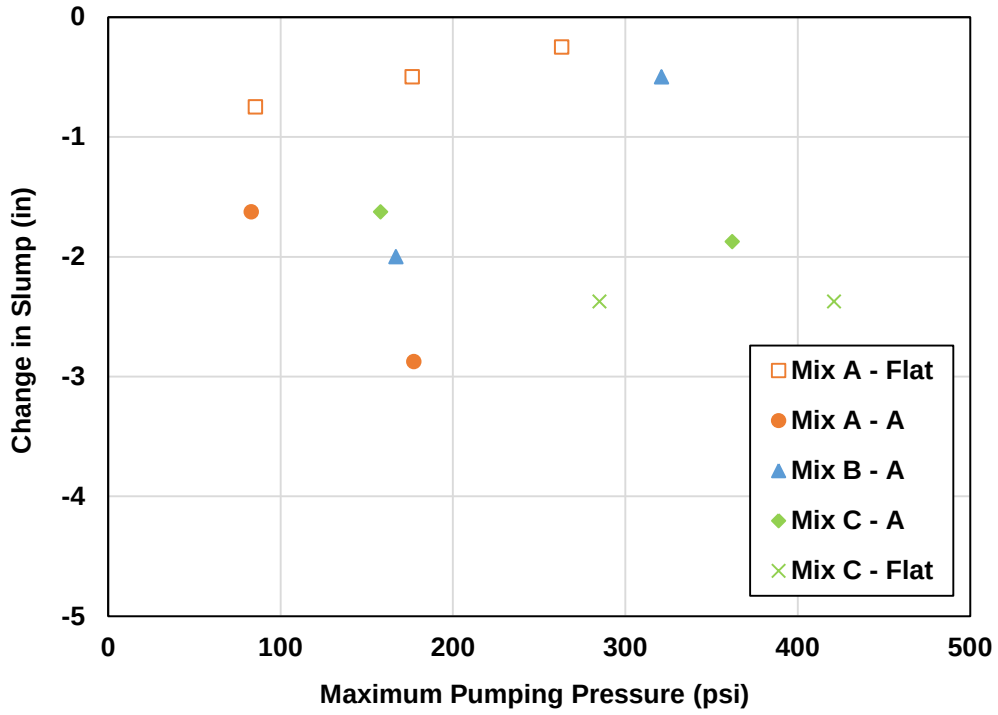

Figure 5.25: Change in Slump vs. Pumping Pressure – Pumping Experiment

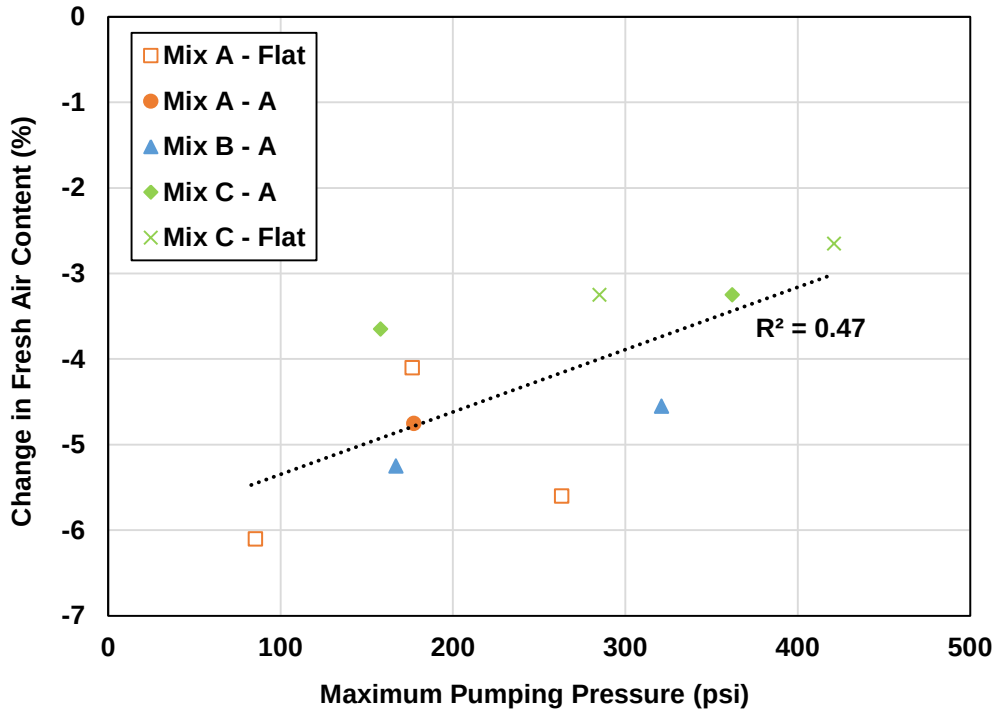

Figure 5.26: Change in Fresh Air Content vs. Pumping Pressure – Pumping Experiment

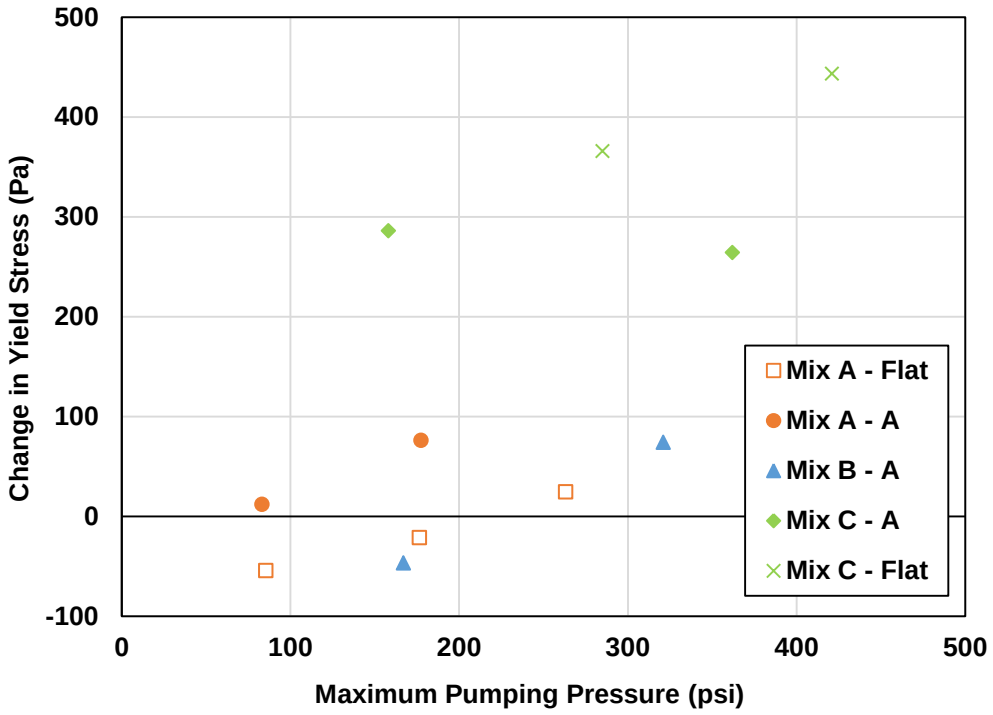

Figure 5.27: Change in Yield Stress vs. Pumping Pressure – Pumping Experiment

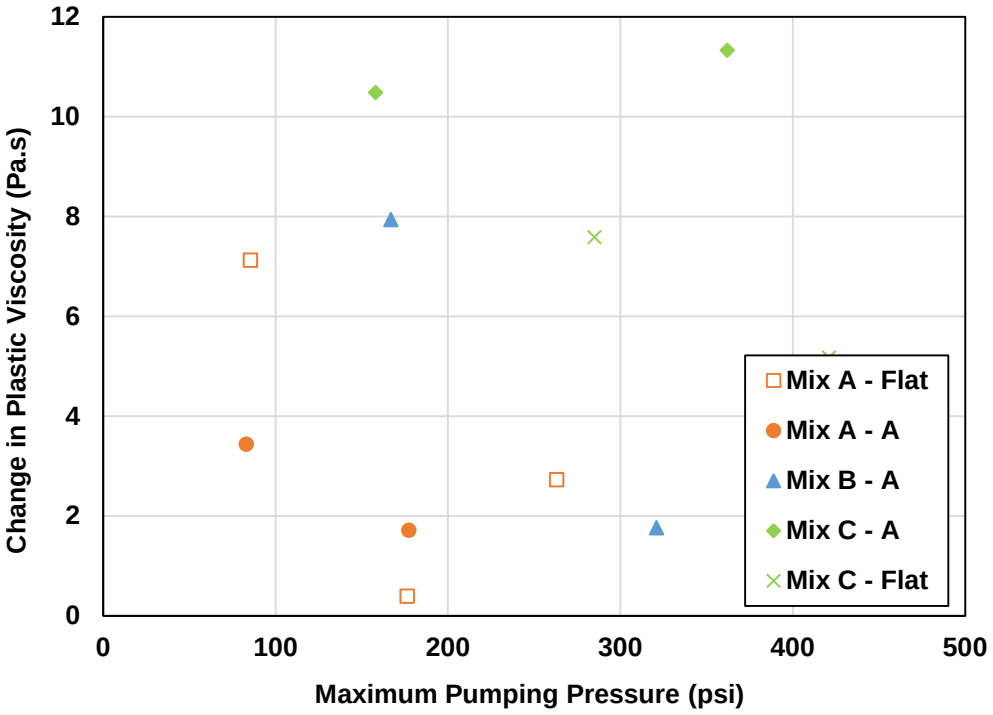

Figure 5.28: Change in Plastic Viscosity vs. Pumping Pressure – Pumping Experiment

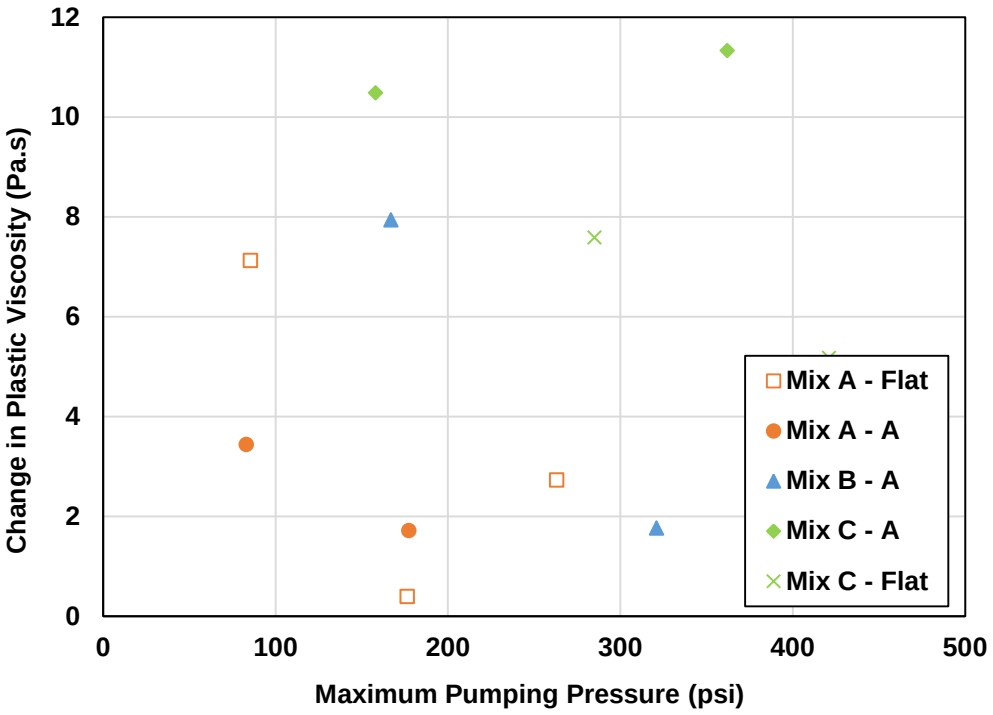

Figure 5.29: Change in Viscous Constant vs. Pumping Pressure – Pumping Experiment

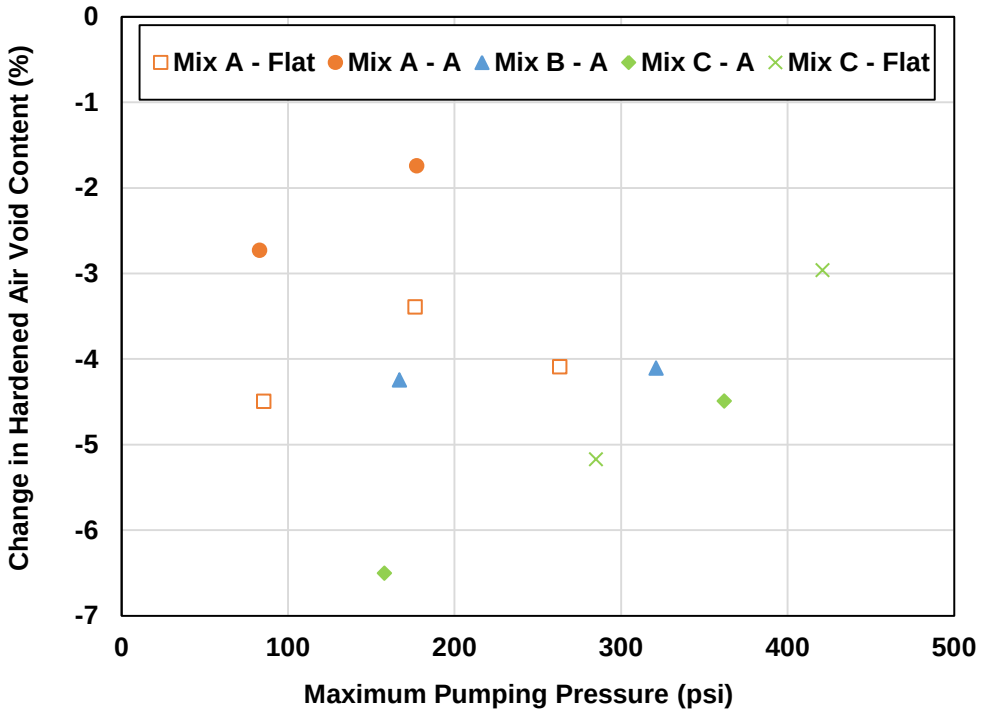

Figure 5.30: Change in Hardened Air Content vs. Pumping Pressure – Pumping Experiment

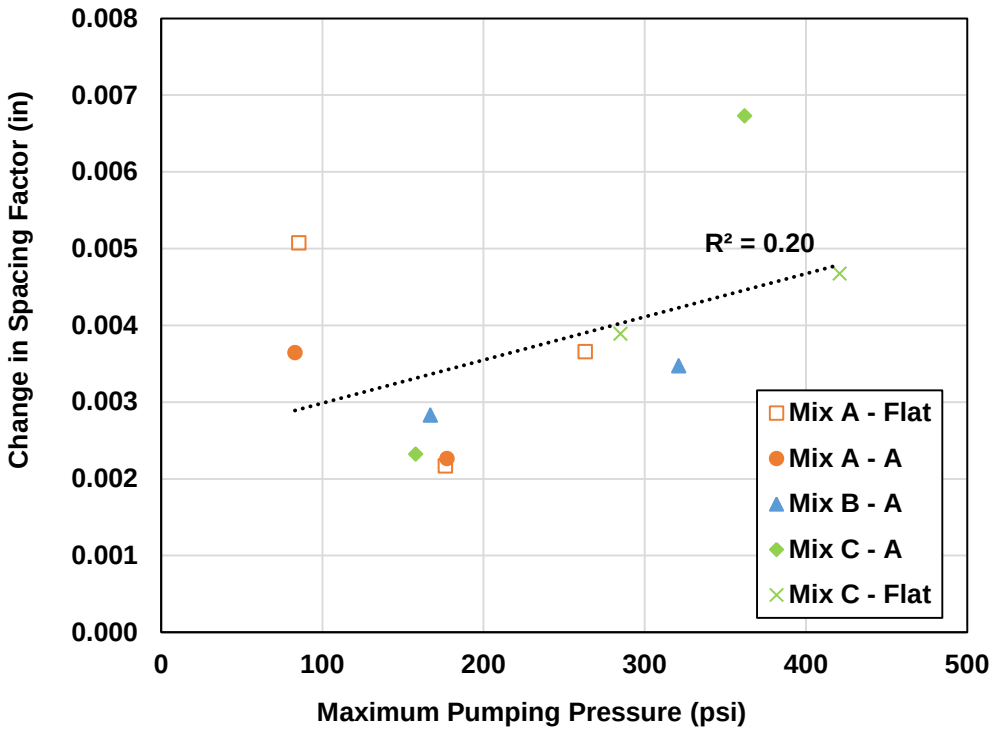

Figure 5.31: Change in Spacing Factor vs. Pumping Pressure – Pumping Experiment

5.4 Summary and Recommendations

A full-scale pumping experiment was conducted in November 2015. Three concrete mixtures were pumped through a 46-meter boom pump using two different boom configurations. Each mixture was pumped at varying pumping rates. In order to record the pressure in the pipeline, the pumping system was instrumented with externally mounted electrical resistance strain gauges. Concrete properties were determined both before and after pumping.

The experiment was in a good agreement with the field study and showed that slump is likely to decrease after pumping. In all 10 cases, slump after pumping was lower than slump of concrete sampled directly from the ready-mix truck. Similarly to the recommendations made in Section 4.4, the authors reiterate the importance of sampling concrete at the point of placement in order to ensure that the mixture maintains the required workability for placement and finishing. KDOT specifications should require that pumped concrete be sampled after placement.

The air void system experienced quantitatively different transformation than what was observed during the field testing campaign. Both the total air void content and spacing factor decreased after pumping in all instances. Additionally, the SAM number after pumping increased in all instances, and in five out of nine cases was greater than the maximum recommended value of 0.20. This implies that the overall quality of the air void system can be significantly compromised after pumping, and therefore it is recommended to require a quantitative performance check (hardened void analysis, freeze-thaw testing) of placed (i.e., pumped) hardened concrete if the structure is expected to experience severe freeze-thaw conditions. However, it is important to note that the pumped concrete was discharged directly onto the ground in this experiment; therefore, the additional concrete mixing action was minimal. Therefore, if concrete is placed in a relatively deep formwork, the detrimental effect of pumping on the air void system is likely to be reduced.

Although the Super Air Meter results exhibited similar trend as the hardened air void analysis results (i.e., increase in the SAM number and spacing factor after pumping), several SAM measurements produced questionable results. The questionable results likely occur because the SAM mechanism is based on changes that occur in the concrete during overpressure. Since the concrete tested is already exposed to higher pressures than the concrete in the SAM, the SAM meter methodology is questionable and should be further investigated.

Two typical boom setups were investigated in this study: the “flat” and the “A” configuration. Results showed that a smaller pumping pressure is required to pump concrete at the same rate when the pump boom is in the “A” configuration. Also, 20% replacement of cement with class F fly-ash resulted in lower pumping pressure.

The maximum recorded pumping pressure correlated well with the absolute change in the spacing factor, suggesting that the greater the pressure acting on concrete, the more significant the change in the spacing factor. Based on this observation, it is advised to make an effort to reduce the pumping pressure as much as possible in order to avoid excessive changes of the air void system. The following measures can be adopted to limit the pumping pressure:

- The position of the pump on the site should be such that the hydraulic head of the pump is as small as possible (i.e., when placing concrete on a bridge deck, avoid pumping from below the deck if feasible).
- The use of the “A” configuration is preferred over the “flat” configuration.
- Adjust the concrete mixture to modify its rheological properties that are directly related to the pumping pressure; see Chapter 6 for additional recommendations.

Chapter 6: Laboratory Program

6.1 Introduction

A series of laboratory tests was performed to investigate factors affecting concrete rheological and tribological parameters, and subsequently its pumpability. The following variables were included in the study: water content, cement content, air content, coarse-to-fine aggregate ratio, and use of fly ash, viscosity modifying admixtures (VMA), and nanoclay particles. Results of laboratory experiments were compared using Kaplan's pressure prediction model, as described in Section 2.5.3.

6.2 Experimental Program

6.2.1 Testing Matrix

In order to work with realistic concrete mixtures, all concrete mixtures contained air entrainment. Several versions of control mixes with various air content were batched so that comparison could be made between concretes with similar air content.

Mix proportions of concretes included in the study are shown in Table 6.1. Three variations of each mix corresponding to the investigated parameter were batched. These variations differed in the total water content, as each set of mixes consisted of concretes with 0.40, 0.43, and 0.45 water-to-cementitious material ratios (w/cm).

Table 6.1: Mix Proportions – Laboratory Study

ID	Cementitious Material		Coarse Aggregate		Fine Aggregate		Water	HRWR
	Type	Weight (lbs)	Type	Weight (lbs)	Type	Weight (lbs)	Weight (lbs)	Dosage (fl.oz/cy)
040 Control	Type I	540	Crushed rock	1599	Natural sand	1579	216	67.5
043 Control	Type I	540	Crushed rock	1577	Natural sand	1557	232	67.5
045 Control	Type I	540	Crushed rock	1563	Natural sand	1543	243	67.5
040 520	Type I	520	Crushed rock	1618	Natural sand	1572	208	67.5
043 520	Type I	520	Crushed rock	1597	Natural sand	1552	224	67.5
045 520	Type I	520	Crushed rock	1583	Natural sand	1538	234	67.5
040 560	Type I	560	Crushed rock	1580	Natural sand	1535	224	67.5
043 560	Type I	560	Crushed rock	1557	Natural sand	1513	241	67.5
045 560	Type I	560	Crushed rock	1542	Natural sand	1498	252	67.5
040 60-40	Type I	540	Crushed rock	1919	Natural sand	1243	216	67.5
043 60-40	Type I	540	Crushed rock	1893	Natural sand	1226	232	67.5
045 60-40	Type I	540	Crushed rock	1875	Natural sand	1215	243	67.5
040 40-60	Type I	540	Crushed rock	1279	Natural sand	1864	216	67.5
043 40-60	Type I	540	Crushed rock	1262	Natural sand	1839	232	67.5
045 40-60	Type I	540	Crushed rock	1250	Natural sand	1822	243	67.5
040 RR	Type I	540	Rounded rock	1537	Natural sand	1553	216	67.5
043 RR	Type I	540	Rounded rock	1516	Natural sand	1532	232	67.5
045 RR	Type I	540	Rounded rock	1502	Natural sand	1518	243	67.5
040 Fly-Ash	Type I	405	Crushed rock	1599	Natural sand	1579	216	67.5
	Class F Fly Ash	135						
043 Fly Ash	Type I	405	Crushed rock	1577	Natural sand	1557	232	67.5
	Class F Fly Ash	135						
045 Fly Ash	Type I	405	Crushed rock	1563	Natural sand	1543	243	67.5
	Class F Fly Ash	135						
040 VMA*	Type I	540	Crushed rock	1599	Natural sand	1579	216	67.5
043 VMA	Type I	540	Crushed rock	1577	Natural sand	1557	232	67.5
045 VMA	Type I	540	Crushed rock	1563	Natural sand	1543	243	67.5
040 Clay**	Type I	540	Crushed rock	1599	Natural sand	1579	216	67.5
043 Clay	Type I	540	Crushed rock	1577	Natural sand	1579	232	67.5
045 Clay	Type I	540	Crushed rock	1563	Natural sand	1543	243	67.5

* VMA was dosed as recommend by manufacturer, i.e., 4 fl oz/cwt (21.6 fl oz/cy).

** Nanoclay particles were dosed as recommend by manufacturer, i.e., 1.35 lbs/cy.

6.2.2 Materials

Standard Type I portland cement manufactured by the Monarch Cement Company, Humboldt, KS, was used throughout this study. Local natural sand provided by Midwest Concrete Materials and meeting KDOT FA-A requirements was incorporated in all mixes. To investigate the effect of aggregate shape on concrete properties, both crushed and rounded aggregate was used: crushed granite obtained from Martin Marietta Materials and pea gravel provided by Midwest Concrete Materials. Aggregate particle size distributions are shown in Figure 6.1.

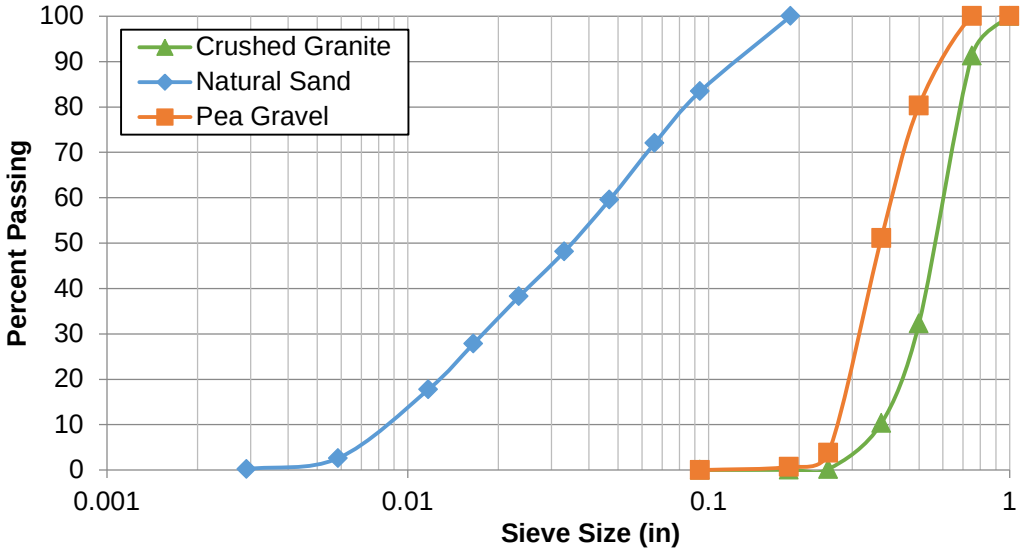

Figure 6.1: Aggregate Gradation – Laboratory Study

Both the air-entraining agent and water reducer used in this study were products of Euclid Chemical: AEA-92S air-entrainer and Plastol 6420 high-range water reducer (HRWR). Both AEA and HRWR are on the current list of KDOT prequalified materials.

In order to investigate the effect of supplemental cementitious materials and chemical and mineral admixtures on pumpability, the following products were incorporated into the testing matrix:

- Class F fly ash: Durapoz F, manufactured by Ash Grove Cement Company;

- Viscosity-modifying admixture: Sika Stabilizer-4R, manufactured by Sika; and
- Nanoclay particles: Acti-Gel 208, manufactured by Active Minerals International.

6.2.3 Experimental Procedure

A Lancaster rotating pan mixer was used in this study to mix the concrete. Mixing was performed according to ASTM C192 (2013). Fresh concrete properties, including rheological and tribological characteristics, were determined as described in Section 3.2. First, the slump test was performed within the first 2.5 minutes upon mixing completion. Second, rheology measurements were performed no later than 5 minutes after the slump test. Finally, the tribological test was carried out within the 5-minute interval following the end of the rheology testing. By implementing this procedure, the stiffening effect of fresh concrete was minimized.

Lastly, based on the obtained rheological and tribological parameters of investigated concretes, an analysis predicting pumping pressure per unit length (1 meter) was carried out. This analysis utilized Kaplan's model, as described in Section 2.5.3. For purposes of this analysis, the flow rate Q was set to 45 cy/hr and the filling coefficient k_r was assumed to be 0.9.

6.3 Results and Discussion

Complete results of the laboratory study are presented in Appendix C.

6.3.1 Air Content

Effects of total air void content on yield stress, plastic viscosity, and viscous constant are shown in Figure 6.2, Figure 6.3, and Figure 6.4, respectively. Presented values represent the set of control mixes (IDs 040/043/045 Control A-C). All three considered parameters decrease with an increase of total air void content. The relationship between all yield stress, plastic viscosity, and viscous constant is linear with a negative slope. The data for mixtures with w/cm of 0.45 deviate from the general trend observed in the rest of the data set. This is not surprising as it was observed that mixes with 0.45 w/cm and high air void content (more than 8% of the total air volume) were on the verge of aggregate segregation; therefore, the rheological and tribological

measurements could have been disrupted by amplified particle migration. Although the rheological and tribological parameters decreased with an increase in air content, definitive conclusions about the effect of air content on pumpability cannot be made because the air bubbles will compress significantly during pumping, decreasing their relative effect compared with unpressurized measurements.

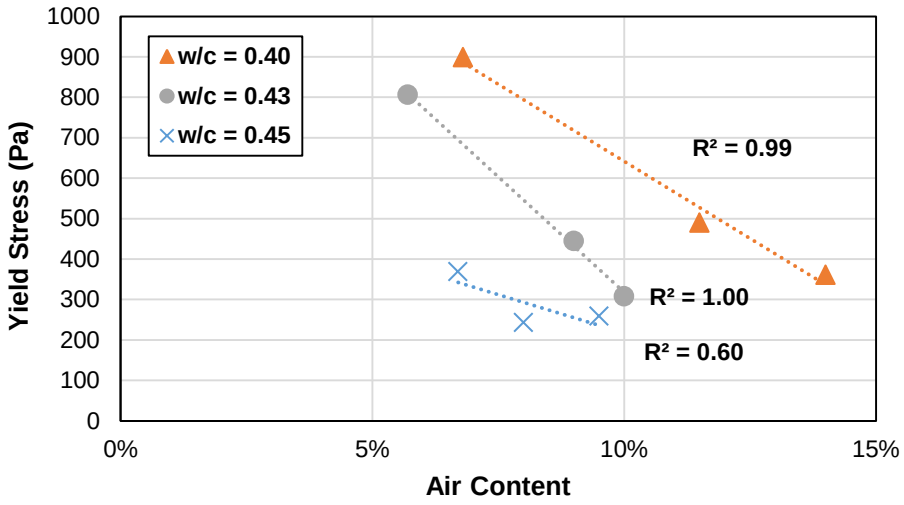

Figure 6.2: Yield Stress vs. Air Content

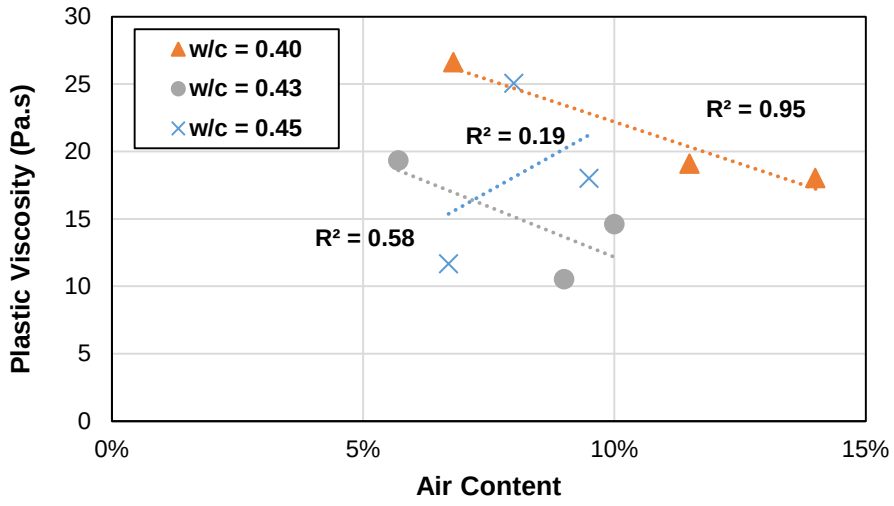

Figure 6.3: Plastic Viscosity vs. Air Content

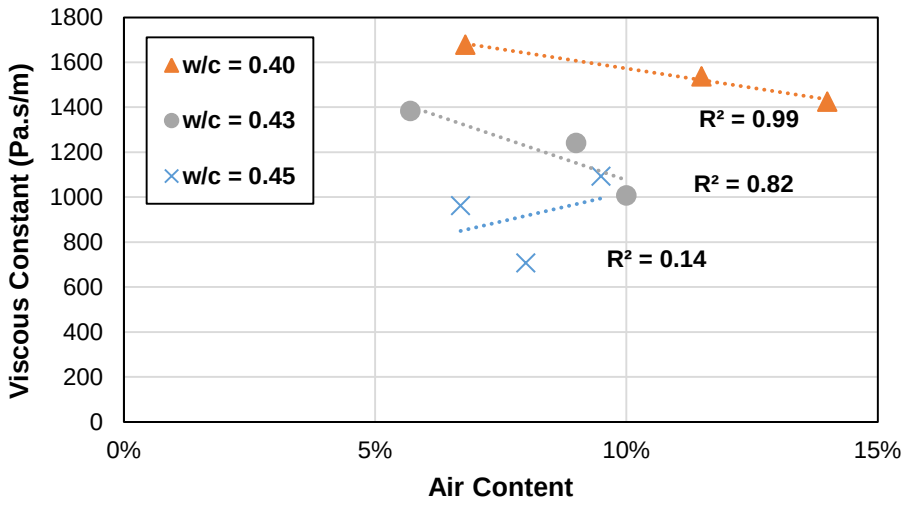

Figure 6.4: Viscous Constant vs. Air Content

6.3.2 Water Content

Figure 6.5, Figure 6.6, and Figure 6.7 show the relationship between water-to-cement ratio and yield stress, plastic viscosity, and viscous constant. In order to avoid misinterpretation of the data by comparing concretes with different air contents, only three sets of mixes are shown to illustrate the effect of water content on rheological and tribological properties. Presented mixes maintained a constant air content throughout the whole set. It is evident that a linear relationship with a negative slope exists between all three investigated fresh concrete parameters; i.e., as the water content increases, yield stress, plastic viscosity, and viscous constant decrease. This is not a surprising outcome as it is a common practice in the industry to increase water content to enhance pumpability.

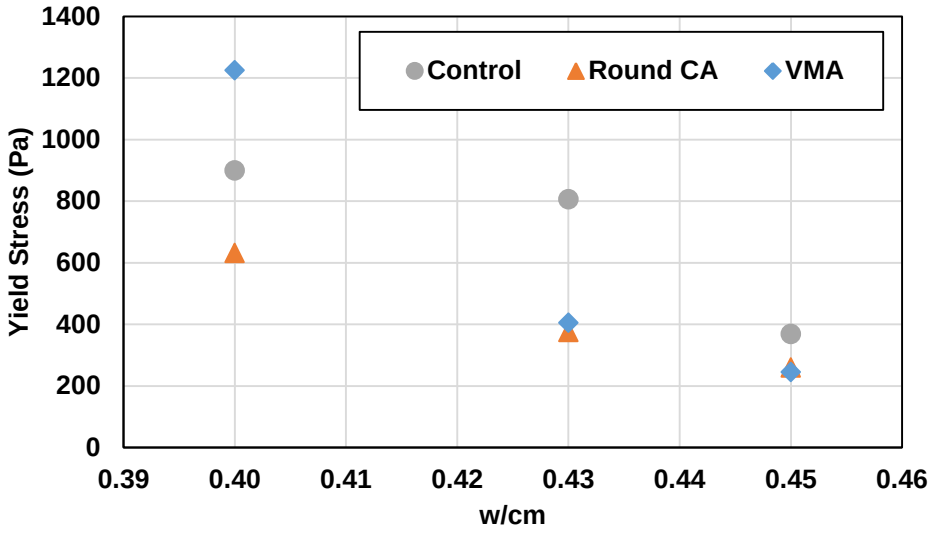

Figure 6.5: Yield Stress vs. w/cm

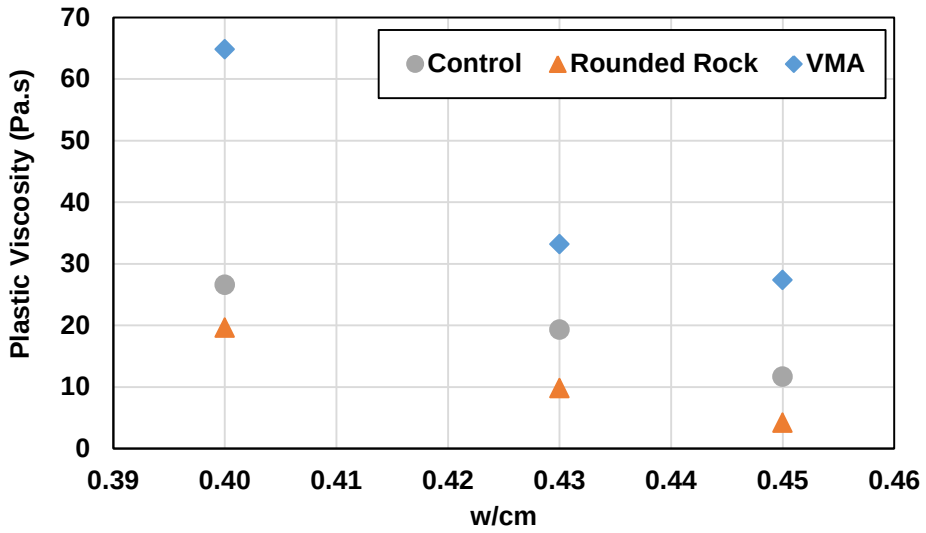

Figure 6.6: Plastic Viscosity vs. w/cm

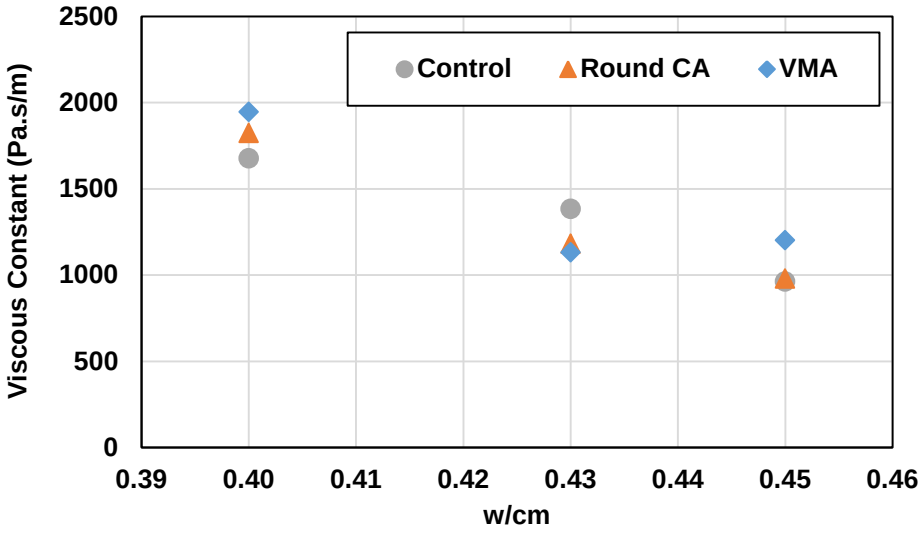

Figure 6.7: Viscous Constant vs. w/cm

6.3.3 Cement Content

The observed relationship between total cement content per cubic yard and yield stress, plastic viscosity, and viscous constant is presented in Figure 6.8, Figure 6.9, and Figure 6.10, respectively. Both yield stress and viscous constant tend to decrease with an increase in cement content, whereas plastic viscosity generally exhibited an opposite trend. However, a decrease of plastic viscosity between 0.45 w/cm-ratio mixes with 540 and 560 lbs of cement/cy was recorded. This can be again contributed to the fact that a slight aggregate segregation occurred in the 0.45 w/cm and 560 lbs of cement mix with water content, hence the rheological measurements could have been disturbed by the aggregate migration during the test.

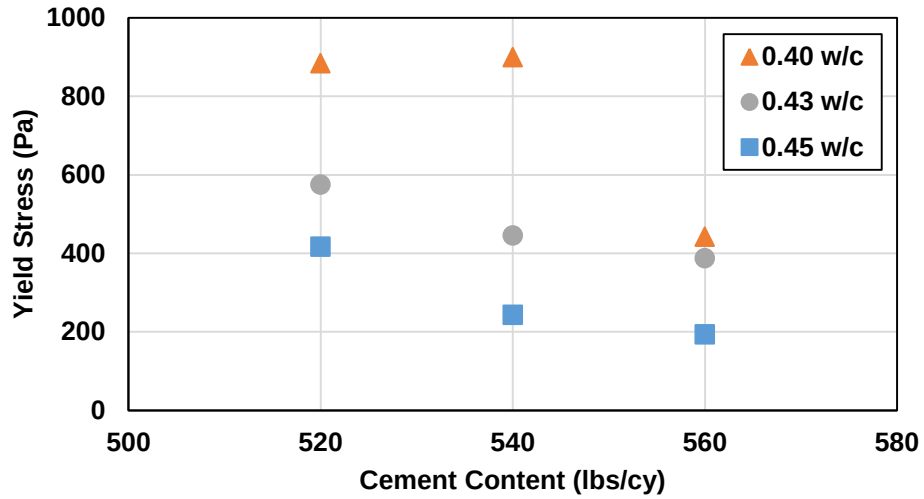

Figure 6.8: Yield Stress vs. Cement Content

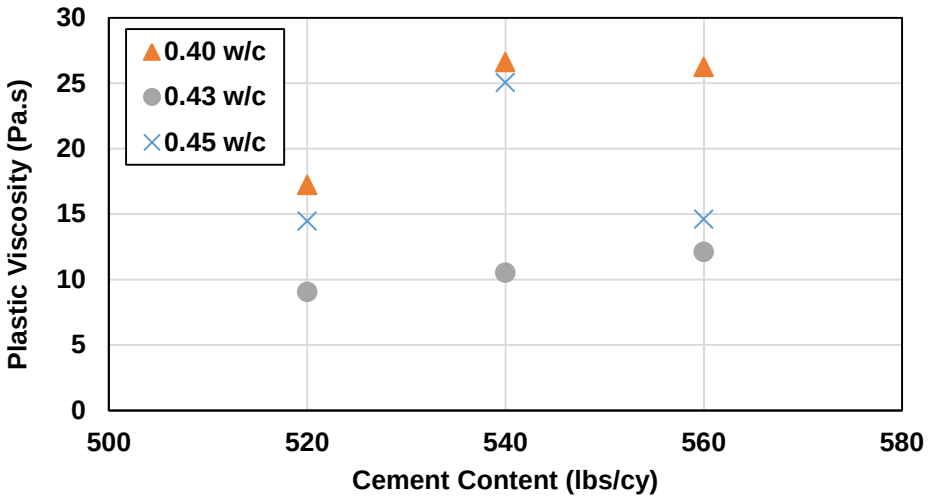

Figure 6.9: Plastic Viscosity vs. Cement Content

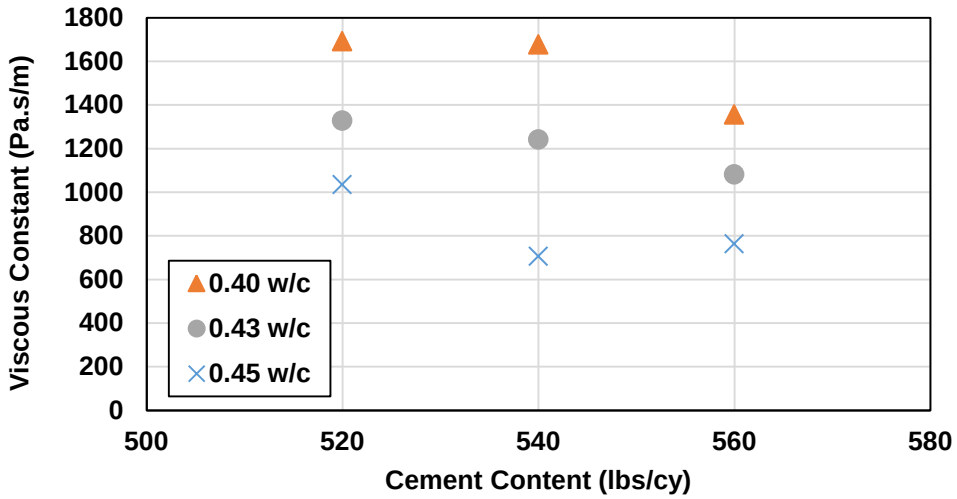

Figure 6.10: Viscous Constant vs. Cement Content

6.3.4 Aggregate Content

Evolution of yield stress with changing coarse aggregate content (by volume) is shown in Figure 6.11. Data points for the yield stress and plastic viscosity were not measured for the 0.40 w/cm, 60-40 mix, due to a high concrete stiffness and subsequently unsuccessful rheological measurements. There was no particular trend observed for the yield stress-coarse aggregate content relationship. For mixes with 0.40 w/cm, a decrease of the yield stress value was recorded with an increase of the total aggregate content; however, only two data points are available, thereby it is not possible to draw a strong conclusion from this observation. For the remainder of the test set, yield stress stayed essentially constant with small variations that can be contributed to the measurement error.

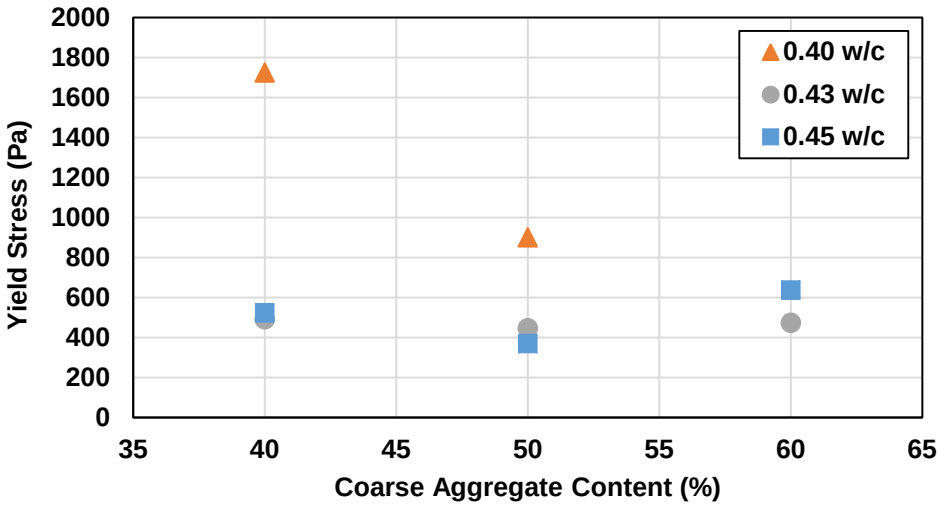

Figure 6.11: Yield Stress vs. Aggregate Content

The relationships between aggregate content and both plastic viscosity and viscous constant are shown in Figure 6.12 and Figure 6.13, respectively. In all cases, plastic viscosity and viscous constant increased with an increase in the aggregate content. Plastic viscosity is often explained as a resistance to flow, hence the plastic viscosity increase with an increase in the coarse aggregate content was to be expected as the higher aggregate content yields a growth in the internal friction of fresh concrete. The increase in the viscosity constant with coarse aggregate content with the 0.40 w/cm mixture could be because the high coarse aggregate content increased the friction between particles, and made it more difficult for particles to migrate away from the tribometer head and lubrication layer.

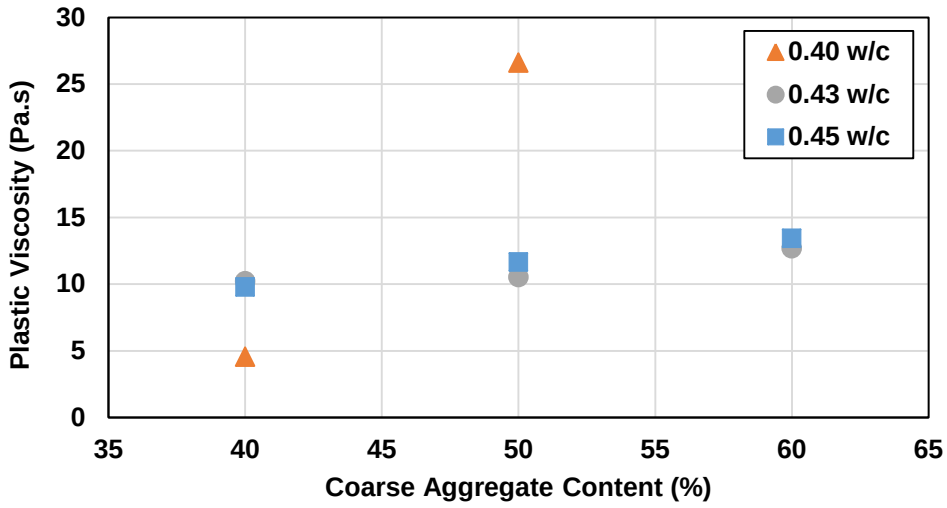

Figure 6.12: Plastic Viscosity vs. Aggregate Content

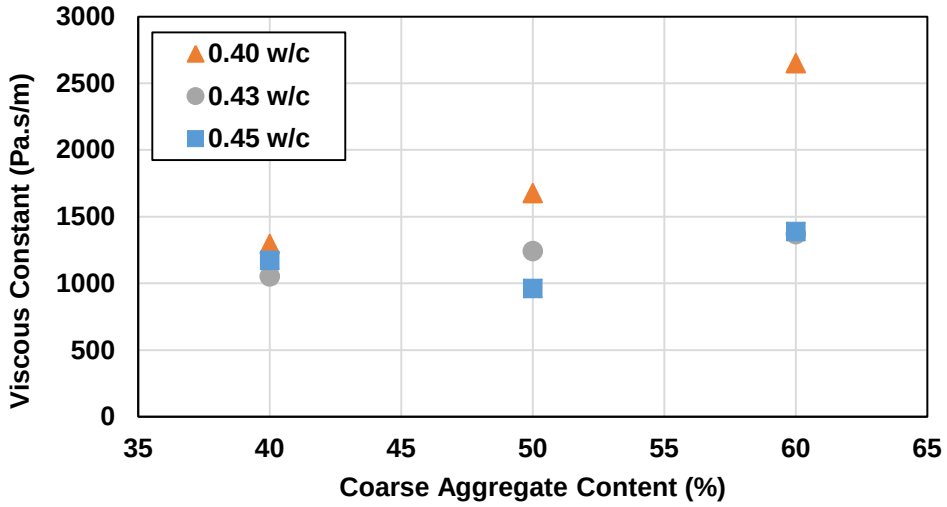

Figure 6.13: Viscous Constant vs. Aggregate Content

6.3.5 Aggregate Roundness

Both yield stress and plastic viscosity decreased in most of the cases when crushed coarse aggregate was replaced with rounded pea gravel, as shown in Figure 6.14 and Figure 6.15. As aggregate shape greatly affects the interaction between particles in the fresh concrete suspension, a decrease in these values is somewhat expected.

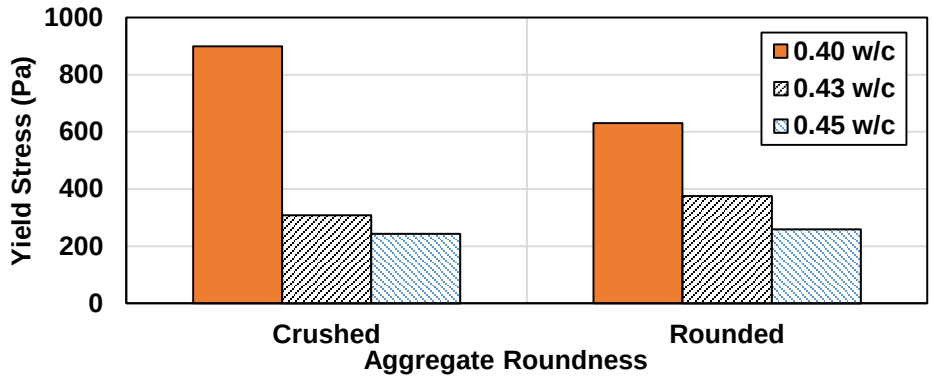

Figure 6.14: Yield Stress vs. Aggregate Roundness

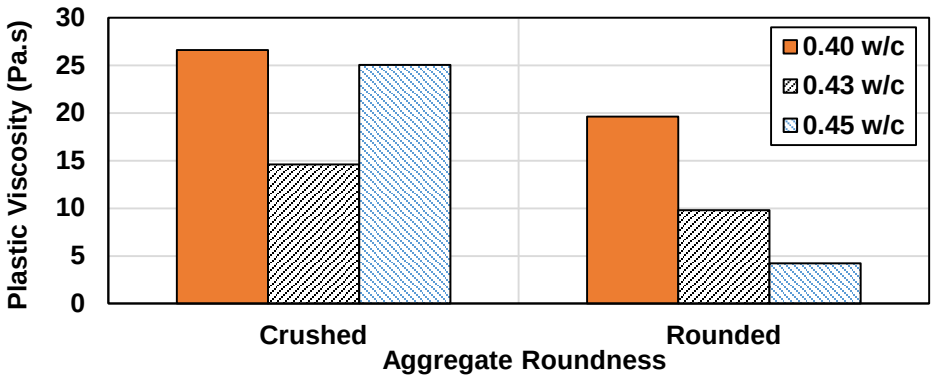

Figure 6.15: Plastic Viscosity vs. Aggregate Roundness

On the other hand, in all cases, greater values of viscous constant were observed when rounded coarse aggregate was substituted in the mix. This could possibly indicate that a thinner lubrication layer was formed when mixes utilizing pea gravel were sheared in the tribometer (assuming the viscosity of the layer remained constant as cement content, sand content, and gradation remained unchanged). Although the exact composition of the lubrication layer is not known, the overall higher amount of very fine particles present in the crushed aggregate could have contributed to an increased thickness of the lubrication layer.

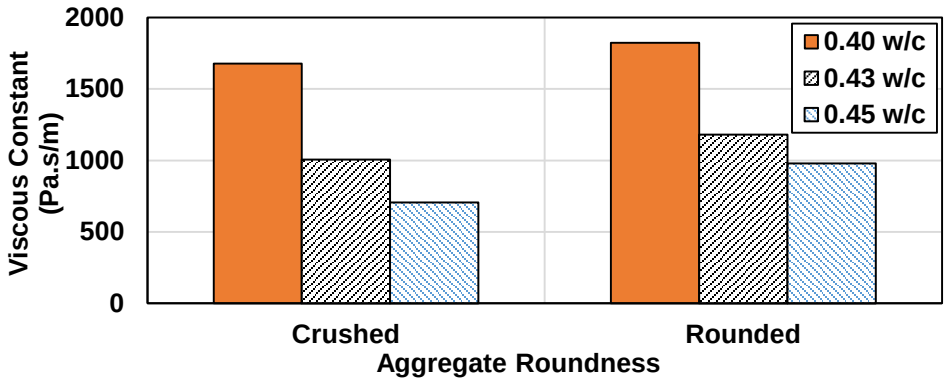

Figure 6.16: Viscous Constant vs. Aggregate Roundness

6.3.6 Use of Supplementary Cementitious Materials

The effects of substitution of 25% of cement (by weight) by Class F fly ash on yield stress, plastic viscosity, and viscous constant in shown in Figure 6.17, Figure 6.18, and Figure 6.19, respectively. A decrease in all three investigated parameters was observed as fly ash was added to the mix. This was very much expected because fly ash particles are perfectly spherical as opposed to grain-like cement particles; thereby, a significant reduction in the internal friction occurs when fly ash is present in a mix. The effect is exaggerated at 0.45 w/cm, most likely due to a slight segregation effect of the mix and coarse particle migration in the rheometer. The benefit to the lubrication layer of adding 25% fly ash to the mixture was as much as increasing the w/cm by 0.03.

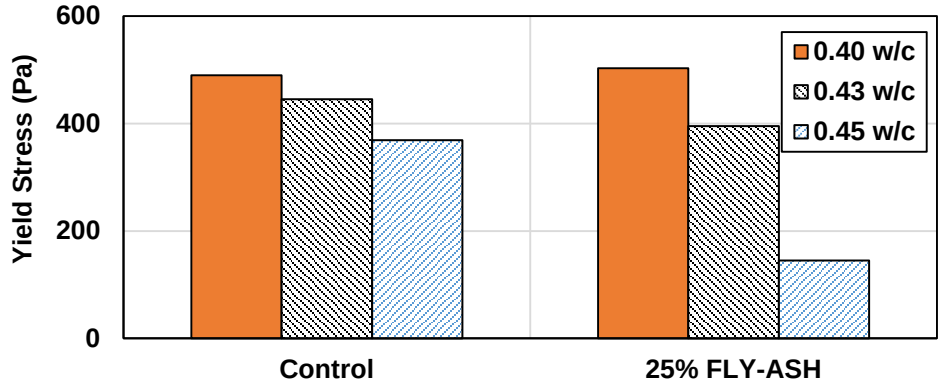

Figure 6.17: Yield Stress vs. Use of Fly Ash

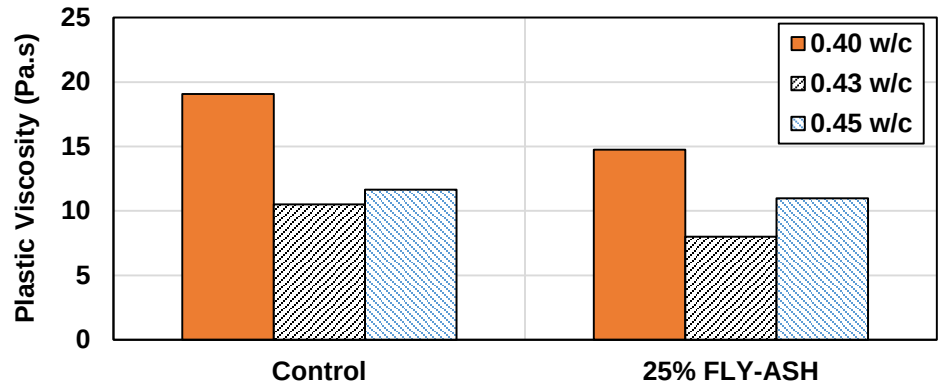

Figure 6.18: Plastic Viscosity vs. Use of Fly Ash

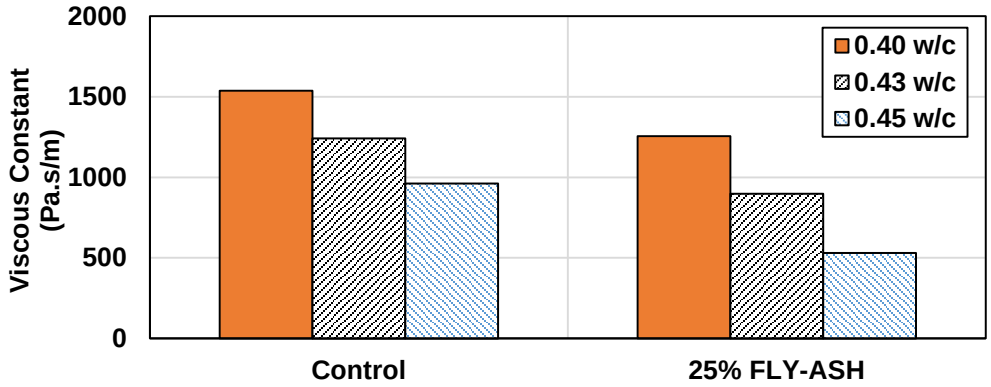

Figure 6.19: Viscous Constant vs. Use of Fly Ash

6.3.7 Use of Viscosity-Modifying Admixture (VMA)

Figure 6.20, Figure 6.21, and Figure 6.22 show the change of yield stress, plastic viscosity, and viscous constant, respectively, with an addition of a VMA. The particular VMA used in this study, according to the manufacturer, is supposed to improve mix cohesiveness without promoting concrete stiffening, ultimately resulting in easier placement. A decrease in yield stress after addition of the VMA was observed for two out of three mixes, whereas an increase in both plastic viscosity and viscous constant was seen in the majority of the test set (five out of six concretes). The decrease in the yield stress supports the manufacturer's claim that the VMA enhances the ease of concrete placement as the initial level of shear stress that is needed to be applied so that concrete starts to move is lowered. However, increased plastic viscosity indicates that a greater amount of shear force must be applied in order to achieve a

certain shear rate (which corresponds to the flow velocity) than what would be required for a mix without the VMA.

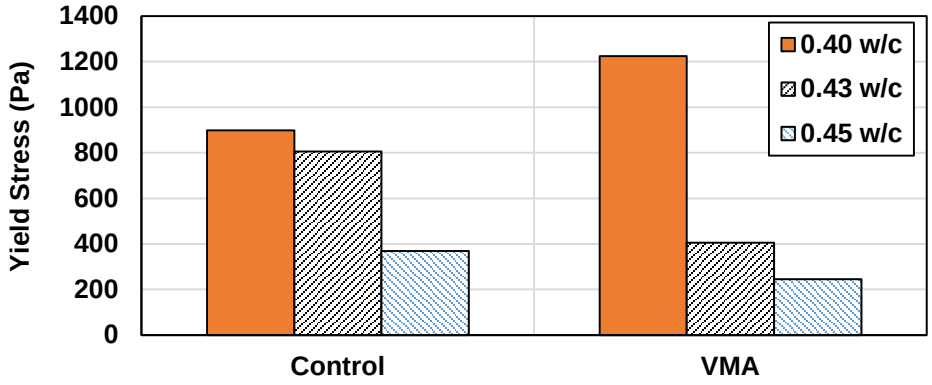

Figure 6.20: Yield Stress vs. Use of VMA

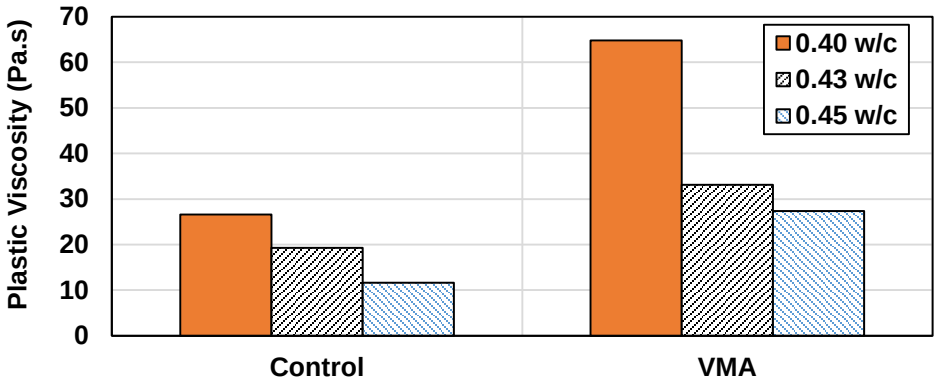

Figure 6.21: Plastic Viscosity vs. Use of VMA

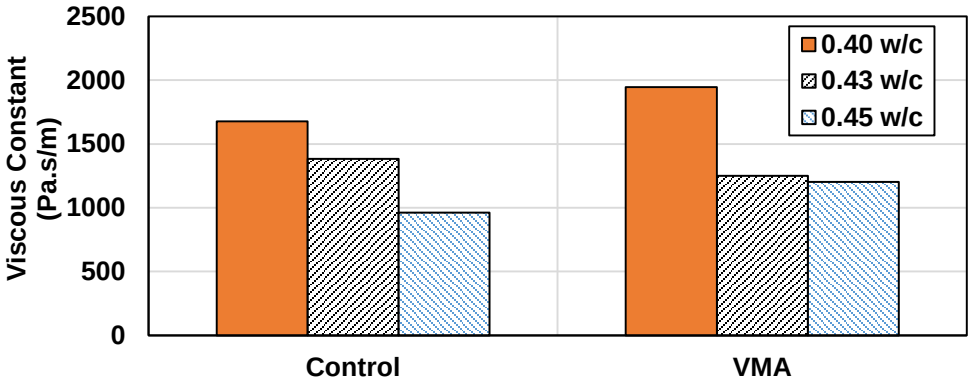

Figure 6.22: Viscous Constant vs. Use of VMA

6.3.8 Use of Nanoclay Particles

Effect of the addition of nanoclay particles on yield stress, plastic viscosity, and viscous constant is shown in Figure 6.23, Figure 6.24, and Figure 6.25, respectively. Both yield stress and viscous constant exhibited both an increase and a decrease in their values after particle addition. However, the value of plastic viscosity decreased in all three cases.

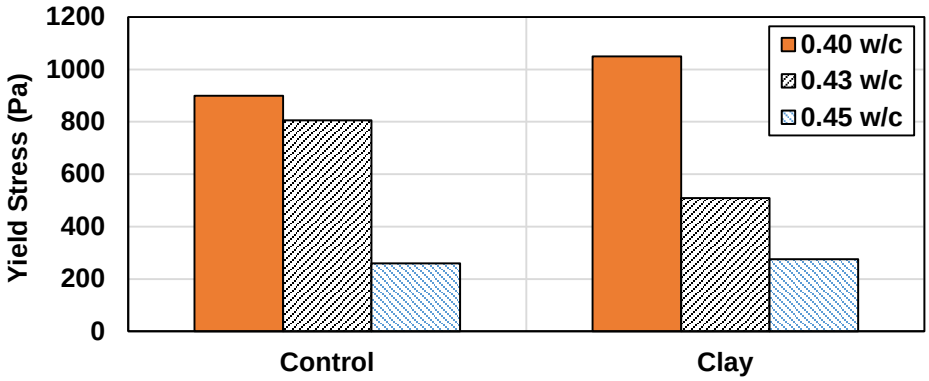

Figure 6.23: Yield Stress vs. Use of Nanoclay Particles

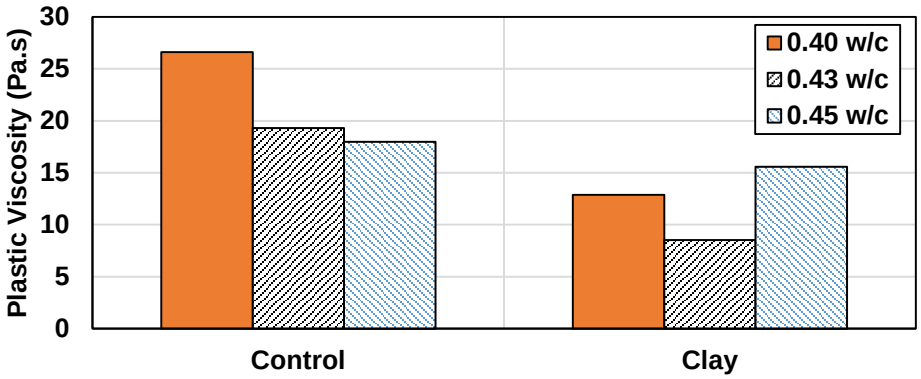

Figure 6.24: Plastic Viscosity vs. Use of Nanoclay Particles

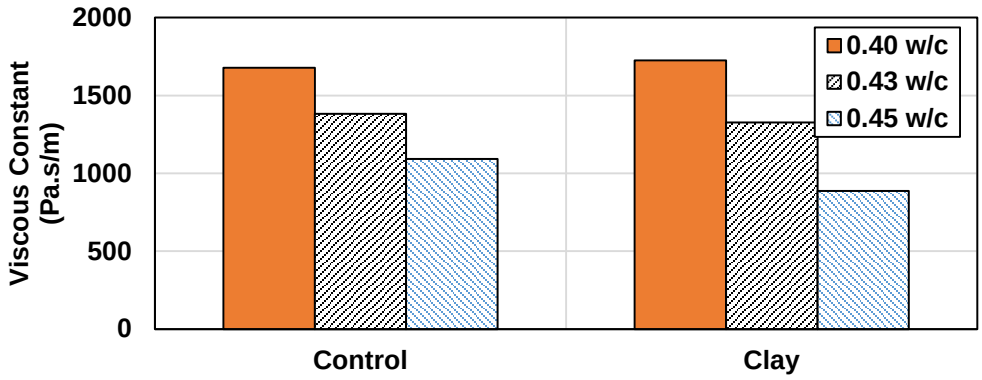

Figure 6.25: Viscous Constant vs. Use of Nanoclay Particles

6.3.9 Pumping Pressure Prediction

Based on measured rheological and tribological properties, Kaplan's pumping pressure model was utilized to evaluate the effect of mix design changes on pumping pressure (Kaplan et al., 2005). All input variables of the model were held constant and the only parameters that changed were the properties of fresh concrete. The following assumptions were made for the modeling purposes: pipe size of 5 inches, 5-inch piston with the filling coefficient of 0.9 (10% of piston remains empty during each pump cycle), and flow rate of 45 cubic yards per hour. The pressure was evaluated in terms of the unit length of the pipeline (psi/ft).

The effect of w/cm and cement content on predicted pumping pressure is shown in Figure 6.26. Results indicated that an increase in mixture water content can reduce the pumping pressure by up to 50%. Similarly, an increase of the total cementitious material content can be beneficial when the pumping pressure needs to be reduced. Considering mixture proportions used in this study, addition of 20 lbs of cement per cubic yard reduced the pressure by approximately 20%. Although increasing the amount of mixing water in the mixture appears to be the most effective measure to reduce the pumping pressure, it is not always possible to add more water due to side effects that such addition can have on other concrete properties (strength, durability, shrinkage). Likewise, the total cement content is very often limited by various performance restrictions. However, when these adjustments are feasible, results of this study suggest they can be effectively used for improving pumpability of a concrete mixture.

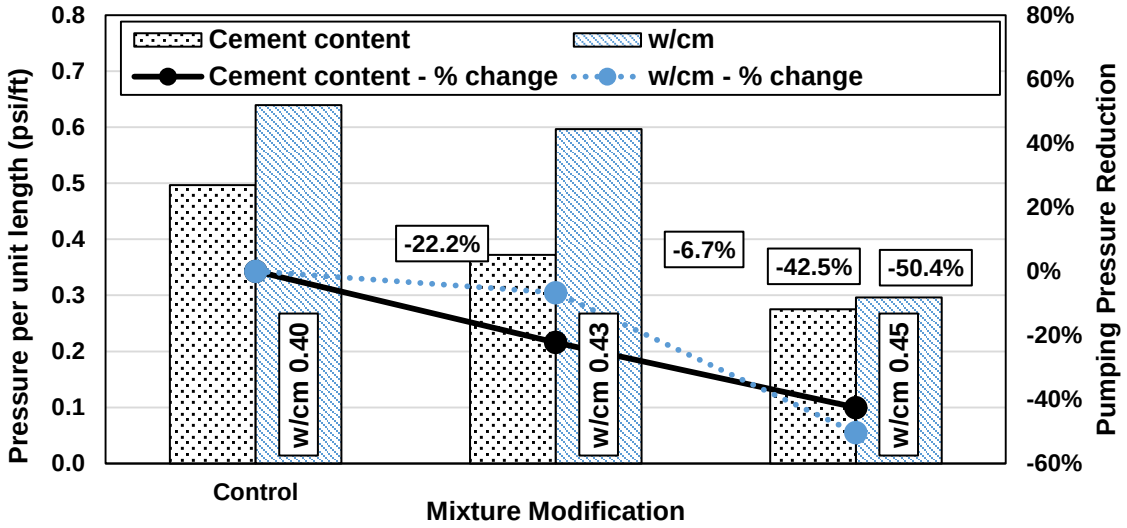

Figure 6.26: Effect of Cement Content and w/cm on Pumping Pressure

The effect of coarse-to-fine aggregate ratio is shown in Figure 6.27. For the particular type of coarse and fine aggregate used in this study, it appears that the 50:50 ratio is the most beneficial in terms of the absolute pumping pressure value. When coarse aggregate content was reduced by 10%, the theoretical pumping pressure increased by 6%. When 10% addition of coarse aggregate took place, the pumping pressure increased by almost 40%. This suggests that there exists an optimal gradation for pumping pressure that may be different than that for other workability parameters.

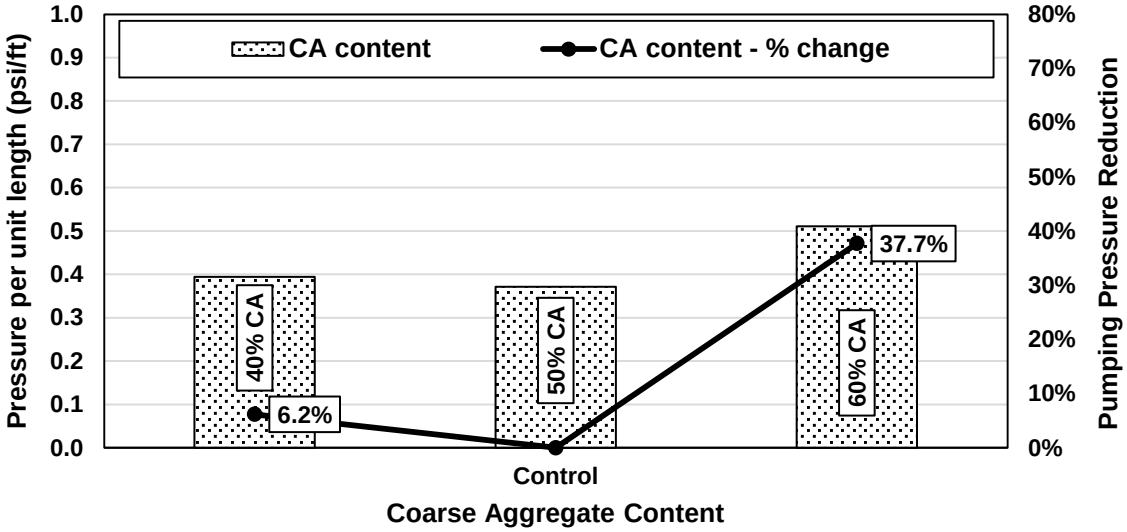

Figure 6.27: Effect of Coarse-to-Fine Aggregate Ratio on Pumping Pressure

The effect of aggregate roundness and 20% fly ash substitution on pumping pressure is shown in Figure 6.28, and the influence of VMA and nanoclay particles is presented in Figure 6.29. The analysis was carried out considering only mixtures with w/cm of 0.43, as these mixtures provided the most consistent rheological and tribological measurements. These design adjustments led to the reduction in the pumping pressure. The absolute decrease in the pumping pressure due to 25% replacement of ordinary portland cement with Class F fly ash was 13%. A similar decrease in the pumping pressure was observed when crushed coarse aggregate was replaced with rounded aggregate particles. Addition of a viscosity-modifying admixture reduced the pressure by 48%, whereas addition of nanoclay particles led to 28% pressure reduction. It is important to reiterate that these values were obtained for a particular mix design used in this study; however, observed general trends are certainly applicable to concrete mixture.

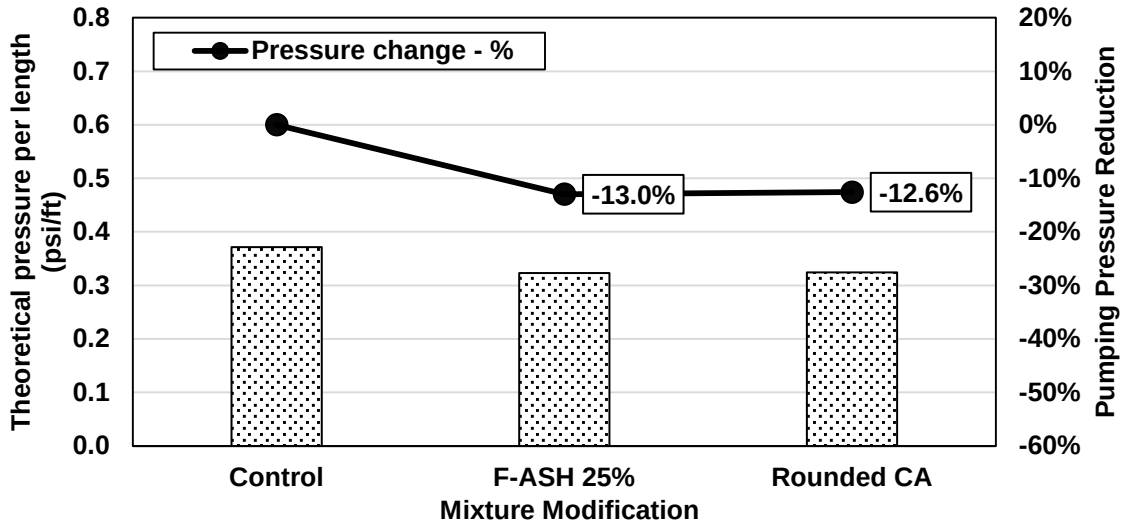

Figure 6.28: Effect of Mix Design (Aggregate Roundness, Fly Ash) on Pumping Pressure

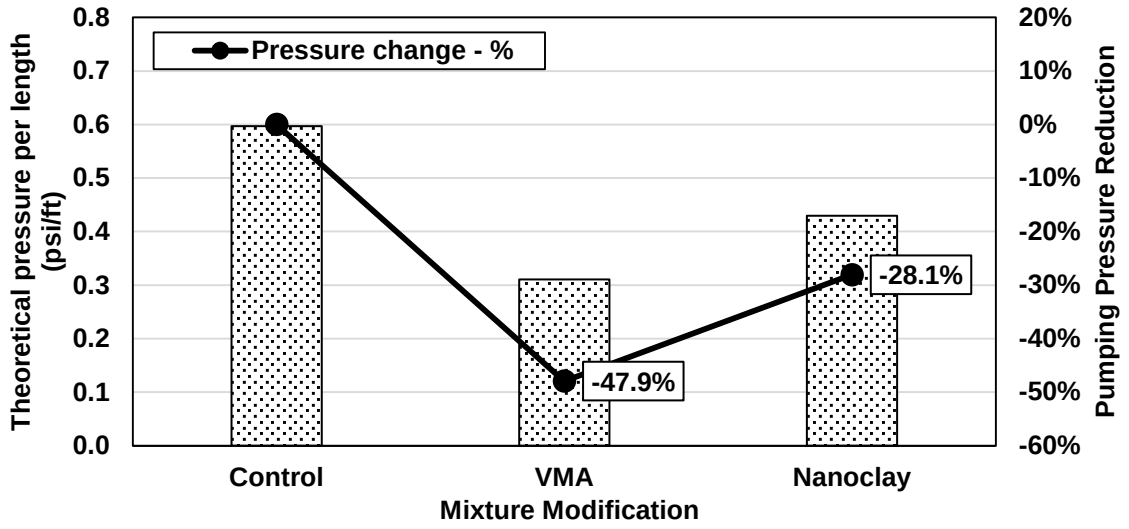

Figure 6.29: Effect of Mix Design (VMA, Nanoclay) on Pumping Pressure

6.4 Summary and Recommendations

A laboratory study was conducted to evaluate the effect of mix design on rheological and tribological properties of concrete, and ultimately on pumping pressure. Variables included in this study included w/c, cement content, coarse/fine aggregate ratio, coarse aggregate shape, and use of fly-ash, viscosity-modifying admixture (VMA), and nanoclay particles. Portable field rheometer and tribometer were used to measure rheological properties of fresh concrete and tribological parameters of the lubrication layer. Kaplan's pumping pressure model was used to analyze the obtained data and to compare effects of mixture modification on the pumping pressure.

The comparative analysis revealed that an increase in the w/cm ratio is possibly the most effective measure to enhance pumpability. However, this might not be always feasible due to performance limitations imposed on the water content. Additionally, excessive water addition can result in an unstable mixture, creating a possibility for segregation and blockage of the pump. Nevertheless, when possible, reasonable increase in the mixing water content can be recommended should the mixture experience pumpability issues.

Addition of nanoclay particles to the mixture substantially reduced the pumping pressure. Moreover, the yield stress remained close to the control mixture value after the particles addition. As yield stress has been found to correlate well with slump measurements, it is recommended to

further investigate use of nanoclay particles in concrete mixtures to enhance their pumpability while maintaining required slump. This could allow KDOT to pump low paste content mixtures without increasing slump and the risk of settlement cracking.

The total cement content was found to have a significant impact on predicted pumping pressure. An increase of cement content from 520 to 560 lbs per cubic yard led to 40% reduction of the pumping pressure. Additionally, replacing 25% of cement with Class F fly ash helped to further reduce the pumping pressure. Therefore, the use of supplementary cementitious materials is encouraged for improving the pumpability of concrete mixture on KDOT projects.

Other corrective measures, such as replacing crushed coarse aggregate with rounded coarse aggregate and addition of viscosity-modifying admixture, were also shown to have a positive effect on reducing the pumping pressure.

Rheometer and rheometer-based portable tribometer have been successfully used in this laboratory study. Although these devices are not field-friendly at this point, their use in the laboratory development can be beneficial and is recommended and encouraged.

Chapter 7: Conclusions and Recommendations

7.1 Conclusions

Based on the results of the field testing campaign, the full-scale pumping experiment, and the laboratory study, the following conclusions have been made:

- Observed changes in the air void system have shown different tendencies during the field testing program and the pumping experiment. The majority of investigated mixtures during the field campaign exhibited an increase in the air content after pumping, whereas all mixes tested during the pumping experiment had a lower air content after pumping. Dissimilar changes in concrete air void system after pumping observed in the field testing and the controlled experiment support the theory that the mixing action after concrete is discharged into the formwork is a significant factor affecting properties of the air void system.
- During the pumping experiment, all tested concrete mixtures showed a decrease in the total air void content and an increase in spacing factor after pumping. Therefore, if the mixing action effect is not present, concrete can be expected to lose a substantial amount of air and small air voids will most likely disappear. A correlation was found between the pumping pressure and absolute change of the spacing factor and the total air void content before and after pumping.
- The SAM number is based on changes in the concrete air system after overpressurization, and pumping subjects the concrete to pressures even higher than seen in the SAM test.
- Pumping pressure is linear along the pipeline for both the “flat” and “A” boom configurations. Higher pumping pressure was required to pump concrete when the boom was in the flat configuration than when it was positioned in the A configuration. Therefore, more substantial changes in the air void system can be expected during pumping operations with the boom in the flat configuration.

- The laboratory study showed that adjustments of mix design parameters can be made to effectively change rheological and tribological properties of concrete, and hence improve its pumpability. The following concrete mixture changes resulted in increased pumpability: an increase in the w/cm, an increase in the paste content, use of fly ash, and use of rounded aggregates instead of crushed aggregates. Some of these factors that improve pumpability such as an increase in the w/cm or paste content conflict with durability requirements and caution should be exercised in attempting to improve pumpability at the expense of durability.
- Nanoclay particles were shown to benefit the concrete viscosity significantly and in some cases have only a minimal effect on the yield stress. This could provide an avenue to enhancing the pumpability of concrete mixtures while still meeting KDOT slump requirements for bridge decks.

7.2 Recommendations

Based on the project findings, it is recommended that KDOT implement the following:

1. Do not use the SAM number as a quality control requirement for pumped concrete.
2. Investigate the use of nanoclay particles to improve pumpability of concrete containing low paste volumes.
3. When having issues with pumpability of a mixture, lower the percentage of coarse aggregate and raise the corresponding percentage of fine aggregate in the concrete mixture. This is often possible with little impact on the paste volume.
4. Sample concrete from the formwork rather than directly from the pump discharge.

References

ACI 304.2R-96. (1996). *Placing concrete by pumping methods*. Farmington Hills, MI: American Concrete Institute.

ASTM C138 / C138M-13. (2013). *Standard test method for density (unit weight), yield, and air content (gravimetric) of concrete*. West Conshohocken, PA: ASTM International. doi: 10.1520/C0138_C0138M, www.astm.org

ASTM C143 / C143M-12. (2012). *Standard test method for slump of hydraulic-cement concrete*. West Conshohocken, PA: ASTM International. doi: 10.1520/C0143_C0143M-12, www.astm.org

ASTM C192 / C192M-13. (2013). *Standard practice for making and curing concrete test specimens in the laboratory*. West Conshohocken, PA: ASTM International. doi: 10.1520/C0192_C0192M, www.astm.org

ASTM C231 / C231M-10. (2010). *Standard test method for air content of freshly mixed concrete by the pressure method*. West Conshohocken, PA: ASTM International. doi: 10.1520/C0231_C0231M-10, www.astm.org

ASTM C1064 / C1064M-04. (2004). *Standard test method for temperature of freshly mixed hydraulic-cement concrete*. West Conshohocken, PA: ASTM International. doi: 10.1520/C1064_C1064M-04, www.astm.org

Barnes, H. A., Hutton, J. F., & Walters, K. (1989). *An introduction to rheology*. Amsterdam, Netherlands: Elsevier.

Bird, R. B., Armstrong, R. C., & Hassager, O. (1987). *Dynamics of polymeric liquids: Vol. 1, Fluid mechanics* (2nd ed.). New York, NY: Wiley.

Browne, R. D., & Bamforth, P. B. (1977). Tests to establish concrete pumpability. *ACI Journal Proceedings, 74*(5), 193–203.

Chapdelaine, F. (2007). *Étude fondamentale et pratique sur le pompage du béton* [Basic and practical study on pumping concrete] (Doctoral dissertation). Université Laval, Québec, Canada.

Choi, M., Roussel, N., Kim, Y., & Kim, J. (2013). Lubrication layer properties during concrete pumping. *Cement and Concrete Research*, *45*, 69–78.

Cooke, T. H. (1990). *Concrete pumping and spraying: A practical guide*. London, England: Thomas Telford.

Dyer, R. M. (1991). *An investigation of concrete pumping pressure and the effects of pressure on the air void system of concrete* (Master's thesis). University of Washington, Seattle, WA.

Ferraris, C. F., & Martys, N. S. (2003). Relating fresh concrete viscosity measurements from different rheometers. *Journal of Research of the National Institute of Standards and Technology, 108*(3), 229–234.

Feys, D., De Schutter, G., & Verhoeven, R. (2013). Parameters influencing pressure during pumping of self-compacting concrete. *Materials and Structures*, *46*(4), 533–555.

Feys, D., Khayat, K. H., Perez-Schell, A., & Khatib, R. (2014). Development of a tribometer to characterize lubrication layer properties of self-consolidating concrete. *Cement and Concrete Composites, 54*, 40–52.

Feys, D., Khayat, K. H., Perez-Schell, A., & Khatib, R. (2015). Prediction of pumping pressure by means of new tribometer for highly-workable concrete. *Cement and Concrete Composites, 57*, 102–115.

Feys, D., Wallevik, J. E., Yahia, A., Khayat, K. H., & Wallevik, O. H. (2013). Extension of the Reiner–Riwlin equation to determine modified Bingham parameters measured in coaxial cylinders rheometers. *Materials and Structures, 46*(1), 289–311.

Fisher, T. S. (1994). *How a concrete pump works: A look at the valves and other components of piston pumps* (Publication #C940629). Boston, MA: The Aberdeen Group.

Ghafoori, N., Diawara, H., Nyknahad, D., Barfield, M., & Islam, M. S. (2012). Pumping influence on fresh properties of self-consolidating concrete. In *Concrete solutions: Proceedings of Concrete Solutions, 4th International Conference on Concrete Repair* (pp. 233–236). London, England: Taylor & Francis Group.

Harris, J. (1977). *Rheology and non-Newtonian flow*. New York, NY: Longman.

Heirman, G., Vandewalle, L., Van Gemert, D., & Wallevik, Ó. (2008). Integration approach of the Couette inverse problem of powder type self-compacting concrete in a wide-gap concentric cylinder rheometer. *Journal of Non-Newtonian Fluid Mechanics, 150*(2–3), 93–103.

Jacobsen, S., Haugan, L., Hammer, T. A., & Kalogiannidis, E. (2009). Flow conditions of fresh mortar and concrete in different pipes. *Cement and Concrete Research, 39*(11), 997–1006.

Jacobsen, S., Mork, J. H., Lee, S. F., & Haugan, L. (2008). *Pumping of concrete and mortar – State of the art*. Oslo, Norway: SINTEF Building and Infrastructure.

Kansas Department of Transportation (KDOT). (2015). Section 401.9: Inspection and testing. In *Standard specifications for state road & bridge construction*. Topeka, KS: Author.

Kaplan, D. (2001). *Pompage des bétons* [Pumping concrete]. Paris, France: Laboratoire Central des Ponts et Chaussées.

Kaplan, D., de Larrard, F., & Sedran, T. (2005). Design of concrete pumping circuit. *ACI Materials Journal, 102*(2), 110–117.

Khatib, R. (2013). *Analysis and prediction of pumping characteristics of high-strength self-consolidating concrete* (Doctoral dissertation). Université de Sherbrooke, Sherbrooke, Québec, Canada.

Koehler, E. P., Fowler, D. W., Ferraris, C. F., & Amziane, S. (2006). A new, portable rheometer for fresh self-consolidating concrete. *ACI Special Publication, 233*, 97–116.

Ley, M. T. (2015, February). *Pushing concrete pavements to new heights of quality and durability* [Presentation slides]. Presented at the WCPA Annual Concrete Pavement Workshop, Oshkosh, WI.

Ley, M. T., & Tabb, B. (2014). A test method to measure the freeze thaw durability of fresh concrete using overpressure. In A. Varma & Gosling, G. (Eds.), *T&DI Congress 2014: Planes, trains, and automobiles* (pp. 79–87). Reston, VA: American Society of Civil Engineers.

Newman, J., & Choo, B. S. (Eds.). (2003). *Advanced concrete technology 3: Processes*. Oxford, UK: Butterworth-Heinemann.

Peterson, K. (2008). *Automated air-void system characterization of hardened concrete: Helping computers to count air-voids like people count air-voids – Methods for flatbed scanner calibration* (Doctoral dissertation). Michigan Technological University, Houghton, MI.

Riding, K. A., Esmaeily, A., & Vosahlik, J. (2015). *Air void clustering* (Report No. K-TRAN: KSU-13-6). Topeka, KS: Kansas Department of Transportation.

Roussel, N. (Ed.). (2012). *Understanding the rheology of concrete*. Cambridge, UK: Woodhead Publishing.

Roussel, N., & Gram, A. (Eds.). (2014). *Simulation of fresh concrete flow: State-of-the art report of the RILEM Technical Committee 222-SCF*. Dordrecht, Netherlands: Springer.

Wallevik, J. E. (2006). Relationship between the Bingham parameters and slump. *Cement and Concrete Research, 36*(7), 1214–1221.

Wallevik, J. E. (2009). Rheological properties of cement paste: Thixotropic behavior and structural breakdown. *Cement and Concrete Research, 39*(1), 14–29.

Wallevik, O. H., Feys, D., Wallevik, J. E., & Khayat, K. H. (2015). Avoiding inaccurate interpretations of rheological measurements for cement-based materials. *Cement and Concrete Research, 78*(Part A), 100–109.

Yazdani, N., Bergin, M., & Majtaba, G. (2000). Effect of pumping on properties of bridge concrete. *Journal of Materials in Civil Engineering, 12*(3), 212–219.

Yingling, J., Mullings, G. M., & Gaynor, R. D. (1992). Loss of air content in pumped concrete. *Concrete International, 14*(10), 57–61.

Yonezawa, T., Yoshioka, Y., Iwashimizu, T., Nanjo, K., Yoneda, S., Sakaue, K., & Nakase, T. (1988). Pumping of lightweight concrete using non-presoaked lightweight aggregate. *ACI Special Publication, 109*, 625–654.

Appendix A: Field Testing Results

Table A.1: Fresh Concrete Properties (Slump, Air Content, and SAM) – Field Testing

Project	Test	Before Pumping			After Pumping		
		Slump	Air Content	SAM Number	Slump	Air Content	SAM Number
		in.	%	-	in.	%	-
K-10 Haskell	1	4.50	6.7	0.12	N/A	N/A	N/A
K-10 Haskell	2	5.75	6.0	0.09	7.25	8.0	0.24
K-10 Haskell	3	5.75	5.6	0.21	6.50	8.6	N/A
I-70 Kaw	1	5.75	6.2	0.06	3.00	7.4	0.22
I-70 Kaw	2	7.75	7.6	0.09	5.75	6.7	0.70
I-70 Kaw	3	5.75	10.3	0.14	5.00	7.1	N//A
K-10 Naismith #1	1	6.00	5.2	0.33	4.75	7.0	0.14
K-10 Naismith #1	2	7.75	5.2	0.25	6.75	7.2	0.14
K-10 Naismith #1	3	5.25	5.5	0.14	6.25	7.0	0.33
K-10 Naismith #1	4	4.00	5.3	0.32	5.00	8.9	0.23
K-10 East	1	5.50	5.2	0.24	6.25	7.5	0.36
K-10 Louisiana	1	4.85	7.5	0.33	4.75	8.7	0.21
K-10 Louisiana	2	6.50	6.2	0.46	6.25	7.0	0.26
K-10 Naismith #2	1	7.50	4.4	0.67	5.75	6.2	0.40

Table A.2: Fresh Concrete Properties (Unit Weight and Temperature) – Field Testing

Project	Test	Before Pumping		After Pumping	
		Unit Weight	Temperature	Unit Weight	Temperature
		lbs/ft³	°F	lbs/ft³	°F
K-10 Haskell	1	N/A	69.2	N/A	N/A
K-10 Haskell	2	N/A	71.0	N/A	75.3
K-10 Haskell	3	N/A	73.6	N/A	73.3
I-70 Kaw	1	145.2	80.3	143.8	84.5
I-70 Kaw	2	142.4	81.0	144.4	83.9
I-70 Kaw	3	138.2	83.2	143.4	85.1
K-10 Naismith #1	1	145.8	80.5	143.0	83.5
K-10 Naismith #1	2	145.8	79.8	142.0	82.5
K-10 Naismith #1	3	144.6	79.4	143.4	82.3
K-10 Naismith #1	4	145.6	80.9	139.4	86.1
K-10 East	1	146.4	81.2	142.4	82.6
K-10 Louisiana	1	142.2	79.6	139.8	81.1
K-10 Louisiana	2	144.4	70.7	142.6	82.5
K-10 Naismith #2	1	146.6	79.6	142.6	81.2

Table A.3: Tribological and Rheological Properties – Field Testing

Project	Test #	Before Pumping			After Pumping		
		PV	YS	Viscous Constant	PV	YS	Viscous Constant
		Pa.s	Pa	Pa.s/m	Pa.s	Pa	Pa.s/m
K-10 Haskell	1	23.5	862	1922	0	0	0
K-10 Haskell	2	46.5	430	1803	28.7	450.3	1410
K-10 Haskell	3	53.7	517	1894	19.7	517	1264
I-70 Kaw	1	16	1294.8	1418	16	893	1735
I-70 Kaw	2	14.4	582.98	1322	16.2	808.8	1879
I-70 Kaw	3	18.4	1042.1	1587	41.8	685.3	1808
K-10 Naismith #1	1	35.9	575.7	1785	13.1	577.1	871
K-10 Naismith #1	2	37.1	611.1	1515	37.1	561.3	1723
K-10 Naismith #1	3	24	862	1653	41.5	630.3	1565
K-10 Naismith #1	4	23.8	1055.4	1471	23.8	954	1038
K-10 East	1	30.8	747.19	1209	16.99	764.54	1345
K-10 Louisiana	1	14.55	928.89	1743	23.63	426.16	1562
K-10 Louisiana	2	27.2	543.74	1518	17.22	776.43	1622
K-10 Naismith #2	1	20.86	1228.86	1871	24	862	1638

Table A.4: Hardened Air Void Analysis – Field Testing

Project	Test #	Before Pumping		After Pumping	
		Air Void Content	Spacing Factor	Air Void Content	Spacing Factor
		%	in.	%	in.
K-10 Haskell	1	N/A	N/A	N/A	N/A
K-10 Haskell	2	N/A	N/A	N/A	N/A
K-10 Haskell	3	N/A	N/A	N/A	N/A
I-70 Kaw	1	6.77	0.00853	7.35	0.00718
I-70 Kaw	2	7.19	0.00565	9.17	0.00652
I-70 Kaw	3	12.02	0.00551	7.08	0.00632
K-10 Naismith #1	1	6.28	0.009590551	8.5	0.007055118
K-10 Naismith #1	2	5.18	0.011523622	7.405	0.007557087
K-10 Naismith #1	3	6.2	0.008834646	7.78	0.007314961
K-10 Naismith #1	4	5.99	0.008185039	7.93	0.007527559
K-10 East	1	6.91	0.00612	7.44	0.00695
K-10 Louisiana	1	7.59	0.008003937	7.28	0.006988189
K-10 Louisiana	2	7.1	0.008661417	8.81	0.005220472
K-10 Naismith #2	1	8.43	0.005374016	9.47	0.007102362

Appendix B: Pumping Experiment Results

Table B.1: Fresh Concrete Properties – Pumping Experiment

Test ID	Sample Source	Mix Design	Boom Setup	Slump	Unit Weight	Air Content	SAM
				in.	lbs/ft³	%	-
1	Truck	A	-	8.75	134.80	11.2	N/A
2	Pump	A	Flat	8.25	142.40	6.9	0.30
3	Pump	A	Flat	8.50	144.52	5.4	0.14
4	Pump	A	Flat	8.00	145.80	4.9	0.22
5	Truck	A	-	8.75	135.60	10.8	0.07
6	Pump	A	A	5.25	144.80	5.7	0.06
7	Pump	A	A	6.50	N/A	N/A	0.00
8	Truck	A	-	7.50	142.00	10.1	N/A
10	Truck	B	-	8.50	141.60	8.4	0.07
11	Pump	B	A	5.25	148.08	3.4	0.30
12	Pump	B	A	6.75	147.20	4.1	0.22
13	Truck	B	-	6.00	139.92	8.9	0.20
20	Truck	C	-	7.25	N/A	7.8	0.00
21	Pump	C	A	5.25	146.00	4.7	0.16
22	Pump	C	A	5.00	145.40	5.1	0.33
23	Pump	C	Flat	4.50	145.40	5.1	0.18
24	Pump	C	Flat	4.50	145.20	5.7	0.42
25	Truck	C	-	6.50	140.20	8.9	0.09

Table B.2: Rheological and Tribological Properties – Pumping Experiment

Test ID	Sample Source	Mix Design	Boom Setup	Yield Stress	Plastic Viscosity	Viscous Constant
				Pa.s	Pa	Pa.s/m
1	Truck	A	-	424.4	6.4	1107
2	Pump	A	Flat	480.2	4.1	828
3	Pump	A	Flat	526.3	6.4	892
4	Pump	A	Flat	447.3	10.8	851
5	Truck	A	-	579.1	1.0	1267
6	Pump	A	A	687.2	4.3	876
7	Pump	A	A	623.4	6.0	825
8	Truck	A	-	643.5	4.2	1033
10	Truck	B	-	494.3	10.1	1240
11	Pump	B	A	601.9	15.4	1152
12	Pump	B	A	723.0	9.3	1302
13	Truck	B	-	803.2	4.9	1786
20	Truck	C	-	0.0	0.0	1065
21	Pump	C	A	672.7	12.7	980
22	Pump	C	A	651.0	13.5	938
23	Pump	C	Flat	752.4	9.8	868
24	Pump	C	Flat	830.2	7.4	938
25	Truck	C	-	773.4	4.4	1346

Table B.3: Pumping Pressures – Pumping Experiment

Test ID	Sample Source	Mix Design	Boom Setup	Maximum Pressure (psi)			Flow Rate
				Gauge A	Gauge B	Gauge C	ft/s³
1	Truck	A	-	-	-	-	-
2	Pump	A	Flat	N/A (176)*	135	73	0.73
3	Pump	A	Flat	N/A (263)*	213	138	1.14
4	Pump	A	Flat	N/A (85)*	64	32	0.20
5	Truck	A	-	-	-	-	-
6	Pump	A	A	N/A (177)*	152	114	0.95
7	Pump	A	A	N/A (83)*	61	28	0.18
8	Truck	A	-	-	-	-	-
10	Truck	B	-	-	-	-	-
11	Pump	B	A	167	201	42	0.78
12	Pump	B	A	321	269	79	1.25
13	Truck	B	-	-	-	-	-
20	Truck	C	-	-	-	-	-
21	Pump	C	A	158	102	34	0.77
22	Pump	C	A	362	205	99	1.25
23	Pump	C	Flat	285	170	84	0.74
24	Pump	C	Flat	421	269	143	1.18
25	Truck	C	-	-	-	-	-

* Extrapolated values.

Table B.4: Hardened Air Void Properties – Pumping Experiment

Mix ID	Sample Source	Mix Design	Boom Setup	Air Content	Spacing factor
				%	in.
1	Truck	A	-	11.45	0.00311
2	Pump	A	Flat	7.20	0.00489
3	Pump	A	Flat	6.50	0.00637
4	Pump	A	Flat	6.10	0.00779
5	Truck	A	-	9.73	0.00233
6	Pump	A	A	8.04	0.00588
7	Pump	A	A	7.05	0.00726
8	Truck	A	-	9.83	0.00490
10	Truck	B	-	8.03	0.00746
11	Pump	B	A	4.48	0.00930
12	Pump	B	A	4.62	0.00994
13	Truck	B	-	9.42	0.00548
20	Truck	C	-	10.40	0.00321
21	Pump	C	A	4.11	0.00602
22	Pump	C	A	6.12	0.01043
23	Pump	C	Flat	5.44	0.00758
24	Pump	C	Flat	7.65	0.00837
25	Truck	C	-	10.82	0.00418

Appendix C: Laboratory Study Results

Table C.1: Fresh Concrete Properties – Laboratory Study, Control Mixes

ID	Slump	Air Content	Unit Weight	Yield Stress	Plastic Viscosity	Viscous Constant	Interface Yield Stress
	in.	%	lbs/ft³	Pa	Pa.s	Pa.s/m	Pa
040 - Control A	4.75	6.8%	148.00	899	26.60	1677	0
040 - Control B	8.00	14.0%	134.88	361	18.02	1424	40.05
040 - Control C	4.25	11.5%	138.64	490	19.08	1537	33.98
043 - Control A	8.00	9.0%	141.44	445	10.51	1241	43.6
043 - Control B	7.25	10.0%	140.08	308	14.60	1007	81.46
043- Control C	3.00	5.7%	145.84	806	19.32	1383	68.28
045 - Control A	9.25	9.5%	139.96	259	18.00	1092	13.02
045 - Control B	8.50	8.0%	142.00	243	25.04	706	38.873
045- Control C	4.00	6.7%	144.36	369	11.66	962	45.37

Table C.2: Fresh Concrete Properties – Laboratory Study

ID	Slump	Air Content	Unit Weight	Yield Stress	Plastic Viscosity	Viscous Constant	Interface Yield Stress
	in.	%	lbs/ft³	Pa	Pa.s	Pa.s/m	Pa
040 - 520	4.50	6.8%	147.60	884	17.2	1692	12.05
043 - 520	7.25	9.0%	141.96	575	9.1	1328	36.86
045 - 520	8.50	9.0%	140.96	417	14.5	1034	52.58
040 - 560	8.00	8.0%	142.16	442	26.3	1356	45.97
043 - 560	8.50	10.1%	139.72	387	12.1	1081	53.2
045 - 560	18.75	7.1%	143.40	193	14.6	763	40.927
040 - 60-40	2.50	4.5%	149.32	N/A	N/A	2649	67.25
043 - 60-40	7.50	9.0%	142.40	473	12.7	1368	57.47
045 - 60-40	4.00	6.7%	144.36	636	13.4	1388	65.37
040 - 40-60	1.50	7.2%	144.92	1724	4.5	1294	70.91
043 - 40-60	8.75	10.5%	138.80	490	10.2	1053	56.48
045 - 40-60	9.00	7.9%	140.68	522	9.8	1172	54.03
040 - F-ASH	8.50	11.5%	137.44	503	14.8	1256	27.74
043 - F-ASH	17.00	8.5%	141.52	395	8.0	899	49.3
045 - F-ASH	19.00	4.6%	146.56	145	11.0	530	37.91
040 - RR	6.00	7.8%	141.00	631	19.6	1824	79.4
043 - RR	7.25	9.5%	137.52	375	9.8	1181	84.83
045 - RR	16.00	8.5%	138.88	259	4.2	980	67.15
040 - VMA	1.50	5.0%	147.24	1225	64.8	1946	98.86
043 - VMA	7.75	6.0%	145.48	405	33.2	1131	103.84
045 - VMA	6.50	5.4%	144.92	245	27.3	1202	50.08
040 - Clay	3.50	6.0%	0.00	1050	12.9	1726	12.79
043 - Clay	0.75	4.7%	149.16	508	8.5	1326	34.69
045 - Clay	8.50	9.6%	140.68	275	15.6	887	44.36

K-TRAN

KANSAS TRANSPORTATION RESEARCH AND NEW-DEVELOPMENT PROGRAM

AD ASTRA PER ASPERA

Kansas

Department of Transportation